8-2020

Signal Processing Combined with Machine Learning for Biomedical Applications

M.D. Shakhawat Hossain
The University of Texas Rio Grande Valley

SIGNAL PROCESSING COMBINED WITH MACHINE LEARNING FOR BIOMEDICAL APPLICATIONS

A Thesis

by

MD SHAKHAWAT HOSSAIN

Submitted to the Graduate College of
The University of Texas Rio Grande Valley
In partial fulfillment of the requirements for the degree of

MASTER OF SCIENCE IN ENGINEERING

August 2020

Major Subject: Electrical Engineering

SIGNAL PROCESSING COMBINED WITH MACHINE LEARNING FOR BIOMEDICAL APPLICATIONS

A Thesis
by
MD SHAKHAWAT HOSSAIN

COMMITTEE MEMBERS

Dr. Yong Zhou
Chair of Committee

Dr. SAMIR IQBAL
Co. Chair of Committee

Dr. NAZMUL ISLAM
Committee Member

Dr. Jia Chen
Committee Member

August 2020

ABSTRACT

Hossain, Md Shakhawat, Signal Processing Combined with Machine Learning for Biomedical Applications, Master of Science in Engineering (MSE), August 2020, 120 pp., 44 figures, 4 tables, and 153 references.

The Master's thesis is comprised of four projects in the realm of machine learning and signal processing. The abstract of the thesis is divided into four parts and presented as follows,

Abstract 1: A Kullback-Leibler Divergence-Based Predictor for Inter-Subject Associative BCI.

Inherent inter-subject variability in sensorimotor brain dynamics hinders the transferability of brain-computer interface (BCI) model parameters across subjects. An individual training session is essential for effective BCI control to compensate for variability. We report a Kullback-Leibler Divergence (KLD)-based predictor for inter-subject associative BCI. An online dataset comprising left/right hand, both feet, and tongue motor imagery tasks was used to show correlation between the proposed inter-subject predictor and BCI performance. Linear regression between the KLD predictor and BCI performance showed a strong inverse correlation ($r = -0.62$). The KLD predictor can act as an indicator for generalized inter-subject associative BCI designs.

Abstract 2: Multiclass Sensorimotor BCI Based on Simultaneous EEG and fNIRS.

Hybrid BCI (hBCI) utilizes multiple data modalities to acquire brain signals during motor execution (ME) tasks. Studies have shown significant enhancements in the classification of binary class ME-hBCIs; however, four-class ME-hBCI classification is yet to be done using multiclass algorithms. We present a quad-class classification of ME-hBCI tasks from

simultaneous EEG-fNIRS recordings. Appropriate features were extracted from EEG-fNIRS signals and combined for hybrid features and classified with support vector machine. Results showed a significant increase in hybrid accuracy over single modalities and show hybrid method's performance enhancement capability.

Abstract 3: Deep Learning for Improved Inter-Subject EEG-fNIRS Hybrid BCI Performance. Multimodality based hybrid BCI has become famous for performance improvement; however, the inherent inter-subject and inter-session variation between participants brain dynamics poses obstacles in achieving high performance. This work presents an inter-subject hBCI to classify right/left-hand MI tasks from simultaneous EEG-fNIRS recordings of 29 healthy subjects. State-of-art features were extracted from EEG-fNIRS signals and combined for hybrid features, and finally, classified using deep Long short-term memory classifier. Results showed an increase in the inter-subject performance for the hybrid system while making the system more robust to brain dynamics change and hints to the feasibility of EEG-fNIRS based inter-subject hBCI.

Abstract 4: Microwave Based Glucose Concentration Classification by Machine Learning. Non-invasive blood sugar measurement attracts increased attention in recent years, given the increase in diabetes-related complications and inconvenience in the traditional ways using blood. This work utilized machine learning (ML) algorithms to classify glucose concentration (GC) from the measured broadband microwave scattering signals (S11). An N-type microwave adapter pair was utilized to measure the sweeping frequency scattering-parameter (S-parameter) of the glucose solutions with GC varying from 50-10,000 dg/dL. Dielectric parameters were retrieved from the measured wideband complex S-parameters based on the modified Debye dielectric dispersion model. Results indicate that the best algorithm can achieve a perfect classification accuracy and suggests an alternate way to develop a GC detection method using ML algorithms.

DEDICATION

The completion of my master's studies would not have been possible without the love and support of my family. I would like to dedicate my thesis to my father, Mr. Abu Bakar Siddique, my mother, Mrs. Suraya Siddique, and my younger brother Md. Zihad Talukder and my elder sister Mrs. Rabeya Sultana, who wholeheartedly inspired, motivated and supported me to accomplish this degree. Thank you for your continuous support, love and patience.

ACKNOWLEDGEMENTS

I will always be grateful to both of my thesis supervisors and co-chairs of my dissertation committee, Dr. Yong Zhou and Dr. Samir M. Iqbal, for all the guidance that they provided me with my research. I cannot ask for better mentors and advisors during my master's degree. They always helped me with my research and article writings. They encouraged me to complete this process through their infinite patience and guidance. My many thanks to my committee member: Dr. Nazmul Islam, who gave me his valuable guidance during summer 2019 when I needed his guidance the most. He gave me valuable advice throughout my entire degree and helped me every time I was in need. I would also like to thank my committee member: Dr. Jia Chen, who suggested some critical changes in the methods to solve the research problem that I was facing. All their advice, input, and comments on my dissertation helped to ensure the quality of my intellectual work.

I would also like to thank my Graduate College at UTRGV to make me financially stable by providing Presidential Graduate Research Assistantship and Summer Graduate Assistantship. I would also like to thank all my friends at NanoBio Lab in UTRGV.

I would also like to acknowledge the contributions made by the coauthors of my published and unpublished works. Coauthors of the unpublished and submitted manuscripts that have been used for the writing of this thesis are Dr. Khawza I. Ahmed, Dr. Raqibul Mostafa,

Mr. Simanto Saha, and Dr. Mathias Baumert. The contributions from the coauthors are mainly editorial.

The writings of the thesis are adopted in-part or in-full form from the articles published, and manuscripts submitted for publication containing parts or full results of the research works done in the thesis. Multiple manuscripts are in preparation based on the results obtained from the research and discussion presented in the thesis. The manuscript articles are listed below,

1. M.S. Hossain, Samir M. Iqbal, Yong Zhou, “Microwave Based Glucose Concentration Classification by Machine Learning,” 2020 IEEE Texas Symposium on Wireless & Microwave Circuits & Systems, 2020.
2. M.S. Hossain, S. Saha, K. Ahmed, R. Mostafa, M Baumert, Samir M. Iqbal “A Kullback-Leibler Divergence-Based Predictor for Inter-Subject Associative Brain-Computer Interface”– submitted in Biomedical Signal Processing and Control.
3. M.S. Hossain, K. Ahmed, R. Mostafa, Samir M. Iqbal "Quad-class Motor Movements Brain-Computer Interface Classification from Simultaneous EEG and fNIRS Recordings using ECOC Classifier" – in the final stage of preparation.
4. M.S. Hossain, Samir M. Iqbal, Yong Zhou, “Application of Deep Neural Network to Design Inter-subject Hybrid Brain-Computer Interface from Simultaneous EEG and fNIRS Recordings,” in preparation.

TABLE OF CONTENTS

Page

LIST OF TABLES

Page

LIST OF FIGURES

Page

CHAPTER I

A KULLBACK-LEIBLER DIVERGENCE-BASED PREDICTOR FOR INTER-SUBJECT ASSOCIATIVE BRAIN-COMPUTER INTERFACE (BCI)

1.1 Organization of The Thesis

The objective of this thesis is to implement state-of-the-art signal processing algorithms and combine that with standard machine learning algorithms to improve the understanding of the brain-computer interface and non-invasive glucose detection. The thesis is divided into four chapters, each chapter dedicated to one of the four projects.

Chapter 1 reports experimental works done for the quantification of cross-subject associativity of sensorimotor brain dynamics in the inter-subject brain-computer interface (BCI). Variation of brain dynamics across subjects and sessions affects the control performance of BCI across participants. Research studies showed that subjects share associativity in sensorimotor rhythm (SMR) dynamics for inter-subject BCI. In this work, we have proposed a predictor of the associativity using an information-theoretic approach and shown that the proposed predictor can predict the performance of inter-subject BCI based on their shared SMR dynamics.

Chapter 2 reports research works in multimodal BCI using simultaneous EEG-fNIRS recordings for multiple motor execution tasks classification. Binary class EEG-fNIRS based hybrid BCIs are promising for motor rehabilitation; however, multi-class BCIs are necessary to extend the technology for more degrees of freedom. In this work, we have proposed a classification algorithm for four-class motor execution BCIs and shown that multimodal combination improves the classification over single modality. Chapter 3 is dedicated to an experimental work designed for the implementation of inter-subject BCI using multimodal simultaneously recorded EEG-fNIRS recordings. EEG-fNIRS based BCIs have been shown in studies to improve BCI control performance; however, inter-subject variability of SMR dynamics can reduce the performance enhancement in EEG-fNIRS BCI. In this work, we have proposed an application of a deep learning algorithm for the inter-subject BCI design using simultaneous EEG-fNIRS recordings.

Chapter 4 reports non-invasive detection of blood glucose concentration using microwave scattering parameters and machine learning algorithms. Non-invasive glucose measurement is essential due to the hazard posed by the uncomfortable conventional method of glucose detection using blood droplets. We have measured microwave scattering parameters for in-vitro glucose solution with binary concentration and utilized machine learning algorithms to classify the glucose concentrations with high accuracy.

Finally, Chapter 5 concludes the thesis by explaining the major achievements of the thesis.

1.2 Introduction

Brain-Computer Interfaces (BCIs) are ways of communication exclusively between the brain and the computer. BCIs enable users to control computer software or a hardware device by brain

activity [1]. In BCI technology, brain signal is acquired, processed, and converted into some commands to controls external devices [2]. Besides its original goal of assisting motor impaired persons in enabling or enhancing their motor functions [3,4], after the recent advancement in BCI [5], it is becoming promising for healthy individuals too. BCI can be used to play games [1], lie detection [1], mood assessment [6], and other healthy activities [7]. In BCI, the brain activity of the brain can be acquired using different recording techniques, i.e., Electroencephalography (EEG), Magnetoencephalography (MEG), functional near-infrared spectroscopy (fNIRS), functional magnetic resonance imaging (fMRI). All the techniques mentioned above have their advantages. EEG captures the electrical activity of the brain, and it has the advantage of higher temporal resolution over other methods, while fMRI has a higher spatial resolution. This higher temporal resolution, along with low cost and easy maintenance, has made EEG the most widely used signal acquisition method for BCIs [8]. BCIs can be of different types based on the stimulus given as well as based on the task performed in the BCI. The stimulus can be given in the form of voice command, image stimulus, video stimulus. Different types of tasks can be performed in a BCI like physical tasks, mental tasks. Based on the tasks, BCI can be of several types like motor imagery (MI) BCI, motor execution (ME) BCI, mental arithmetic (MA) BCI. MI is the imagination of performing a motor task rather than performing it. MI-BCI provides its user to use an exclusive channel to convey a user's intention to a computer [9]. ME is the execution of motor tasks like moving motor organs, i.e., hand, leg. MA refers to performing some tasks in the brain that is not related to motor activity. The task can be counting, doing some mathematics, etc.

In our project, we focused on MI-based BCIs. The main reason is the vast availability of online open-source dataset. This experiment is focused on motor imagery (MI) based BCI (MI-BCI). Beginning in the 1990s until now, many kinds of MI-BCI have been developed [10].

Although MI-BCIs have been designed to improve living standards of peoples with severe motor dysfunction or impairment (e.g., those with spinal cord injuries and by born motor disfunction) by augmenting their motor function or communication possibilities [2,11,12]. Besides these applications, BCI has several other up-and-coming fields in rehabilitation, e.g., for stroke rehabilitation [4,11,12,14], and multimedia and virtual reality [5,13,15] for which motor imagery based BCI brings innovative perspectives.

1.3 Challenges in MI-BCI (Literature Reviews)

Even though MI-BCIs offer some promising technologies, those technologies are not available on the public market due to the BCI control inability also generalized as "BCI illiteracy" of a significant section of users [16]. Even for the individuals who do fall in the "BCI illiterate" group, the average MI-BCI performance measured as classification accuracy is around 75% [17]. Nevertheless, with proper training, a group of users can attain higher performance accuracy in the range of (80-100) % for binary class MI tasks [18]. However, there are other factors besides "BCI illiteracy" that affect the BCI control performance. Inter-subject and inter-session variability of brain dynamics can cause variation in BCI control performance. It is now well known that the EEG data varies from subject to subject and session to session, and this causes BCI protocols to lack adaptability. However, the non-adaptable characteristics of training protocols have yet to answer the inter-subject BCI performance variability. There are several previous works reported to address this across subject performance variability.

A recent study consisting of offline and online analyses with neurofeedback to users to enhance mental states focusing on the application for Major Depressive Disorder (MDD) explains the inter-subject and intersession variability of different brain states [19]. For the first instance, Reuderink et al. [20] proposed a second-order baselining algorithm for smoothing

across subjects and the across-session difference in MI classification. In [21], the authors suggested a plausibility of designing a subject independent MI-BCI. This paper focuses on decoding five different mental imagery tasks instead of MIs. In [22], the authors proposed an online across-subject BCI using P300 speller for the first time. Besides explaining the difference and similarity in P300 patterns, this study also showed a comparison of inter-subject performance variation between pooled-subject and cross-subject paradigms. The results showed that the classification accuracies notably decrease in cross-subject experiments compared to pooled-subject. In [23], Saha et al. showed how the performance of MI-BCI varies in inter-subject and inter-session experiments for multiclass MI tasks. The paper uses a relatively new experimental method; a) it trains the BCI using data of one subject and tests it on other subject b) trains the classifier using data of one session while tests it on another session and vice versa. They have found some associativity in the BCI performance across the subject and termed it as Pairwise Performance Associativity. These types of variation in MI-BCI control performance over subjects and sessions have generated an interest in finding suitable parameters to predict users' MI-BCI control performance.

Additionally, learning the control of BCI, also known as training, can be both time and resource consuming. The training time can be reduced by finding some suitable predictors of BCI control performance. Moreover, predictors can provide further information regarding the adaptability of a generic BCI for a particular group of subjects. So far, two types of predictors have been explored: neurophysiological and psychological. A brief description of the predictors can be found in the following paragraphs.

Neurophysiological Predictors: In a recent work [24], A predictor was adopted from the preceding resting period sensorimotor rhythms (SMRs) amplitude to predict the performance of

following MI-BCI activity. A μ rhythm from the sensorimotor areas was proposed as a neurophysiological predictor. The predictor is dubbed "Blankertz's SMR predictor" by the authors. Laplacian EEG channels were used to record the brain activity of relaxing with eyes open for two minutes and used for predictor calculation. A strong correlation ($r = 0.53$) between the BCI performance and the predictor was reported for a database containing eighty subjects. The modulation of SMRs induced by left-hand or right-hand MI activity demonstrated to have a positive correlation with frontal and occipital γ-oscillations power while having a negative correlation with central-parietal γ-oscillations power [25]. Again, in [26] Grosse- Wentrup and Schölkopf provided evidence that γ-oscillations power from frontoparietal networks can be a predictor of performance variation on different trials. In [27], Suk et al. proposed the use of a novel Bayesian Spatio-Spectral Filter Optimization (BSSFO) method to investigate similarity and difference of different spatiospectral parameters across the subject. Subject groups with similar physiological characteristics were formed by clustering individual BSSFO patterns. Three groups were formed containing μ-bands, β-bands, and BCI-illiterate. These three groups of subjects show distinct spatial topographies, and subjects' BCI performance was highly correlated with the grouping. A two minutes recording of preceding resting-state EEG using three channels was shown as a predictor of the BCI performance. They have shown a strong correlation of ($r = 0.581$) between the prediction and classification accuracy. In [28], the authors suggest that resting-state functional connectivity networks can be analyzed to predict SSVEP responses and performance. They have analyzed three different network topologies. A strong negative correlation between SSVEPs of the frequencies with average functional connectivity, clustering coefficient was reported, and also a negative correlation was shown with the characteristic path length. The authors also argued that the classification accuracy could be predicted by three

averaged network measures, while their combination can further improve the prediction performance. In [29], for amyotrophic lateral sclerosis (ALS) patients, three different EEG features were reported as a good predictor of P300-based brain-computer interface (BCI) performance. In [30], Fazli et al. used NIRS activity before a task to predict performance fluctuation in EEG-based BCI. Spectral band power was used to find dissimilarity between the BCI-literate group with BCI-illiterate groups [31]. The authors have compared non-task related state (NTS) for the eyes-open state, with the resting by a ready state the state just before MI and during MI. The results show a high level of θ-power and a low level of α-power in the case of the BCI-illiterate group compared to the BCI-literate group. In [32], the authors showed that prefrontal area γ-activity and MI performance has a strong positive correlation. Psychological predictors of MI-BCI performance was obtained by calculating the laterality index (LI), and cortical activation strength (CAS) from EEG signals during paretic hand MI tasks and showed a significant correlation between L1 values and binary BCI performance and CAS values shows the strong positive correlation for brain-switch BCI tasks performance[33].

Lastly, the authors of [34] proposed a novel predictor that can reflect the attentional level. Their proposed predictor was determined from the spectral power calculated from EEG data before task cue for specific rhythms across brain regions. The predictor showed a significant positive correlation of $r = 0.53$ with the MI accuracies. The authors observed that BCI classification accuracies could be improved if a higher frontal θ power and lower posterior α power can be achieved before MI task onset, and this also reflects a higher attention level. Interestingly, the results reported in [34] show signs of contradiction with the findings of [31]. However, the authors of these two papers focused on different areas of the brain. The frontal theta and lower posterior alpha were the focus of [34], while sensorimotor areas were considered

in [31]. Moreover, the authors of [35] used criticism for the statistical analyses employed by Ahn et al. [31]. The inconsistency observed in the analyses might explain the discrepancy too. Although finding neurophysiological predictors looks appealing, studies showed the BCI-control performance could be attributed to the user's psychological profile.

Psychological Predictors: Several psychological parameters were proposed in articles as predictors for BCI performance. Daum et al. [36] showed that the capability of regulating the slow cortical potentials (SCP) could be correlated to memory span and attention for epileptic patients. A relation between the BCI performance and mood of the patients, along with other neutral predictors (e.g., quality of caregiving, sleep, headache, and the room temperature), was found for some patients by N. Neuman in [37]. Nijober et al. showed a correlation between SMR-BCI performance and the mood and motivation [38]. The authors correlated higher SMR regulation capabilities with a higher score of mood and mastery confidence, also showed that lower SMR regulation is related to higher rates of fear of incompetence. Burde et al. found that the accuracy of BCI control is positively correlated with the locus of the score of technology control [39]. Hammer et al. [40] argued that their investigated psychological parameters (such as personality, motivation, and attention span) play a significant part in single-season control performance in an SMR-BCI. A personalized neurofeedback protocol was proposed as a solution for the BCI-inefficacy issue [41]. In [42], Ahn et al. showed that the user could predict their BCI performance if they were trained to do so. The paper showed a positive correlation ($r = 0.64$) between the subject self-prediction score and their BCI performance.

Participants' personality, cognitive profile, and neurophysiological markers were correlated with BCI control performances in [43]. While the MI-BCI performances were not correlated with neurophysiological markers, it was strongly correlated with mental-rotation scores.

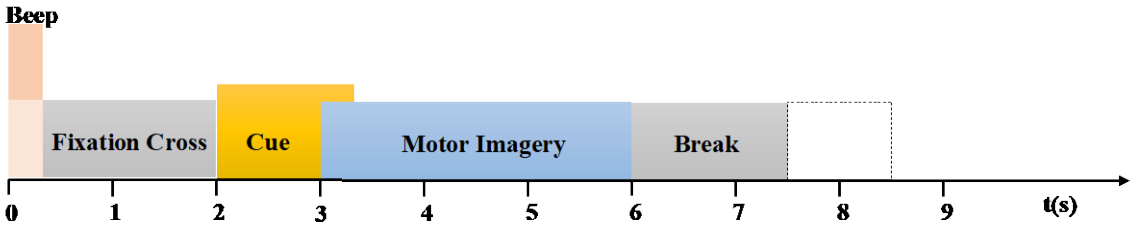

Figure 1.1: The timing scheme of single trial motor imagery-based brain-computer interface. [61]

Performance of different types of predictors on MI-BCI performance is reviewed in [44]. The authors have found that the brain network is less developed in low-performance groups in MI-BCI. A lacking in research works was suggested, although there are significant studies in intra-subject and clinical patients. Integrative studies between different types of variables were suggested for a better understanding of the variation, and a strategic approach was proposed for solving the variation and improve the performance and reliability. However, in [45], Botrel et al. suggested that while there are several existing proposed predictors of BCI performance, their reliability and validity must be specified in the BCI realm.

In Summary, previous studies on BCI-performance predictors focused on Band Power values for SMR-BCIs and, or Slow Cortical Potentials (SCP), to quantify the BCI control performance. Most of the previous works used information from a single session or single trials. Most of the neurophysiological predictors were calculated using a different method than the actual BCI settings. Hence, it is essential to use a standard BCI system to quantify the BCI control performance of MI-BCI. In recent times, there is an increase in the research works performed on inter-subject paradigms. Designing an inter-subject BCI can necessarily reduce the time required for the training session. However, since in inter-subject BCI is trained on one subject and tested on another subject to achieve higher inter-subject BCI classification accuracy, it is crucial to

have a relation between the brain dynamics of participating subjects. It can be very troublesome to find such a relation between human brain dynamics without having information regarding the subjects' anatomical, neurological, and psychological similarities.

1.4 Motivation

Inherent intra-subject (inter-session) and inter-subject variability in sensorimotor rhythm (SMR) dynamics displayed in the electroencephalogram (EEG) hinders the reproducibility of brain-computer interface (BCI) performance [46] and necessitates individual training sessions that are tedious and sometimes frustrating for users. Motor imagery (MI), i.e., the covert anticipation of a motor task, is suitable for rehabilitating patients that have some degree of motor disability. It can also be used to augment motor performance for healthy individuals [47], [48]. However, the nonstationary nature of EEG signals impedes the generalization of MI-BCI [46], [23], [49], [50].

Covariate shift is an illustration of altered test data distribution relative to the training data, while conditional distribution remains unchanged [51]. Transfer learning-based data-driven strategies have been well-studied for the use of BCI models across sessions/subjects [52]. However, not all subjects share collective SMR dynamics due to the differences in individual cognitive and neurophysiological traits [46], [53], [54]. Moreover, 15-30% of users are incapable of producing a robust signal to drive a BCI because of BCI illiteracy [55].

Recent work has concentrated mostly on the assessment of inter-subject associativity as an exclusive predictor for subject independent BCI performance [46], [23], [49], [50]. Saha et al. demonstrated BCI performance variation in the context of intra- and inter-subject BCI based on

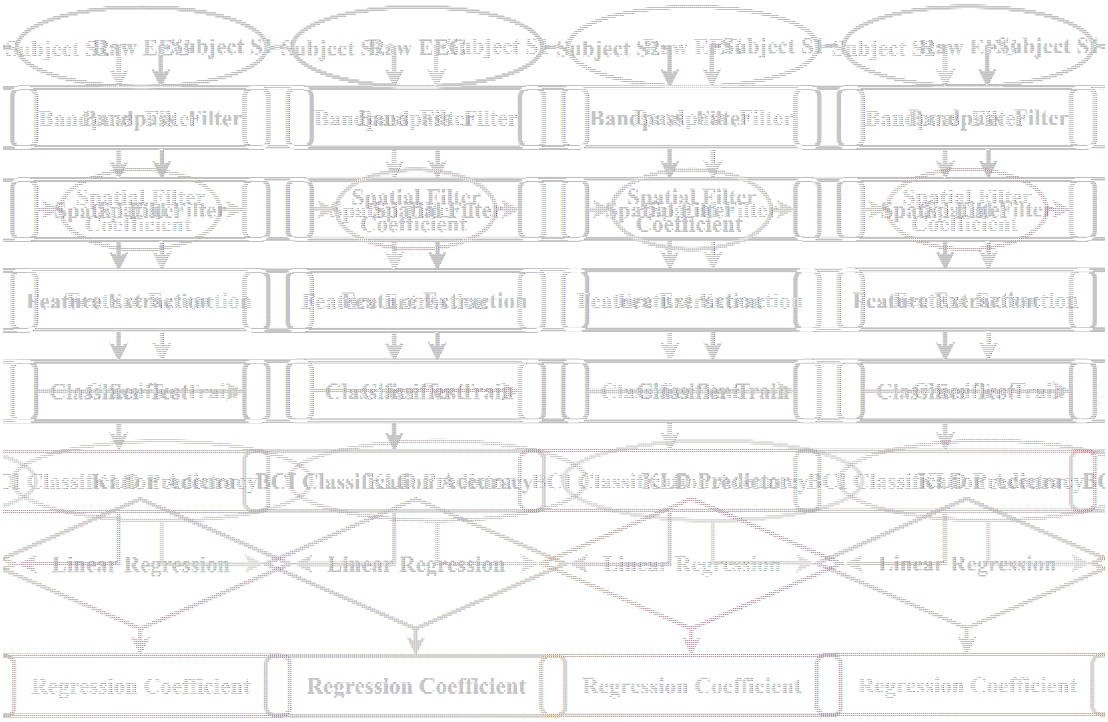

Figure 1.2: Simple Block Diagram of BCI Classification Accuracy Calculation.

multiclass MI [23]. Other studies have shown source- or sensor-space analyses derived features for developing inter-subject associative BCI [49], [50], [56]-[58].

Common spatial pattern (CSP) has been a widely used filtering technique for subject-specific MI classification [59]. Kang et al. extended the use of CSP for subject-to-subject information transfer, where Kullback-Leibler Divergence (KLD) was applied to identify subjects with similar characteristics [58]. Arvaneh et al. integrated KLD into a transfer learning strategy for MI-BCI [60]. Most of the studies on transfer learning have considered just reducing the number of

training trials from the target subject. In this work, however, we evaluated a fully subject-independent MI-BCI, where no training trials from the target subject were considered. Besides, a KLD-based predictor of inter-subject associativity was shown that provides new insights on inter-subject BCI performance [46,23].

1.5 Methodology

1.5.1 Dataset IIa, BCI Competition IV

The publicly available dataset IIa from BCI Competition IV was used for this work [61]. As per [61], The dataset consisted of EEG signals recorded using 22 Ag/Ag-Cl electrodes from 9 healthy subjects. The electrodes were placed with an inter-electrode distance of 3.5 cm. All signals were recorded monopolar. The left mastoid was used as a reference, and the right mastoid was used as the ground. The data were recorded using an amplifier with 100 μV sensitivity, sampled at 250 Hz, while bandpass filtered between 0.5 Hz to 100 Hz along with a notch filter at 50 Hz to eliminate powerline interference. The data were recorded for four MI classes, i.e., left-hand (LH), right-hand (RH), both feet (F), and tongue (T). The EEG signals were recorded in two different sessions for each subject. Each session contained six runs and each run comprised of 48 trials (12 trials for each class), yielding a sum of 288 trials per session. The subjects sat in a cozy armchair in front of a computer screen. Figure 1.1 illustrates the timing diagram of the experiments [61]. At the beginning of each trial (t = 0 s), a brief audible sound was played along with a fixation cross appearing on the computer screen. At t = 2 s, an arrow directing either toward left, right, down or up (representing one of the four classes, LH, RH, F, or T, respectively) was presented and remained on the screen for 1.25 s. The cue prompted the subject

to carry out any of the four MI tasks. The subjects were requested to perform the task until the fixation cross disappeared from the screen A short break was given before starting the next trial.

1.5.2 Experimental Design

The experiments were divided into two parts. First, the BCI performance in subject-independent context was evaluated. Then, the inter-subject KLD predictor associated with MI tasks was

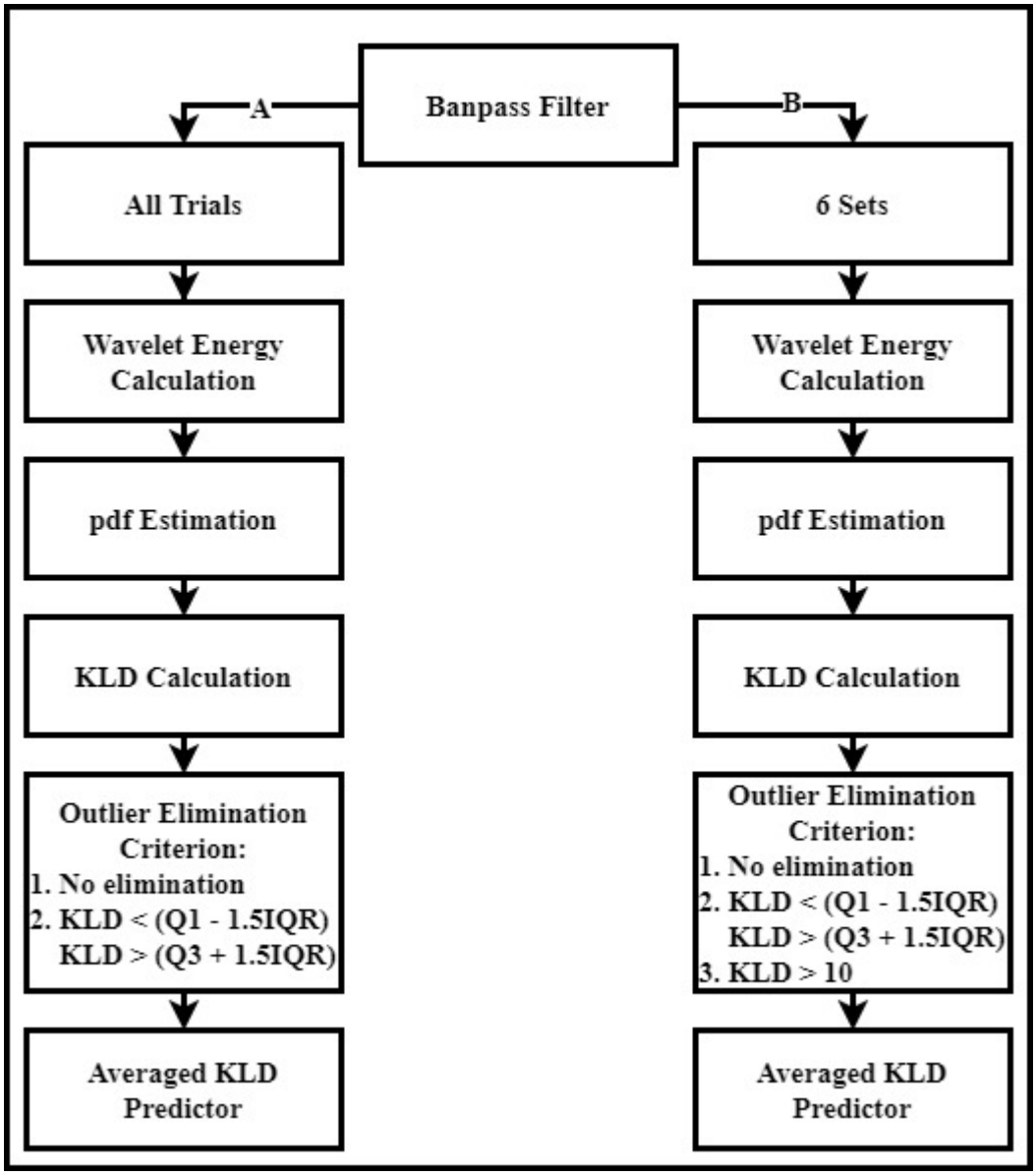

Figure 1.3: A simple block diagram of the algorithm of KLD Predictor Calculation.

calculated. The relationship between BCI performance and KLD predictor was finally established.

Figure 1.2 shows the block diagram of the presented inter-subject BCI approach. We investigated the performance of a fully subject-independent two-class BCI paradigm. Six binary class pairs were considered, i.e., LH-RH, LH-F, LH-T, RH-F, RH-T, and F-T. An inter-subject BCI experiment was conducted where EEG signals from two subjects were used to train and evaluate a classifier [23]. The dataset consisted of EEG from two different days for each subject. Two sessions were considered as two different sets of data. Considering a cross-subject experiment, i.e., EEG signals from one subject for training and EEG signals from another subject to evaluate, a total of $2 \times {}_9P_2 = 144$ inter-subject combinations were possible for all nine subjects. We evaluated BCI performance for only 45 combinations, as presented before in [23]. The previous study [23] showed that BCI performance varied over season and across-subjects. However, it did not provide any quantification for the performance variation. This work is focused on designing a predictor of inter-subject BCI performance across subjects and seasons for binary class BCI. In order to reduce computational complexity, we chose 45 subject-pair combinations, as described in [23]. From the available 288 trials of two sessions, only 144 trials were extracted for each binary class combination. Thus, the BCI model was trained using 144 trials from one subject, while 144 trials from another subject were used to evaluate the performance.

The signals were filtered using a Butterworth bandpass filter of order 4 with corner frequencies of 8 Hz and 40 Hz. The EEG signals collected from subject S1 were used to train both CSP with regularization (RCSP) and classifier models. The BCI performance was evaluated

for EEG signals collected from another subject, S2. Notably, four spatially filtered components were considered for two classes, i.e., two components for each class. The energy was calculated for each sub-band after decomposing each component using db9 (Daubechies family) up to level 3 wavelet basis, resulting in 16 attributes. Similarly, Shannon entropy was calculated using db3 wavelet basis, resulting in further 16 features. Several mother wavelets were tested before selecting the above-mentioned mother wavelets. We tested db1-db11 for both cases and selected the mother wavelet that gave us the highest accuracy. It has been found that energy calculated from db9 decomposed signals better differentiates the classes, and similar attribute has been observed for db3 mother wavelet in case of the calculated entropy. A two-layer feed-forward neural network with 12 hidden layers was trained by data from subject S1 and evaluated on data from another subject S2.

Figure 1.3 illustrates the flow chart of KLD-based predictor calculations. Initially, the EEG signals were processed using a 4th order Butterworth bandpass filter with corner frequencies of 8 and 40 Hz to extract MI-related features [23]. The KLD-based predictor was estimated in two different ways and indicated as Category A and B. In Category A, and all trials were treated as a single set while in Category B all the available trials were divided into six subsets representing six runs in the dataset. Each of the six subsets consisted of 24 trials for two classes. Discrete wavelet decomposition up to level 3 was then applied to EEG signals. Two different mother wavelets were used for Category A (db27) and Category B (db7). We used db1-db31 and selected the mother wavelet that attributed the optimal performance. It was found that db27 and db7 showed the best performance for Category A and B, respectively. Probability density functions (PDF) were estimated for each of the inter-subject EEG channels independently. For Category A, the number of acquired PDF was equal to the number of

channels multiplied by the number of trials. For Category B, the number of acquired PDF was equal to the number of channels multiplied by the number of subsets.

The KLD was calculated from the PDF either by one vs. one or one vs. all paradigms. The KLD was calculated across the channel. Hence, the number of KLD values was equal to the number of EEG channels. The calculated KLD values were then averaged. There were some outliers in the calculated KLD values that were significantly higher than the remaining values, which could potentially lead to misinterpretation of the overall data and, consequently, SMR dynamics. It is to be noted that RCSP was not applied for KLD calculations. For Category A, two approaches were used to investigate the impact of outliers on KLD-based inter-subject BCI predictor, namely:

Approach 1: All the calculated KLD values were averaged without considering the outliers.

Approach 2: Divergence values lower than the first quartile $-$ 1.5 $\times$ interquartile range (IQR) and values higher than the third quartile + 1.5 $\times$IQR were eliminated before averaging.

For Category B, the above two approaches, along with a third approach, were applied. The third approach was:

Approach 3: Values of KLD > 10 were considered outliers since most of the values were in the range of [0 1]. Those values were discarded before averaging.

A linear regression model was developed between inter-subject BCI performance and KLD predictor to observe correlations. To address the effect of spatial brain dynamics on the

inter-subject MI-BCI, three different cases were considered based on the number of channels used in the study from the region of interests [23], [62]. These cases were:

Case I: All the available 22 channels were used.

Case II: Only nine channels from the sensorimotor areas and parietal lobe were used.

Case III: Only nine channels from the sensorimotor areas were used, assuming that sensorimotor areas were mostly activated during MI [46], [23], [49], [50].

1.5.3 Kullback-Liebler Divergence

The KLD is an information-theoretic measure of the distance between two probability distributions [63], [64], [65], [66]. It is a non-symmetric measure of the difference between two probability distributions p(x) and p(y), quantifying the information lost when the distribution p(x) is approximated by the distribution p(y).

Let X and Y be two discrete random variables representing EEG signals from two subjects S1 and S2, where p(x) is the PDF of X, and p(y) is the PDF of Y. KLD between X and Y is defined as:

$$D_{kL}(p(x)\|p(y)) = \sum_{x\in X} p(x)\, ln\frac{p(x)}{p(y)} \qquad (1.1)$$

Thus, if p(y) can be used to approximate the distribution of p(x), then both subjects S1 and S2 have similar MI-EEG dynamics. KLD is zero when p(x) = p(y). The KLD value is either 0 or a non-negative number.

If both p(x) and p(y) are zero, then the KLD is undefined. To avoid such a case, a smoothing method is typically applied, where the KLD would not be calculated when both p(x) and p(y) are zero, but the values of p(y) would be replaced with values very close to zero, i.e., eps (ε), where ε= 2.22×10-16.

In this work, we hypothesized that the KLD between subjects was associated with the performance of inter-subject BCI. If KLD between two subjects was low, they were more likely to share similar SMR characteristics.

1.5.4 Regularized Common Spatial Pattern

Common spatial pattern (CSP) is a filtering technique used to maximize the separability of class-specific features and thereby the classification accuracy. CSP projects multichannel EEG, where MI-related features are contained in fewer channels [59].

RCSP introduces one or more regularization parameters for covariance matrix estimation [67], [68], [69]. It is assumed to be more robust to outliers and small training trials. Let E represent N×P EEG signals, where N is the number of EEG channels, and P is the number of samples per trial. $\bar{S}_c$ is then the covariance matrix of E that is calculated as follows:

$$\bar{S}_c = \frac{1}{M}\sum_{m=1}^{M} S_{(c,m)} \qquad (1.2)$$

Here, $S = \frac{EE^T}{trace[EE^T]}$, C∈{1,2} and it represents either of the two classes of the trial, i.e., Class 1 or Class 2 for binary class, and *m=1,2,…M* is the number of trials with *M* denoting the total number of trials.

Table 1.1. Correlation between BCI performance and KLD predictor.

(Case: 1, 2 or 3 based on the number of used channels; Category: A (no group) or B (6 groups) based on trial grouping; KLD Calculation: G (one vs. one inter-subject channel) or H (one vs. all inter-subject channel; Approach: outlier elimination rules (1, 2 or 3); R: regression coefficient; LH: left hand; RH: right hand; F: Foot; T: tongue.)

Class Pair	Case	Category	KLD Calculation	Approach	R
LH-T	2	B	G	3	-0.55
LH-T	2	B	H	3	-0.59
RH-F	2	A	H	1	-0.42
RH-F	2	A	H	2	-0.43
RH-F	2	B	G	3	-0.42
RH-F	2	B	H	2	-0.40
RH-F	2	B	H	3	-0.41
RH-T	1	A	H	1	-0.46
RH-T	1	A	H	2	-0.46
RH-T	2	A	G	1	-0.43
RH-T	2	A	G	2	-0.42
RH-T	1	B	G	1	-0.42
RH-T	1	B	G	2	-0.45
RH-T	1	B	G	3	-0.55
RH-T	1	B	H	1	-0.43
RH-T	1	B	H	2	-0.45
RH-T	1	B	H	3	-0.52
RH-T	2	B	G	3	-0.62
RH-T	2	B	H	3	-0.62
RH-T	3	B	G	3	-0.44
RH-T	3	B	H	3	-0.44

The CSP projection matrix was derived from the sample-based covariance matrix estimated from the training trials. The relation can be given as follows:

$$E_{CSP} = W^T E \qquad (1.3)$$

where W is the projection matrix. To implement the RCSP, the covariance matrix calculation was biased using γ and β known as regularization parameters for RCSP. γ controlled the shrinkage of the training sample covariance matrix estimate to the pooled estimate, and β controlled the degree of shrinkage towards a multiple of the identity matrix. The following values were used in combination during regularization [23],[49], [50]:

$\beta = (0,0.001,0.01,0.1,0.2,0.3,0.4,0.5,0.6,0.7,0.8,0.9)$

$\gamma = (0,0.01,0.1,0.2,0.3,0.4,0.5,0.6,0.7,0.8,0.9)$

1.6 Results and Discussion

In this study, both KLD-based predictor and BCI classification accuracy were calculated asymmetrically, i.e., independently for S1-S2 and S2-S1. Figure 1.4 shows the BCI performance for the class pair RH-T with the effects of used channels from different areas of interest [46], [23], [49]. The highest accuracy was achieved for subject pair A04E-A01E in Case III (93.75%). Notably, not all subject pairs showed good BCI performance; presumably, not all subjects shared common CSP-extracted features of MI tasks [46], [23], [49].

Table 1.1 lists the correlation coefficients between KLD-based predictor and BCI performance. The strongest correlation ($r = -0.62$) was found for RH-T in Case II using Approach 3. The stronger was the correlation, the better the BCI performance is suggested. Figure 1.5 demonstrates the linear regression between KLD-based predictor and BCI performance using three separate criteria for reducing the effects of outliers during KLD estimation. Approach 3 seems more robust estimation due to the elimination of outliers. Averaging the KLD values may produce unreliable BCI performance predictor, while outliers are inherently present in the

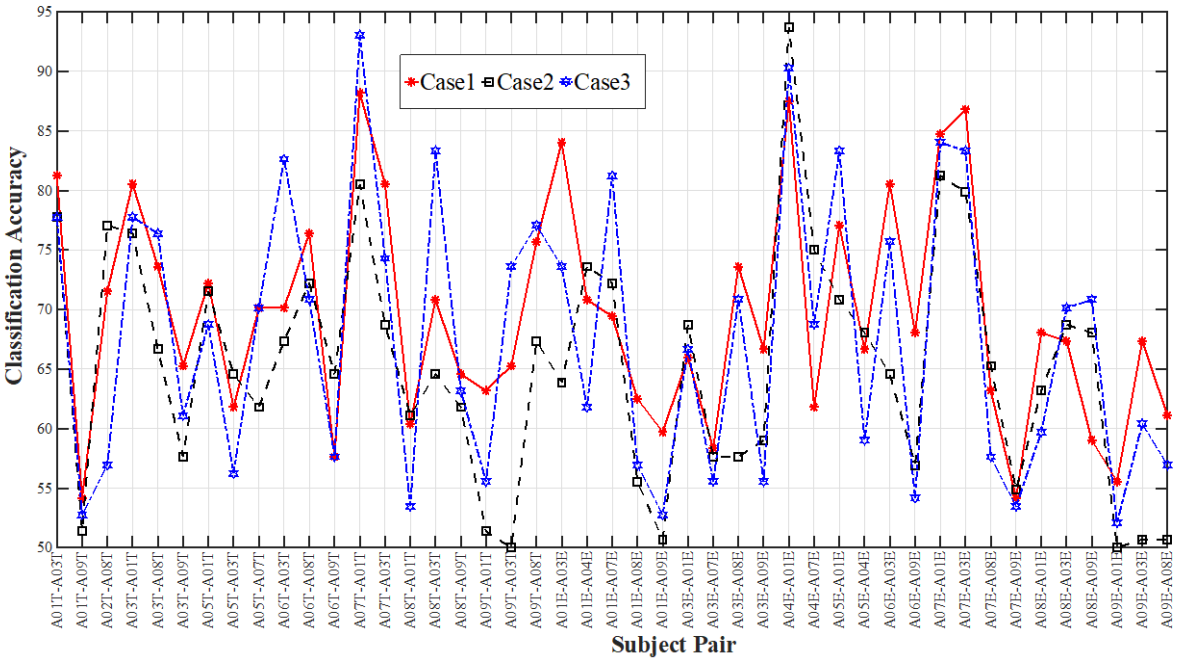

Figure 1.4: Comparison of binary MI-BCI classification accuracies between three cases of class pair RH-T.

The x-axis shows the subject pair while the y-axis is inter-subject BCI classification accuracy. The *T* in the subject pair represents that the signals were recorded on Day-1 while *E* represents that the recordings were for Day-2.

measurement. Figure 1.5 indicates that eliminating KLD values greater than ten improves the presented inter-subject BCI performance predictor.

Diverse cognitive and neurological factors, including brain anatomy and functions and underlying emotional and mental processes, give rise to variability in SMR-EEG dynamics, thus influencing BCI [46]. Previous studies have shown that two subjects may share common sensorimotor rhythms in EEG signals, which can be modeled in an inter-subject associative BCI context [23], [49], [50]. The reported dataset does not contain any secondary information required for the identification of sources of intra- and inter-subject variability. The experimental setup was inspired by the previously shown strategy to quantify inter-subject variability in cases where no secondary information was available [23], [49], [50]. The advantage of such a cross-

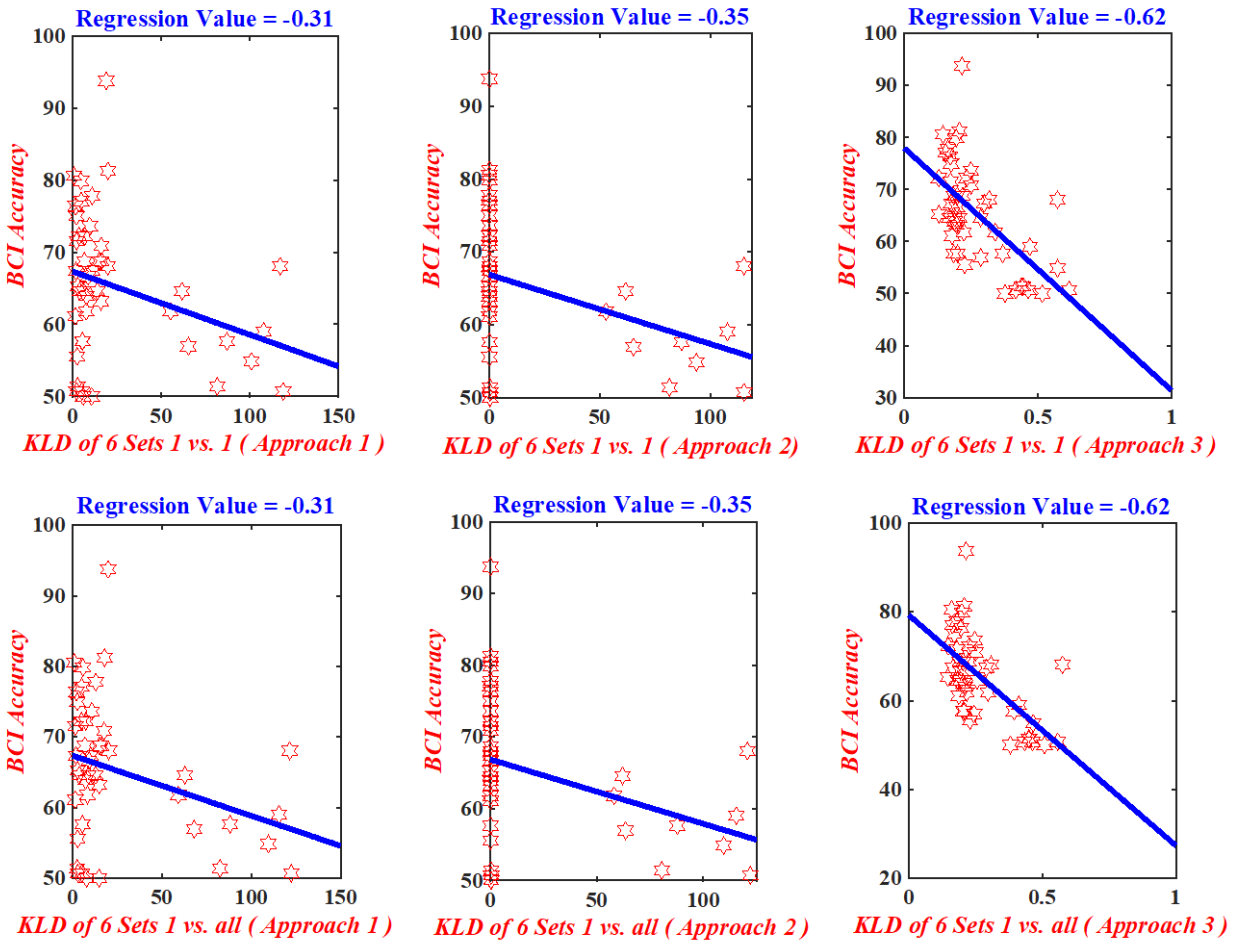

Figure 1.5: Linear regression between KLD-based predictor and BCI performance for right hand versus tongue motor imagery tasks classification.

Usually, KLD values vary from 0 to 1; however, some KLD values are higher than 1 (sometimes very high). Three approaches were used to find out a reliable BCI performance predictor in terms of the outliers. These figures show examples of the elimination of outliers with these approaches.

subject experiment over pooled-subject experiment is the ability to explicitly investigate if any two subjects share similar SMR dynamics. To the best of our knowledge, this is the first work to show a KLD-based predictor for inter-subject BCI.

The amplitude of sensorimotor EEG signals was shown as a predictor for BCI performance, in which a strong correlation (r = 0.53) was found [24]. Resting the EEG-based predictor estimated prior to the actual BCI experiment showed promising results (r = 0.581).

Nijober et al. demonstrated that greater SMR regulation capability was associated with a higher confidence level while lower sensorimotor rhythm regulation was related to fear of incompetence [53], [70], [71]. Most of the previous works concerning BCI performance predictor were based on the subject-specific setups. However, this study has directly established a relationship between KLD-based predictor and BCI performance using a completely subject-independent setup. The results would be beneficial to investigate the impacts of inter-subject variability in BCI design, implicating a significant reduction in the tedious calibration time.

1.7 Summary of Study 1

A list of predictors has been calculated to quantify the BCI performance. The KLD-based predictor has been shown for the first time to improve inter-subject associative BCI performance. Results implicating the presence of similar MI-related features across subjects could lead to further quantification of inter-subject associativity.

CHAPTER II

MULTICLASS SENSORIMOTOR HYBRID BRAIN COMPUTER INTERFACE BASED ON SIMULTANEOUS EEG AND FNIRS

2.1 Introduction

Brain-Computer Interface (BCI) enables alternate pathways of communication between brain and computer, which further enable converting brain thoughts into computers [72]. Hybrid BCI (hBCI) is designed using two or more imaging modalities to take advantage of each independent modalities [73, 74]. There has been a significant increase in the use of hBCI in recent years, especially for the classification of sensorimotor tasks, i.e., motor execution (ME) and motor imagery (MI). An hBCI employing EEG and fNIRS has shown promise because of its capability of monitoring simultaneous electrophysiological and hemodynamic brain activities noninvasively [73, 75]. This remarkable characteristic had given rise to the growing interest in combining the modalities to improve the understanding of brain activity for the design of a better BCI system. The first implementation of the combined modality in BCI can be traced back to 2012 when Fazli et al. implemented a hBCI using NIRS and EEG [76]. The hybrid system improved binary classification accuracy for both ME and MI tasks.

Another study proposed an online hBCI using EEG and NIRS for self-paced MI tasks; however, the method did not significantly improve classification performance compared to the performance achieved by a single modality [77]. These findings encouraged others to design the BCI system combining EEG-fNIRS for hBCI. In [78], the authors used EEG-fNIRS hBCI for the classification of force and speed of hand clenching in MI BCI. The right thumb finger tap was used to design an hBCI, and the study reported a new classification technique using a modified vector phase diagram and used EEG power for early detection of hemodynamic responses [79]. The combined modality improves the control performance over single modalities; however, the hBCI often suffers from the problem of combining to a different type of database having different dimensions. Hence, performance improvement can often be time-limited due to this problem. Selecting more relevant information and reducing the data dimension was studied to solve this problem. Channel selection-based method was shown with a significant increase in EEG-fNIRS BCI classification accuracy [80]. An hBCI was designed using a few-channel EEG-fNIRS by performing source analysis to select three optimal EEG channels [81]. Task-related channel selection has been a well-studied strategy for enhancing EEG-based BCI accuracy [25, 49, 50].

Apart from the earlier studies, there have been other attempts to improve the combined performance further. In [82], the outputs of the EEG classifier were fused with the outputs of the fNIRS classifier to improve the classification accuracy significantly. Recently, deep learning has been used for the classification of EEG-fNIRS hBCI to classify MI tasks [83]. Thanawin et al. applied a convolutional neural network (CNN) for the classification of rest, right-hand, and left-hand ME tasks from fNIRS signals and showed an increase in classification accuracy with CNN when compared to support vector machine (SVM) and artificial neural network (ANN) [84].

Sinem et al. achieved notable classification accuracies for binary classes of sensorimotor tasks, i.e., MI vs. Rest, ME vs. Rest, and ME vs. MI tasks

The previous studies focus on the classification of one type of task vs. another on a binary-class paradigm. While the binary-class hBCI can be used for improved control performance for BCI technologies, multiclass ME-hBCI classification extends the use of such a system with higher degrees of freedom. To date, the multiclass classification of ME-hBCI has not been investigated comprehensively. In this study, we propose a multiclass ME-hBCI

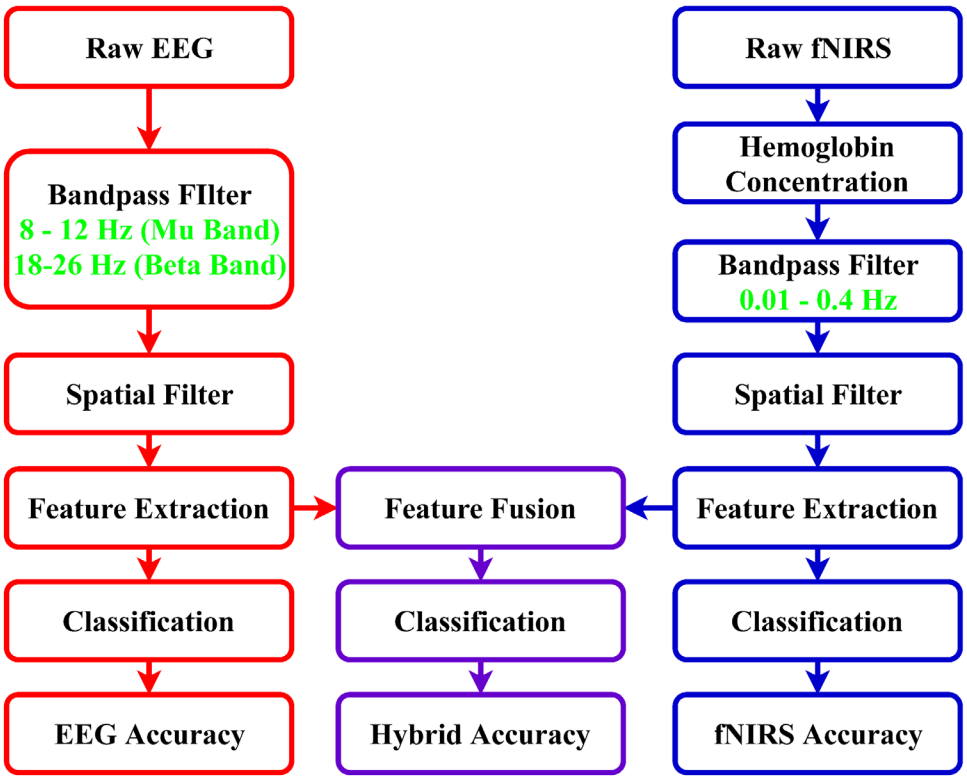

Figure 2.1: Block Diagram of Proposed hBCI.

classification paradigm.

2.2 Methodology

2.2.1 Multimodal Dataset Using EEG-fNIRS

We used a publicly available dataset containing simultaneous recordings of EEG and fNIRS acquired from 15 healthy participants [85]. The EEG system had 21 channels, and the fNIRS system had 12 sources and 12 detectors resulting in 34 channels. The fNIRS probes were mounted on the EEG cap (actiCAP 128) along with EEG electrodes. The fNIRS sources and detectors were placed 3.4 cm apart, and the fNIRS wavelengths were set to 760 nm and 850 nm. The EEG signals were sampled at 250 Hz, while fNIRS recording was sampled at 10.42 Hz. There were five blocks of ME tasks. Each block contained 20 trials divided into 4 ME tasks (Right-Arm—Left-Arm raising, Right-Hand—Left-Hand gripping). A total of 100 trials of ME tasks were recorded with 25 trials per class. Each trial started with a 6 s rest period followed by 6 seconds of recording. The subjects were given visual instructions in the form of textual writing on a laptop screen placed at 1 m from their eyes [86].

2.2.2 Pre-Processing

Figure 2.1 shows a block diagram of the experiments. The EEG signals were filtered with a 4th order Butterworth filter (bandpass) with two sets of cutoff frequencies to capture Mu (8-12 Hz) and Beta (18-26 Hz) rhythms. The fNIRS signal is optical light intensities. We need to convert the light intensities to hemoglobin concentration. We have solved Modified Beer-Lambert law to convert the NIRS signal to hemoglobin concentrations. Oxy-hemoglobin concentration (ΔC_{HbO}), de-oxy-hemoglobin concentration (ΔC_{HbR}) were estimated from the raw light intensities. Modified Beer-Lambert law for fNIRS concentration changes can be given as

$$\begin{bmatrix}\Delta C_{HbO}(t)\\ \Delta C_{HbR}(t)\end{bmatrix} = \begin{bmatrix}\alpha_{HbO}(\lambda_1) & \alpha_{HbR}(\lambda_1)\\ \alpha_{HbO}(\lambda_2) & \alpha_{HbR}(\lambda_2)\end{bmatrix}^{-1} \begin{bmatrix}\Delta A(t,\lambda_1)\\ \Delta A(t,\lambda_2)\end{bmatrix} \frac{1}{l\times d} \qquad (2.1)$$

Where ΔA (t; λj) (j = 1,2) is the absorbance variation of wavelength λj. The factor $\alpha_{HbX(\lambda j)}$ is the extinction coefficient of HbX (HbX = HbO, HbR) in μM−1 mm−1, d is the differential pathlength factor (DPF), and l denotes the distance between an emitter and a detector in cm. The wavelength of the infrared light was 760 nm and 850 nm. We have also calculated the total hemoglobin concentration (ΔC_{HbT}), which was the vector summation of ΔC_{HbO} and ΔC_{HbR}, as:

$$\Delta C_{HbT} = \frac{\Delta C_{HbO} + \Delta C_{HbR}}{\sqrt{2}} \qquad (2.2)$$

The fNIRS concentrations were bandpass filtered with a 4th order Butterworth filter from 0.01 to 0.4 Hz. After filtering, the fNIRS time series were normalized by subtracting the average of each channel from the original amplitude and dividing by the standard deviation of all channels. A common spatial pattern without (CSP) and with (RCSP) regularization was applied to EEG and fNIRS signals, independently [86, 87]. The CSP provided a supervised class-specific decomposition of signals to enhance the separability of two tasks.

2.2.3 Regularized Common Spatial Pattern

Common spatial pattern (CSP) and regularized common spatial pattern (RCSP) was applied to the dataset during the preprocessing [25, 49, 50]. A detailed explanation of CSP and RCSP can be found in Section 1.4.4. Both CSP and RCSP are generally applied to binary class paradigms; however, in our experiments, there were four classes (right hand, right arm, left hand, left arm); hence, the CSP and RCSP were applied in one vs. all paradigm. Two optimum

channels were selected for each ME class resulting in eight channels per trial for Mu and Beta rhythms each. Eight optimal channels were selected for each fNIRS concentration changes.

2.2.4 Feature Extraction and Classification

The features were extracted from the CSP and RCSP filtered signals. The last 4 second signals for each channel were used in the feature extraction for EEG, and for fNIRS, the last 56 samples among total 63 samples were used for feature extraction (Fs_{fNIRS} = 10.42 Hz, total samples $10.42 \times 6 \cong 63$ samples).

Commonly used features such as wavelet energy, band power, sample entropy were extracted from EEG. For wavelet energy, the time series were decomposed up to level 4 with Daubechies 1 (db1 or Haar) wavelet basis. The energy was calculated (1 from the approximated coefficient and three others from the last three detailed coefficients excluding the highest frequency components). In order to calculate band power, the time series were divided into eight 1-second overlapping windows (4 windows for each second starting from 0 s, and four windows for each second starting from 0.5 s). Power was calculated for each window, and finally, the first four windows were averaged to find a single value and last four windows for another power value. The sample entropy was then calculated from a total of 4 sec with 0.1 tolerance. All features were normalized to zero mean and unit variance across trials. Seven features per channel were extracted, thus making 56 features per trial for Mu and Beta each.

For the fNIRS signal, the maximum, signal average, slope indicator (SI), and sample entropy were calculated as features. In order to calculate the SI, the available 56 samples were divided into five 14-samples windows, and 4 SI values were calculated using the formula $SI = Average_{window2} - Average_{window1}$. Sample entropy was estimated with tolerance set to

$0.9 \times standard\ deviation(signal)$. Seven features per channel were calculated for each fNIRS concentration changes, thus making 56 features per trial (8 channels per trial). The features of each fNIRS concentration changes were normalized to 0-1 across trials. In hBCI, the features of EEG and fNIRS were combined. A multiclass support vector machine (SVM) is used to classify the four classes. SVM separates two classes by introducing a hyperplane as a separator of the features for two classes and try to increase the hyperplane separation by learning specific data points called support vectors along the hyperplane boundary. SVM well designs for binary-class classification; however, it can be modified for a multiclass paradigm considering one vs. one or one vs. all scenarios. Often the resultant classifier becomes computationally heavy. In our experiment, we have implemented a multiclass error-correcting output code to implement the multiclass SVM [88].

2.3 Results and Discussion

Table 2.1 the obtained classification accuracies. The highest accuracy of 98% for fNIRS-based BCI was achieved for subject S2 with RCSP, while the accuracy is 96% using hBCI. The highest accuracy for EEG-based BCI, i.e., 87% using both CSP and RCSP, while hBCI results 91%. The highest accuracy achieved by the hBCI was 96% with RCSP. The best overall accuracy improvement in hBCI was recorded for subject S3 with CSP (25% improvement compared to EEG and 23% compared to fNIRS) and S13 with RCSP (19% compared to EEG and 12% compared to fNIRS). The classification accuracy increased for most of the subjects with an exception for subject S2, S5, S9, S11 for CSP and subject S2, and S10 for RCSP where hBCI classification accuracies were lower than those for the fNIRS system.

The average classification accuracies for EEG, fNIRS, and hBCI with CSP were 54.3±13.6%, 70.5±11.8%, and 77.5±6.8%, respectively. The average accuracies for EEG, fNIRS, and hybrid systems with RCSP were 61.0±12.1%, 80.3±10.1%, and 86.2±6.8%, respectively. Increased average accuracy in hBCI compared to any single modality was around 7% and 6% using CSP and RCSP, respectively. Accuracies achieved using the EEG signal were reduced compared to those for the fNIRS system. This reduction could be due to lower signal to noise ratio and the integration of both EEG and fNIRS modalities using a single cap. Some (4-5) subjects had more hair on their heads, as mentioned in the dataset [85]. As a result, the accuracy of fNIRS is lowered for those subjects compared to EEG. Accuracy improvements with hBCI system occurred for the subjects with comparable EEG and fNIRS accuracies and vice versa (exception is subject S1). Notably, higher accuracies were achieved using RCSP as more resilient to outliers [86, 87, 25, 49, 50].

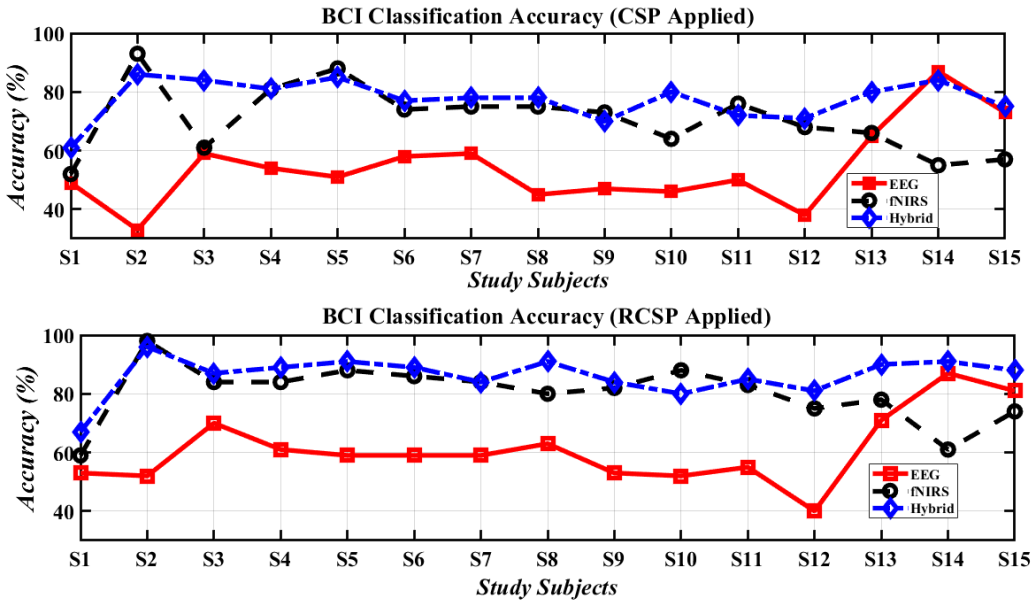

Figure 2.2: Comparison of classification accuracy for EEG, fNIRS, and Hybrid modality based BCI systems.

The figure in the up showed the comparison when CSP was used as the spatial filter, and the lower figure is for RCSP based spatial filtering.

Table 2.1: Classification Accuracies (SD: Standard Deviation).

Spatial Filter	**CSP**			**RCSP**		
Subject	**EEG (%)**	**fNIRS (%)**	**Hybrid (%)**	**EEG (%)**	**fNIRS (%)**	**Hybrid (%)**
S1	49	52	61	53	59	67
S2	33	93	86	52	98	96
S3	59	61	84	70	84	87
S4	54	81	81	61	84	89
S5	51	88	85	59	88	91
S6	58	74	77	59	86	89
S7	59	75	78	59	84	84
S8	45	75	78	63	80	91
S9	47	73	70	53	82	84
S10	46	64	80	52	88	80
S11	50	75	72	55	83	85
S12	38	68	71	40	75	81
S13	65	66	80	71	78	90
S14	87	55	84	87	61	91
S15	73	57	75	81	74	88
Mean $\pm$ SD	54.3 $\pm$ 13.6	70.5 $\pm$ 11.8	77.5 $\pm$ 6.8	61.0 $\pm$ 12.1	80.3 $\pm$10.1	86.2 $\pm$ 6.8

A. Buccino et al. Designed an hBCI using EEG-fNIRS signals and decoded four-movement tasks [84]. They have done the classification using binary class classifiers and have not shown an actual measurement of multiclass classification accuracy for their work. For arm movement vs. hand movement classification, they have shown the highest of 83.6% average binary classification accuracy for the hybrid system with an increase of 3.2% from fNIRS to hybrid system. On the contrary, our proposed methods have provided an average accuracy of 86.2% for 4 class classifications using the hybrid system, which is a 6% improvement from the fNIRS system. There are other notable multiclass works reported in the articles; however, best of our knowledge, there is no four-class motor movement detection work reported yet.

Improvement in classification accuracy can be better understood from Figure 2.2. In the Figure, the classification accuracies for EEG, fNIRS, and Hybrid modality has been compared. Classification accuracy in the hybrid system has either reduced or the improvement is lower when the individual classification accuracy of the standalone systems is far apart and not comparable. On the other hand, when the classification accuracy for standalone systems are close and comparable, the hybrid system shoed the highest accuracy improvement. This improvement is because the same machine learning algorithms with similar structures and hyperparameters were used in the experiment for every modality. Hence, when the features have a better correlation, the resultant hybrid system yields better accuracy that the standalone system.

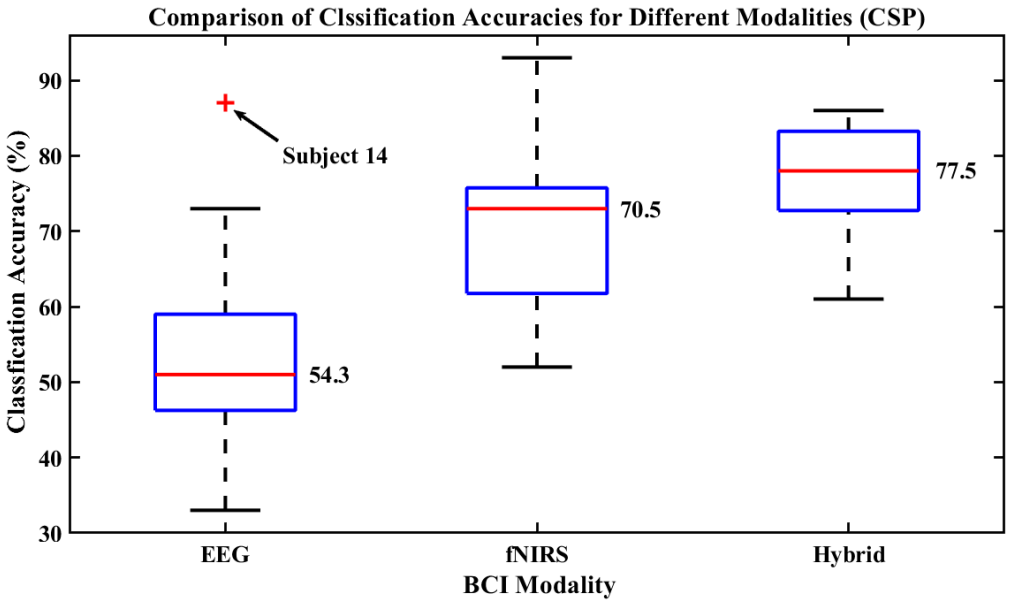

Figure 2.3: Boxplot of classification accuracy for different BCI modalities when CSP is used as spatial filtering.

The numbers accompanying the redline of the box plots show the mean value. The red plus sign represents the subject with accuracy considered as the overshoot for the box plot.

In our experiment, we have combined two feature spaces with different dimensions. To combine the figure spaces, we have calculated the features of EEG and fNIRS in a manner that

yields a feature matrix that has at least one dimension that is the same. Hence, when the two features have a better correlation between them, the resultant feature matrix provides a better generalization of the system and yields better classification accuracy.

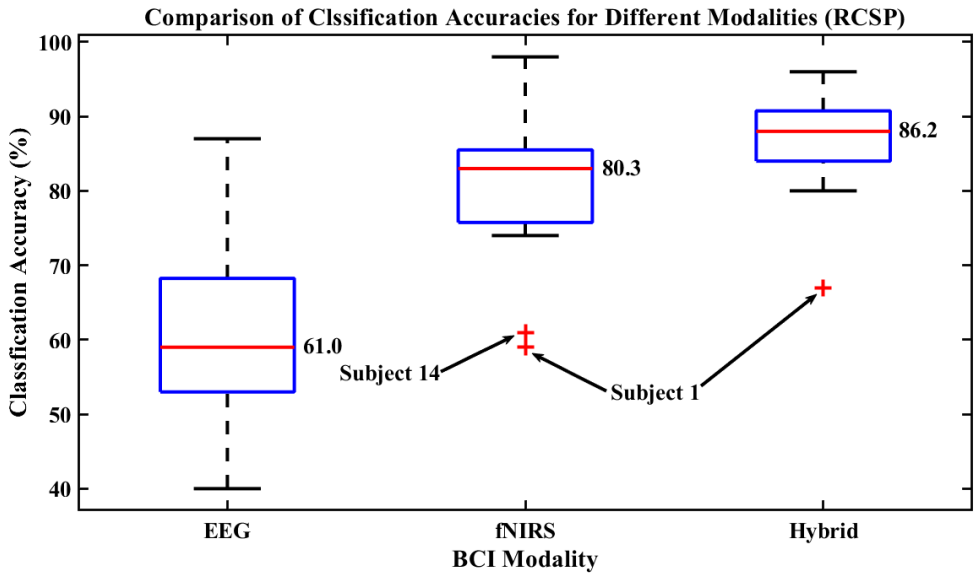

Figure 2.4: Boxplot of classification accuracy for different BCI modalities when RCSP is used as spatial filtering.

The numbers accompanying the redline of the box plots show the mean value. The red plus sign represents the subjects with accuracies considered as the undershoot for the box plot.

Box plot in Figures 2.3 and 2.4 better describes the classification accuracy of different modalities. For EEG and fNIRS based systems, the classification accuracies vary widely for different subjects. On the contrary, the classification accuracy variation over different subjects is very low for the hybrid system. As we can see from the table as well as the figures that the standard deviation for EEG based system is 13% and 12% and for fNIRS 11% and 10% using CSP and RCSP respectively when for the hybrid system the standard deviation is reduced to 6.8%. The reduced standard deviation further shows that the generalization of the combined hybrid system is better than the standalone systems. Better generalization yields better classification/detection accuracy for BCI tasks that is unknown to the classification algorithms.

Earlier works performed the classification of different types of BCI tasks, i.e., ME vs. MI, MI vs. MA, and the works often classify binary-class paradigm. Multi-class classification in ME-hBCI is yet to be done using EEG-fNIRS. In this work, we performed the classification of four-ME classes using simultaneously recorded EEG-fNIRS signals on the multi-class paradigm. The classification accuracy improvement is notable among the literature.

2.4 Summary of Study 2

The multiclass classification of hBCI is essential to enabling users to perform multitasking using the hBCI system. This study successfully presented a classification scheme for multiclass ME tasks in hBCI paradigm with a significant increase in performance as compared to singular modality.

CHAPTER III

APPLICATION OF DEEP LEARNING FOR IMPROVED INTER-SUBJECT EEG-FNIRS HYBRID BCI PERFORMANCE

3.1 Introduction

Brain-Computer Interface (BCI) is a communication pathway between a human brain and a peripheral device, such as a computer, which enables to record brain signals and transfer messages or commands from the brain straight to the device [89], [90]. The brain signals can be attained using several different modalities which includes electroencephalogram (EEG) [92], near-infrared spectroscopy (NIRS), functional magnetic resonance imaging (fMRI) [97], magnetoencephalography (MEG), and many more [92]. Primarily, the main aim of the BCI development was to serve individuals with physical disabilities, but as the decades passed, the technology has evolved such that it is used for applications like lie detection [93] as well as gaming [94]. Among all the approaches mentioned above, EEG has the highest popularity due to its high temporal resolution, proportionately low cost, and non-invasive technique [95], [96]. Apart from EEG, functional near-infrared spectroscopy (fNIRS) is a popular approach with high spatial resolution [97], [98]. fNIRS picks on the changes in the oxygenated (HbO) and deoxygenated (HbR) hemoglobin concentrations and analyzes the physical activity effects on cerebral hemodynamics and oxygenation [98].

EEG has better temporal resolution with relatively lower spatial resolution, and fNIRS has a high spatial resolution. Hence, it is expected that the combination of these two modalities provides both good temporal and spatial resolutions. Thereby, a hybrid BCI is a system wherein either there is a combination of different brain signals or one brain signal with any other type of bio-signal, such as electromyogram (EMG) [91], electrooculogram (EOG) [15]. Normally, hybrid-BCI or hBCI provides better classification accuracy over a single modality-based BCI due to its ability to compensate limitations of one modality with others [99].

The first study pointing out the fNIRS feasibility for BCI was reported by Coyle et al. [106]. There, the subjects were assigned an MI task to squeeze and release a softball to determine brain activity. Naseer et al. used fNIRS to classify BCI development revealing different patterns for the left- and right- wrist MIs [107]. In [100], a further analysis was carried out using the two patterns of EEG, ERD, and SSVEP BCIs along with the near-infrared spectroscopy (NIRS), revealing the use of input from different brain signal techniques for hBCIs. Henceforth, encouraging researchers to implement hBCI using different approaches such as to control a machine using EEG and EOG to control motion [101]. Here, Punsawad discovered that an average of 95% classification accuracy was possible to achieve with the use of 2-channel bio-signals, further proof that hybrid is the key to BCI universality. In 2012, Fazli et al. introduced the idea to enhance the BCI performance using an EEG-NIRS hybrid [108]. Although the result predicted a successful increase of 5% in the performance, the study was based on subject-specific classifiers. In [109], a multimodal brain-imaging dataset was provided for EEG and fNIRS, along with the validation on the hBCI prosper. Furthermore, Buccino et al. conducted an hBCI research classifying four executed movements, and his methods indicated a depreciation of the delay caused by fNIRS [84]. A review of the use of different modalities for the design of

hBCI can be found in [110]. The authors showed the benefits of combing EEG, EMG, EOG, fNIRS signals for designing hBCI. They have also compared the performance of hBCI using different types of stimuli. In [111], Corsi et al. proposed the integration of EEG and MEG signals to improve the classification accuracy of MI-BCI. The experiment recorded multimodal data from fifteen subjects and showed that the combined multimodal signal could improve the classification accuracy significantly. Authors of [112] used multimodal EEG and functional transcranial Doppler ultrasound (fTCD) recording for the implementation of hybrid moto imagery BCI. They have utilized the mutual information between the modalities as the features and SVM were used for classification. Their reported results showed that they had achieved an increase of 4 – 5 % using the multimodal signal for a left-arm, right-arm, baseline task classification. In 2015, an investigation was conducted for affect detection at the time of human-technology interaction (HTI) [102], where Pollmann came up with the idea of neuroscientific methods for the purpose, explicitly using EEG and fNIRS. In the beginning, the resemblance of an fNIRS device to that of an EEG concerning size and portability grabbed the attention and later, the fact that fusing the high temporal resolution data of EEG with the high spatial resolution data of fNIRS might compensate for the limitations of each technique. From the simultaneous measurements of both modalities, the study result showed that each of the two methods does not influence the other as they record different correlates of brain activity. Hence, using both modalities at the same time provides a more extensive data set as well as there is an opportunity to analyze EEG, fNIRS, and their hybrid approach separately.

The classification accuracy of EEG-based BCI may decline significantly due to the presence of outliers' effect from multiple channels [103]. Furthermore, the majority of the BCIs are subject-specific, resulting in tedious calibration sessions. Consequently, the concept of inter-

subject BCI came into account. However, developing it has various challenges, such as the inherent brain dynamics variations from subject to subject caused by the difference in individual brain growth [104]. In [105], Neuper et al. carried out a project involving Graz-BCI using MI and EEG data to control a mechanical device to help assist patients with challenging motor functions. Even this project depended on event-related desynchronization (ERD) and was subject-specific, making it not suitable for a universal model.

For this experiment, we are focusing on inter-subject BCI design using multimodal brain imaging. Inter-subject BCI is referred to as a system that is designed and trained on a subject while it is tested on other subjects. Brain signal variation across different subjects and sessions significantly impairs the accuracy of most brain-computer interface (BCI) systems. The target is to minimize the subject dependent information learning in the classification so that the system can provide good classification accuracy for a subject entirely unknown for the classifier [25,49,50]. In our first experiment, we have reported an inter-subject BCI system using EEG signals recorded for MI tasks. Fazli et al. proposed one of the earliest subject independent BCI using EEG recordings from forty-five subjects [116]. Their proposed experiment reports an ensemble of classifiers designed for the MI classification extracted from subject-specific spatial and temporal filters. The results showed that when using the subject independent BCI, even a BCI-naïve user can achieve acceptable classification accuracy without any calibration or subject-specific training. In [117], the authors designed an fNIRS BCI system to minimize inter-subject variability. They have used a linear programming SVM to learn subject/session-invariant features from the oxy-hemoglobin data. The paper reports a good classification accuracy for mental tasks BCI recorded from seven subjects and eight seasons. In a recently published article, Li et al. reported an inter-subject P300 based BCI designed using simultaneous EEG-fMRI

[118]. The authors have suggested that their designed system can identify the variability in P300 across individuals, which can be used to design biomarkers to predict the potentiality of a personalized BCI.

Halme et al. published an article in 2018 [119] that reports the first implementation of an across-subject BCI using simultaneous MEG and EEG for the classification of MI (left, right-hand imagery) and passive movement tasks. They have trained the inter-subject classifiers on subjects that showed good intra-subject accuracy and tested the classifier for the total datasets. The results showed better performance for MEG over EEG. However, the hybrid system provided the best performance. A subject independent BCI has been reported by Gaur et el. In [120] to classify MI tasks from EEG recordings. The article proposes the use of a novel filtering method designed based on the multivariate empirical mode decomposition using subject independent BCI. The proposed filter helps using cross-channel information and enhances localization. They have shown that their proposed filter can improve the classification accuracy by more than 11% when used before CSP calculation compared to general subject independent BCI without the filter. Fahimi et al. proposed an inter-subject BCI using end-to-end deep CNN for EEG based BCI [121]. A classification algorithm designed for mental attention using CNN classifier from single-channel EEG data in the inter-subject paradigm was reported in the article. The authors achieved 79.26% average classification accuracy for a dataset of one hundred and twenty subjects. Herff et al. proposed a cross-subject BCI using fNIRS recordings and classified speaking tasks [122]. They have achieved 71% and 61% classification accuracy for overt and silent speech classification from fNIRS recordings. The authors have suggested that the proposed system can be an essential step toward designing subject independent BCI. Liu et al. [123] took a slightly different approach for the subject independent BCI design using EEG-fNIRS recordings.

They have used multisubject learning algorithms for classification of the mental workload from EEG, fNIRS, and Physiological measurements. Finally, in [124], Kwon et al. designed a subject independent BCI based on CNN for the classification of left and right-hand MI tasks performed on two different days. The classification was performed on a dataset containing EEG recordings from 54 subjects. They have shown that the subject-independent model outperforms subject dependent models designed using different filtering algorithms.

In recent times, deep neural networks have been extensively used for BCI task classification [131]. Both strains of the neural network can be found in research studies, both the convolutional neural network (CNN) and the recurrent tensor neural network (RTNN). While CNN is considered a better contender for image-based classification, RTNN is considered to perform better in signal-based classification, making it the perfect candidate for EEG-fNIRS based BCI classification. RTNN is often implemented using a long short-term memory algorithm known as the LSTM network. In [125], Wang et al. used a long short term (LSTM) neural network for the classification of motor imagery tasks from EEG data. They have also employed CSP based channel weighting methods to enhance the effectiveness of the classification algorithm. Zhang et al. implemented a combination of both CNN and RTNN algorithms to extract the patterns in a subject independent BCI designed using EEG [126]. CNN was used for detecting the high-level representation of EEG, and RTNN is used for exploring the temporal dynamics of the EEG signals and find the most discriminative temporal patterns. Authors of [127] implemented a hand movement classification from the EEG signal using the LSTM network. They have verified that the implemented classifier can improve the classification accuracy in both subject dependent and subject-independent experiments.

LSTM is also used for fNIRS classification. In [128], Yoo et al. proposed the use of LSTM networks for the classification of mental arithmetic, mental counting, and puzzle-solving task from fNIRS. The fNIRS data were recorded from the prefrontal cortex. The authors have shown that the LSTM based network can improve the classification accuracy significantly compared to LDA and SVM. Huve et al. classified the mental state of drivers from fNIRS based BCI using deep neural network (DNN) and recurrent neural network (RNN) [129]. They have tried to measure the effect of weather conditions, type of road, and the manual driving vs. autopilot condition in the mental state of drivers. Their experiment showed that they had achieved the same performance using both RNN and DNN, and the classifiers over-performed typical machine learning classifiers. Authors in [130] compared the performance of the LSTM network with LDA, SVM, and KNN for fNIRS based BCI system classification. They have also compared the performance of the LSTM network in subject-related and subject-related paradigm and showed that LSTM provided better accuracy for the subject-unrelated paradigm. A hybrid classifier designed with a combination of both DNN and RNN is used for the classification of simultaneous EEG-fNIRS signals by Ghonchi et al. [131]. The proposed experiment showed a 99.6% classification accuracy. A novel DL framework utilizing CNN and LSTM was proposed in [132] for classification of the multiclass mental workload from the fNIRS signal recorded from the prefrontal cortex. The study compared the classification performance of SVM, kNN, ANN, with the DL framework and showed the DL outperformed the other methods by a large margin for a dataset of fifteen subjects. Authors in [133], performed an experiment to record brain activity using simultaneous EEG-fNIRS system for supervised left-hand and right-hand MI BCI tasks. The authors used DNN for the classification of the binary class MI tasks and showed

that there was a synergistic effect present when multimodal recordings were classified using DNN, and that improved the classification.

In summary, the articles mentioned above showed experiments in the realm of BCI in both subject-dependent and subject-independent. The studies used different types of brain imaging techniques, including EEG, EOG, EMG, MEG, fNIRS, fMRI, and fTCD. The focus of the BCI tasks in diverse (i.e., MI, MA, Mental workload, Speech recognition). Different types of machine learning algorithms were studied as classifiers, including ANN, SVM, LDA, kNN, DNN, CNN, RNN, and LSTM for the classification of binary or multiclass BCIs. There are several articles on hybrid BCIs using EEG-fNIRS, some of them are subject-specific while some are subject independent, some are across subject or inter-subject.

Some articles already applied CNN based deep NN as a classification algorithm for EEG-fNIRS based BCIs. However, until now, based on the article reviews done already, I haven't found any article deals with the issue of inter-subject EEG-fNIRS BCI classification using the LSTM neural network. In this research, I have targeted to work on inter-subject BCIs using simultaneously recorded EEG-fNIRS signals. For the classification, I have selected two separate versions of LSTM NN; one is deeper than the other. This research focuses on an inter-subject BCI. That is, the BCI is trained using features from one subject while tested with features from another. Simultaneous EEG and NIRS recordings are available for twenty-nine subjects. In the experiment, one subject (Ex. Subject 1) is used for testing while the training subject has been changed from subject 2 to subject 29. Thus, every time we are testing the BCI on the same subject while training it using different subjects. This procedure was repeated for all twenty-nine subjects. Hence, all twenty-nine subjects were used for training and testing the BCI.

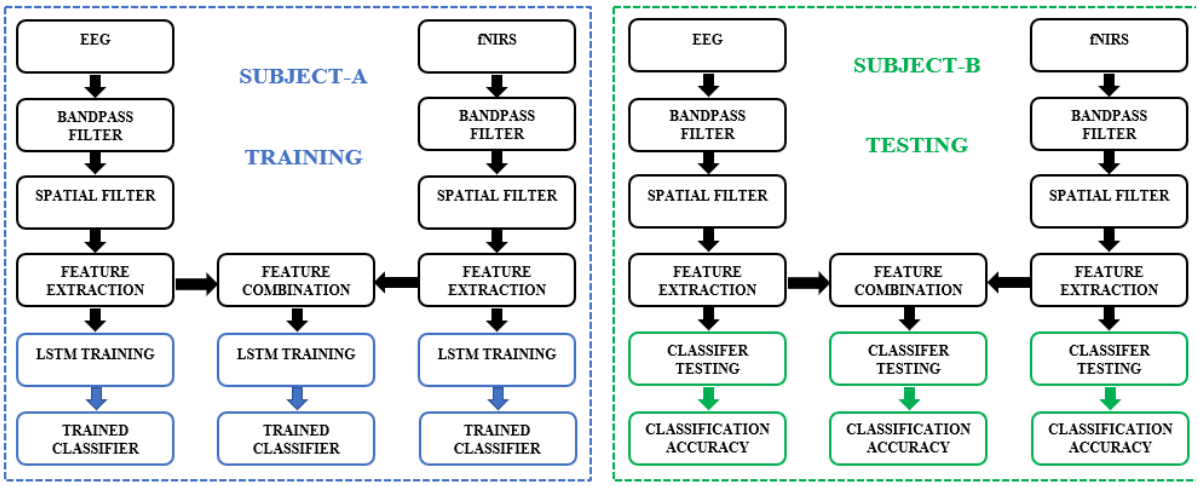

Figure 3.1: Flowchart of the Proposed Experiment.

3.2 Methodology

3.2.1 Dataset

For the validation of our proposed experiment, we have used a publicly available dataset recorded by J. Shin [113] containing simultaneous EEG and fNIRS signal recordings of twenty-nine healthy participants. EEG data were recorded using a multichannel BrainAmp amplifier with thirty active electrodes placed in the 10-5 system. NIRS data were collected by NIRScout with a 12.5 Hz sampling rate. Thirty-six physiological channels from fourteen sources and sixteen detectors were placed at frontal, motor, and visual areas with an inter-optode distance of 30 mm. The subjects relaxed in a comfortable chair, forbidden to move any body part during recording, with a 50-inch white projection screen 1.6 m away. Three seasons of left- and right-hand MI tasks and of Mental Arithmetic (MA) and baseline tasks were recorded for each subject. Here, only MI seasons are used. Every season had a 1 min pre-experiment resting period followed by 20 repetitions of the given task and finally a 1 min post-experiment resting period. At the start of the task, a 2-s visual instruction was given followed by a 10 s task period and 15-17 s random resting period and a short beep of 250 ms at the beginning and end of each task

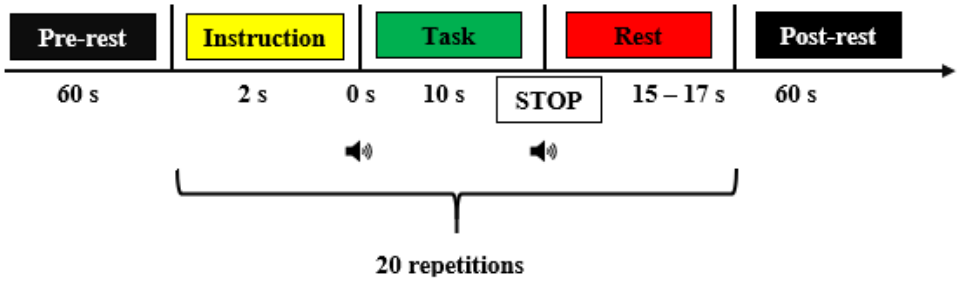

Figure 3.2: Schematic sequence diagram of the experimental paradigm.

Every season has one minutes recording during resting period before the experiment, twenty repetitions of tasks followed by one-minute recording of the post-experiment resting period. At the start of the task a visual instruction was given for two seconds which followed by a ten seconds task period and a fifteen to seventeen seconds resting period. A short beep was played to mark the stop and start of the task [113].

period. The subjects performed kinesthetic MI tasks; that is to imagine opening and closing their hands like grabbing a ball, at 1 Hz speed for 10 s. Figure 3.2 shows the schematic sequence diagram of the experimental paradigm of the dataset recording. The same procedure was repeated 20 times in a season 10 trials for each hand yielding to 30 trials per class in all three seasons.

3.2.2 EEG Processing and Feature Extraction

The experiment is designed as an inter-subject experiment, which referred to as the training will be done on Subject A, and the testing will be done on subject B. Figure 3.1 shows the experiment flowchart. As the flowchart refers, signal processing is similar for both subjects up to feature extraction. Raw EEG data often contains interference and noise distortion from subject physical activity as well as noise from the environment like electrical interference, muscle activity, eye movements. The bandpass filter is a way of capturing the frequencies of

interest and subtract or reduce the interference from signals of other frequencies. Before filtering, the signal was normalized by subtracting the average amplitude of each channel from each channel signal and then dividing the resultant signal using the standard deviation of all channels signal for the subject. Fourth-order Butterworth bandpass filter has been utilized for the filtering task. The filtering was performed in two steps. First, a fourth-order filter is designed with cutoff frequencies set at 0.5 to 49 Hz. After that, five separate fourth-order bandpass filter was designed to filter the EEG signals in 5 different frequency bands. The cutoff frequencies are 0.5 – 3.5 Hz for Delta-wave, 4-7.5 Hz for Theta-wave, 8-13 Hz for Mu-wave, 18-32 Hz for Beta-wave, and finally 8-32 Hz a customized frequency band specially used for MI BCI signals. The filtered signals from stage one was filtered again using these five filters. Hence, six different frequency signals were generated from the original EEG signals. After this step, the resultant signals from subject A is utilized for training the spatial filter RCSP. All the available sixty trials of subject A are used to train the filter, and the trained filter is applied to all the available trials from subjects A and B, a total of one hundred and twenty trials combining both subjects. The RCSP algorithm shaped the filtered data in such an alignment that the first channels show maximum covariance for left-hand motor imagery (MI) while showing minimum covariance for right hand MI. On the contrary, the last channels show maximum covariance for right hand MI and minimum covariance for left hand MI. To train the RCSP filter, the covariance matrix is calculated for each MI activity from subject A. After the competition of the spatial filtering, eight optimal channels were selected from the outputs of RCSP, the first four channels, and the last four channels. The selected channels were used for the feature extraction process. Three types of features making a total of thirteen features were calculated; wavelet energy, wavelet entropy, frequency band power. Each trial contains 2000 samples for each channel. The last 1000 samples for each trial is

wavelet decomposed up to level 3 using ‘db1’ mother wavelet. Four wavelet energy is calculated from the decomposed signals, three detailed coefficients, and one approximate coefficient is calculated. The last 1500 samples were again wavelet decomposed up to level 6 using ‘db3’ mother wavelet. Seven decomposed signals were generated. Five Shannon entropies were calculated from the decomposed signals, excluding the second and final component, which is the lowest and highest frequency components, respectively. Finally, four-band powers were calculated from the signals. The bands are divided based on the sample. Each band is composed of 500 samples starting from 1 and ending in 2000. The band power is calculated using MATLAB band power command using sampling frequency and appropriate frequency range, which is varied for each frequency band. Hence, a total of thirteen features were calculated per trial per channel for EEG. Features were normalized. LSTM neural network was trained on Subject A and tested on subject B. Classification is performed using the LSTM network. The description of the classifier is given in section 3.2.E. The only difference for EEG classification is that the number of inputs for the network is thirteen, which means the features for each channel were used as the feature for the classifier, and the classifier structure is also different. The structure is given below,

- Sequence input layer: Input dimension is 13
- LSTM layer: 100 hidden neurons. The output mode is last.
- Fully connected layer: 2 fully connected layer.
- Softmax layer: Outputs a vector that represents the probability distributions of a list of potential outcomes. The loss function is crossentropyex
- Classification layer: Classification output layer. Provides an output class label.

Figure 3.3: LSTM network structure used for EEG classification and fNIRS classification.

The structure is the same for fNIRS; however, it is different for the hybrid system. The LSTM structure is shown in Figure 3.3. The training and testing options are the same for all the classifiers used in the experiment, and the options are described in sub-section 5. Finally, based on filter frequency bands, six different experiments were created to test the effect of each bandpass filter on the classification accuracy.

3.2.3 NIRS Processing and Feature Extraction

The experiment is designed as an inter-subject experiment, which referred to as the training will be done on Subject A, and the testing will be done on subject B. The Figure shows the experiment flowchart. As the flowchart refers, signal processing is similar for both subjects up to feature extraction. NIRS signals are optical light intensities. We need to convert the light intensities to hemoglobin concentration. We have solved Modified Beer-Lambert law [48] to convert the NIRS signal to hemoglobin concentrations. Oxy-hemoglobin concentration (ΔC_{HbO}), de-oxy-hemoglobin concentration (ΔC_{HbR}) were estimated from the raw light intensities. Modified Beer-Lambert law for fNIRS concentration changes can be given as

$$\begin{bmatrix}\Delta C_{HbO}(t)\\ \Delta C_{HbR}(t)\end{bmatrix} = \begin{bmatrix}\alpha_{HbO}(\lambda_1) & \alpha_{HbR}(\lambda_1)\\ \alpha_{HbO}(\lambda_2) & \alpha_{HbR}(\lambda_2)\end{bmatrix}^{-1} \begin{bmatrix}\Delta A(t,\lambda_1)\\ \Delta A(t,\lambda_2)\end{bmatrix} \frac{1}{l\times d} \qquad (3.1)$$

Where ΔA (t; λj) (j = 1,2) is the absorbance variation of wavelength λj. The factor $\alpha_{HbX(\lambda j)}$ is the extinction coefficient of HbX (HbX = HbO, HbR) in μM−1 mm−1, d is the differential pathlength factor (DPF), and l denotes the distance between an emitter and a detector in cm. The wavelength of the infrared light was 760 nm and 850 nm. We have also calculated the total hemoglobin concentration (ΔC_{HbT}), which was the vector summation of ΔC_{HbO} and ΔC_{HbR}, as:

$$\Delta C_{HbT} = \frac{\Delta C_{HbO} + \Delta C_{HbR}}{\sqrt{2}} \qquad (3.2)$$

The NIRS signals could be contaminated by physical noises like muscle movement, eye movements. Removing the noise or reducing the noise contamination level is essential to get acceptable control performance. Fourth-order Butterworth bandpass filter was utilized to filter the signals. Three different frequency band was used for three hemoglobin concentrations. The frequency ranges are 0.01 to 0.25 Hz for ΔC_{HbO} , 0.01 to 0.4 Hz for ΔC_{HbR} , and 0.01 to 0.5 Hz for ΔC_{HbT}. It has been found that these are the optimal frequency ranges for the three types of fNIRS concentrations. Normalization has been done by subtracting the mean from the data and dividing the resultant by the standard deviation. At this point, the filtered signals were used to separate all the trails. After this point, the signals for subject A is used to train the spatial filter RCSP, and the filter is applied to both subjects. To train the RCSP covariance matrix has been created from the filtered signals. A description of the RCSP filter has been provided in the earlier chapter. Sixty trials from subject A have been used for the training, and the filter has been applied to a total of one hundred and twenty trials from both subjects. Outputs of RCSP has been feed to feature extraction algorithm after selecting six optimal channels. The first three channels of the RCSP output is selected along with last three channels. It is expected the first channels

provide better classification performance for class 1, and the last three channels provide better performance for class 2. Each channel of fNIRS concentrations contains 100 samples for 10 seconds of activity. All the 100 samples were selected as features. The classification is performed using the LSTM network. The description of the classifier is given in sub-section 5. The only difference for fNIRS classification is that the number of inputs for the network in six, which means the data for each channel was used as the feature for the classifier, and the classifier structure is also different. The structure is given shown in the figure. A detail of the structure is given below,

- Sequence input layer: Input dimension is 6
- LSTM layer: 100 hidden neurons. The output mode is last.
- Fully connected layer: 2 fully connected layer.
- Softmax layer: Outputs a vector that represents the probability distributions of a list of potential outcomes. The loss function is crossentropyex
- Classification layer: Classification output layer. Provides output class.

The training and testing options are the same for all the classifiers used in the experiment, and the options are described in sub-section 5. Finally, the three fNIRS concentrations are classified as separate signals, and the classification accuracy is compared to see the effect of filtering frequency and the type of hemoglobin concentration on the control performance.

3.2.4 Hybrid BCI And Feature Fusion

In the hybrid experiment, features obtained from EEG and fNIRS is combined to generate the features for the hybrid system. Before combining the features from the EEG and fNIRS signals, few changes were made to the signal processing and feature extraction processes of each method.

Table 3.1: The Combination of Hybrid BCI Experiment

Combination Number	**EEG Signals**	**fNIRS Concentrations**
1	Delta	HbO
2	Theta	HbO
3	Mu	HbO
4	Beta	HbO
5	8-32 Hz	HbO
6	0.5 – 49 Hz	HbO
7	Delta	HbR
8	Theta	HbR
9	Mu	HbR
10	Beta	HbR
11	8 - 32 Hz	HbR
12	0.5 – 49 Hz	HbR
13	Delta	HbT
14	Theta	HbT
15	Mu	HbT
16	Beta	HbT
17	8 – 32 Hz	HbT
18	0.5 – 49 Hz	HbT

For EEG, no changes were made in the signal processing part. However, changes were made in the feature extraction part. Each trial contains 2000 samples for each channel. The last 1500 samples for each trial are wavelet decomposed up to level 3 using db7 mother wavelet. Four wavelet energy is calculated from the decomposed signals, three detailed coefficients, and one approximate coefficient is calculated. The last 1000 samples were again wavelet decomposed up to level 6 using 'db3' mother wavelet. Seven decomposed signals were generated. Five Shannon entropies were calculated from the decomposed signals, excluding the 2nd and Final component, which is the lowest and highest frequency components, respectively. Finally, four-band powers were calculated from the signals. The bands are divided based on the sample. Each band is composed of 500 samples starting from 1 and ending in 2000. The band power is calculated using MATLAB band power command using sampling frequency and appropriate frequency range, which is varied for each frequency band. Hence, a total of thirteen features were calculated per trial per channel for EEG.

For fNIRS, the cutoff frequencies for each of the HbO, HbR, and HbT concentration filters. The new cutoff frequencies are 0.01 to 0.4 Hz for HbO, 0.01 to 0.2 Hz for HbR, and 0.01 to 0.3 Hz for HbT. For the purpose of RCSP filtering, eight optimal RCSP filtered channels were selected for the hybrid experiment. This was done to match the number of channels selected for EEG. The selected channels are the first four channels and the last four channels. Each fNIRS trial was comprised of 100 samples for 10 seconds of recording as a sampling rate of 10 Hz. For the hybrid experiment, the fNIRS signals are downsampled by a factor of 5 to select only 20 samples for fNIRS. The samples are normalized by scaling the data to unit length using the vector 2-norm. Finally, 13 features of EEG and 20 features of fNIRS were combined from the feature matrix of the hybrid system. The initial feature matrix of the EEG and fNIRS was 8 X 13 X 60

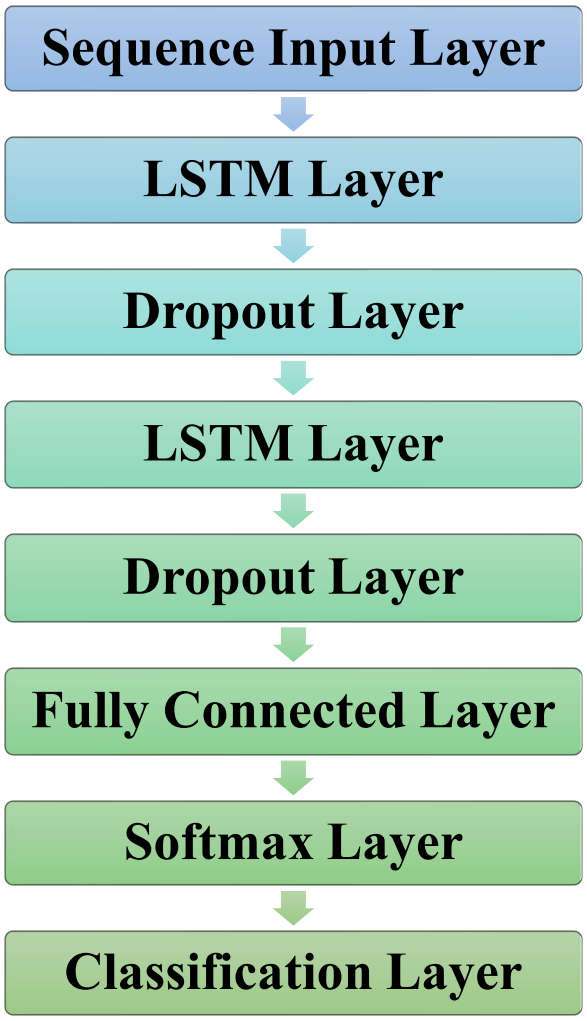

Figure 3.4: Structure Diagram of the Used LSTM Network.

and 8 X 20 X 60, respectively, where the first number is the number of RCSP filtered channels, a second dimension is a number of features, and the final dimension is the number of trials for each subject. The features of fNIRS and EEG are concatenated to form a feature matrix with dimensions equal to 8 X 33 X 120. The combination is done in such a manner that each EEG signal type is combined with each fNIRS concentrations, and the accuracy is calculated. A total of eighteen combinations of EEG-fNIRS was created, and the classification is performed using LSTM is the inter-subject paradigm, and the classification accuracies were compared to see the changes of the accuracies from standalone systems. The combinations are as shown in Table 3.1

3.2.5 Long Short-Term Memory (LSTM)

The classification is performed using a recurrent tensor neural network implemented using long short-term memory (LSTM) framework [114, 115]. LSTM is well known for forecasting future events based on current data. It has also been used for classification problems. One of the best characteristics of the LSTM network is that it performs better for text classification as well as signal-based classification, while convolutional neural network (CNN) is well known for image-based classification problems. The network structure is given in Figure 3.4. The key parts of the network are,

- Sequence Input Layer – Inputs are the features. Sequence input size 33.
- LSTM Layer – 113 hidden neurons. The output mode of the network is set to 'sequence.' Sequence to sequence classification networks.
- Dropout Layer – Dropout factor 0.2 Prevents overfitting.
- LSTM Layer – 90 hidden neurons. The output mode is set to 'last'—Sequence-to-label classification networks.
- Dropout Layer – Dropout factor 0.2. Prevents overfitting.
- Fully Connected Layer –Two fully connected layer (Num of output classes = 2)
- Softmax layer: Outputs a vector that represents the probability distributions of a list of potential outcomes. The loss function is crossentropyex
- Classification layer: Classification output layer. Provides output class.

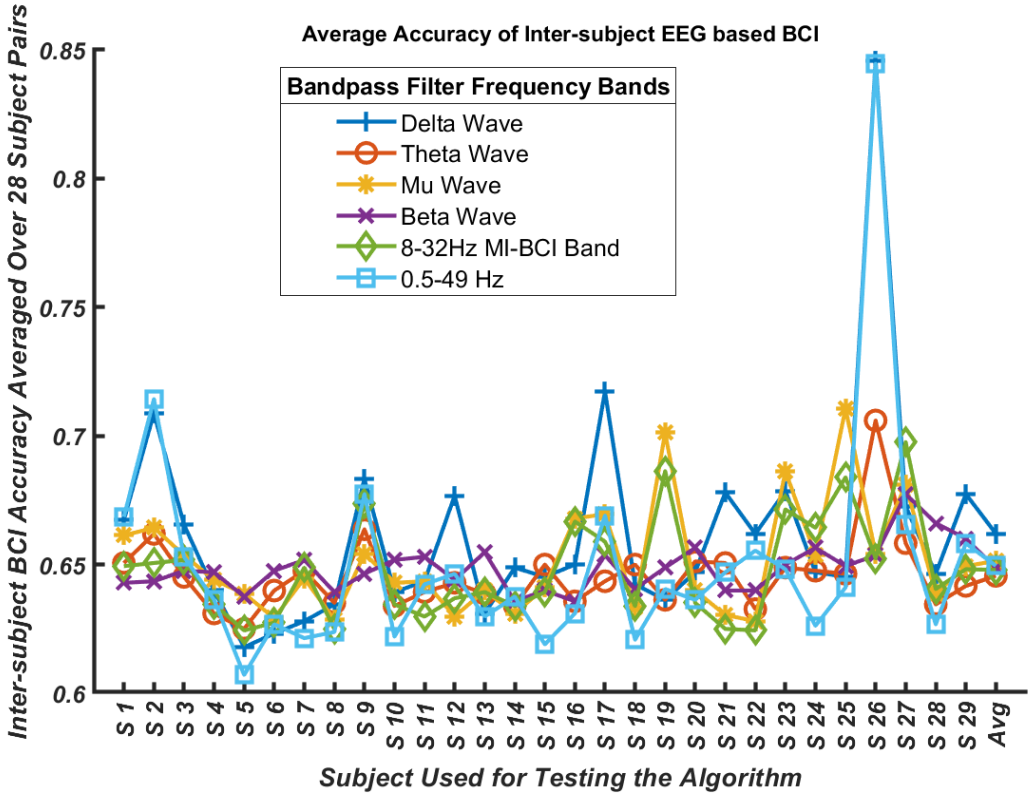

Figure 3.5: Average Accuracy of EEG Based Inter-subject BCI. The X-axis shows the testing subject number, and Y-axis is the average inter-subject classification accuracy. The accuracy is averaged over 28 inter-subject pairs for each testing subject. The six different lines show accuracy for each of the 6 EEG frequencies used for bandpass filtering.

The above-mentioned structure is used for a hybrid system only. However, the standalone EEG and fNIRS systems are classified with a different structure, and the structure is mentioned in each sub-section. For training, the maximum number of epochs was set to 100 epochs, and minibatch size was set to 32. For training, adam was used as the solver, and the training was done on a Linux workstation run on an Intel XEON E5 processor with 64 GB of RAM while all the calculations were performed on a Nvidia RTX 5000 GPU. Gradient descent was used for the optimization algorithm, and the threshold was set to 1, meaning the perfect accuracy. The testing was performed using MATLAB command classify with the same number of the minibatch size used for the training. As mentioned earlier, RCSP is used as a spatial filtering method. RCSP is a modified version of CSP where the CSP algorithm is controlled with two regularization

parameters call gamma and beta. For our experiment, we have tested 12 different values of beta and 11 values of gamma. The values of beta and gamma is,

$$\beta = [0\ 0.001\ 0.01\ 0.1\ 0.2\ 0.3\ 0.4\ 0.5\ 0.6\ 0.7\ 0.8\ 0.9];$$
$$\gamma = [0\ 0.01\ 0.1\ 0.2\ 0.3\ 0.4\ 0.5\ 0.6\ 0.7\ 0.8\ 0.9];$$

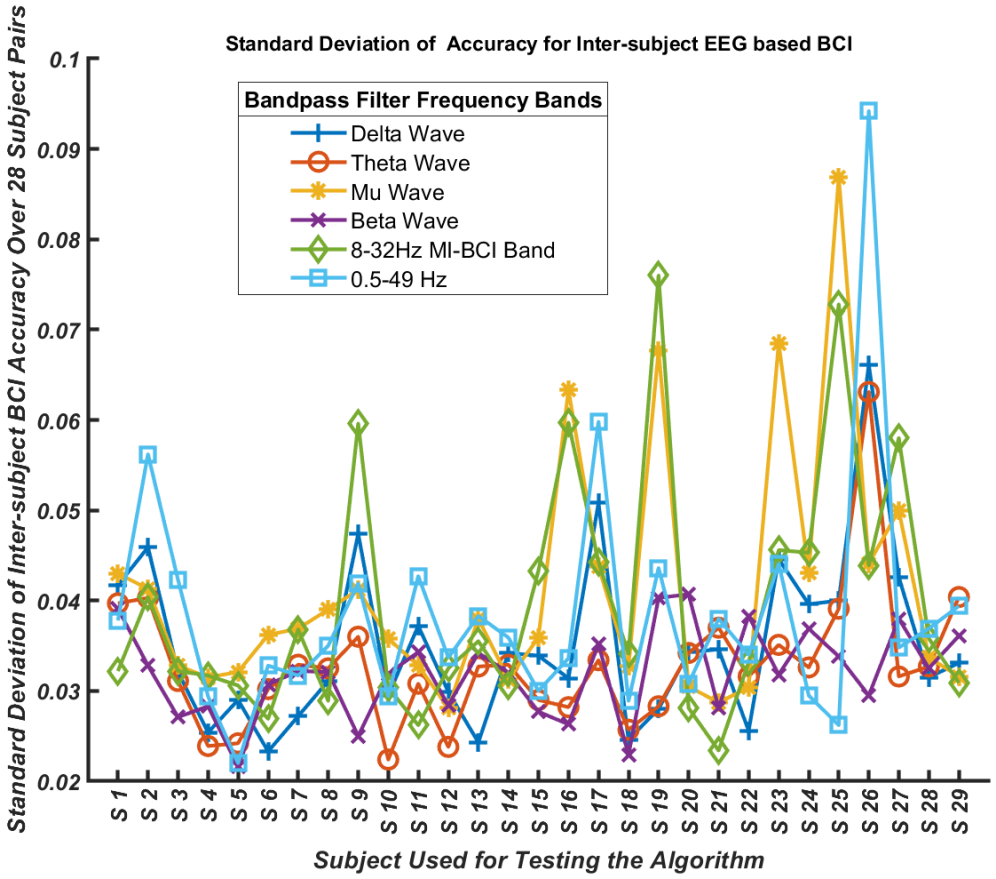

Figure 3.6: Standard Deviation of Accuracy of EEG Based Inter-subject BCI. The X-axis shows the testing subject number, and Y-axis is the standard deviation of inter-subject classification accuracy. The standard deviation is achieved over 28 inter-subject pairs for each testing subject. The six different lines show accuracy for each of the 6 EEG frequencies used for bandpass filtering.

Detailed information about the regularization can be found in subchapter II. Testing all the combinations means that the total number of iterations for each subject combination is 11 X 12 = 132, and each subject is tested with 28 other subjects since the dataset contains 29 subjects. These make the total number of iterations for each to each subject is 132 X 28. This is a large

task to do for any MATLAB programs. Among the 132 iterations of RCSP, we have selected the best classification accuracy among 132 tries, and hence we can eliminate the need for another validation process. Another validation would again increase the computational burden on the required task. Since we have selected the best results from 132 iterations of RCSP, we can certainly say that our data is not contaminated with overfitting or under-fitting. Hence, we can eliminate the necessity of using another validation algorithm.

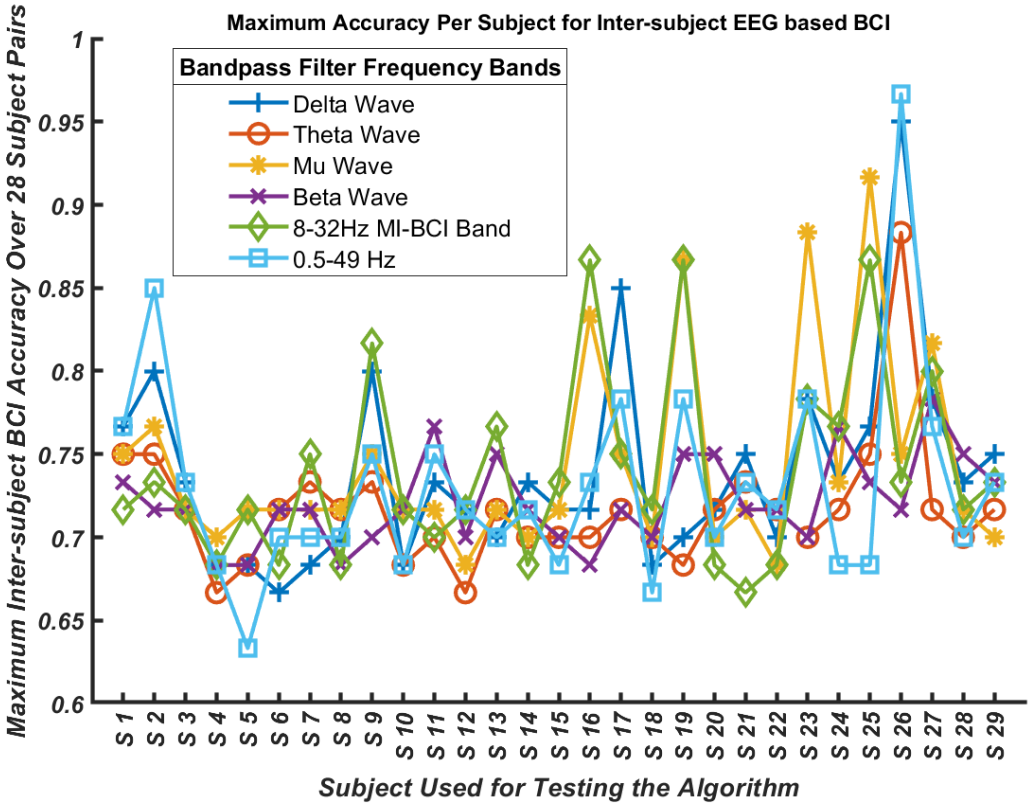

Figure 3.7: Maximum Accuracy of EEG Based Inter-subject BCI. The X-axis shows the testing subject number, and Y-axis is the maximum of inter-subject classification accuracy. The maximum accuracy is the maximum among 28 inter-subject pairs for each testing subject. The six different lines show accuracy for each of the 6 EEG frequencies used for bandpass filtering.

3.3 Results and Discussions

In this experiment, an inter-subject hybrid BCI has been designed using simultaneously recorded EEG and fNIRS recording. The recording is collected from twenty-nine healthy participants. The brain activity was generated for the imagination of hand movement as if the subjects are grabbing the ball in their hand with a certain frequency. Inter-subject has been referred to as a BCI system that is trained with one subject and tested with a different subject. This is done to test the capability of the designed algorithm to perform better on an unknown subject's data. The

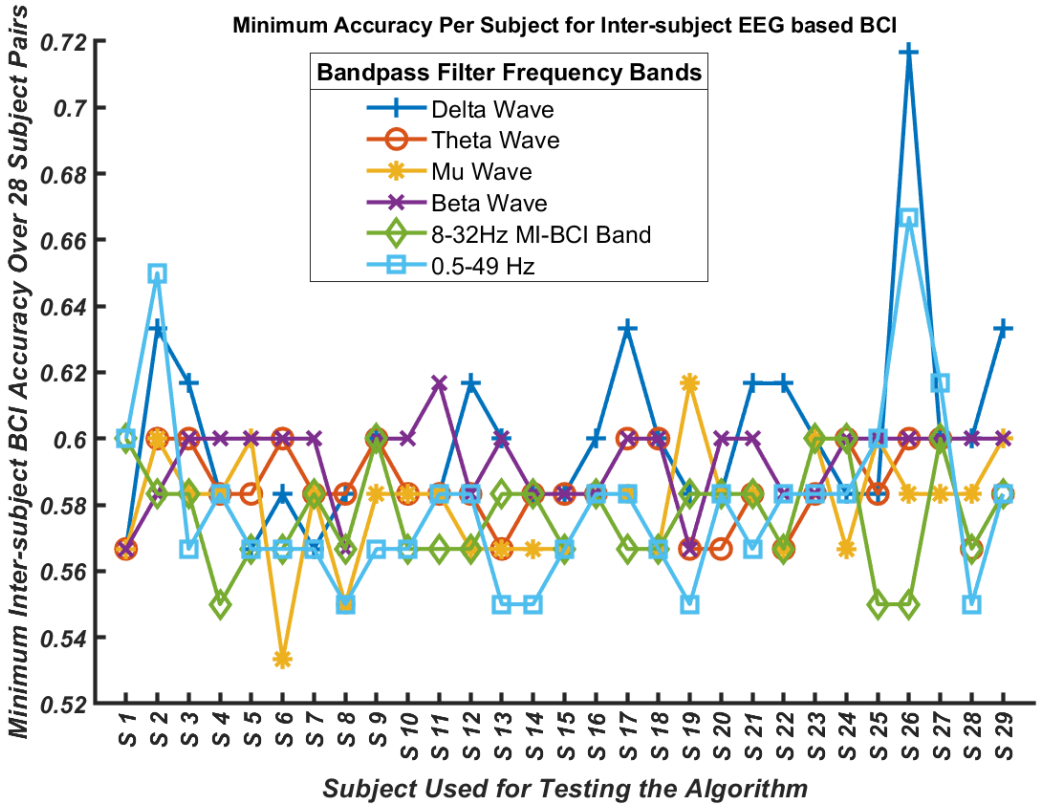

Figure 3.8: Minimum Accuracy of EEG Based Inter-subject BCI. The X-axis shows the testing subject number, and Y-axis is the minimum of inter-subject classification accuracy. The maximum accuracy is the minimum among 28 inter-subject pairs for each testing subject. The six different lines show accuracy for each of the 6 EEG frequencies used for bandpass filtering.

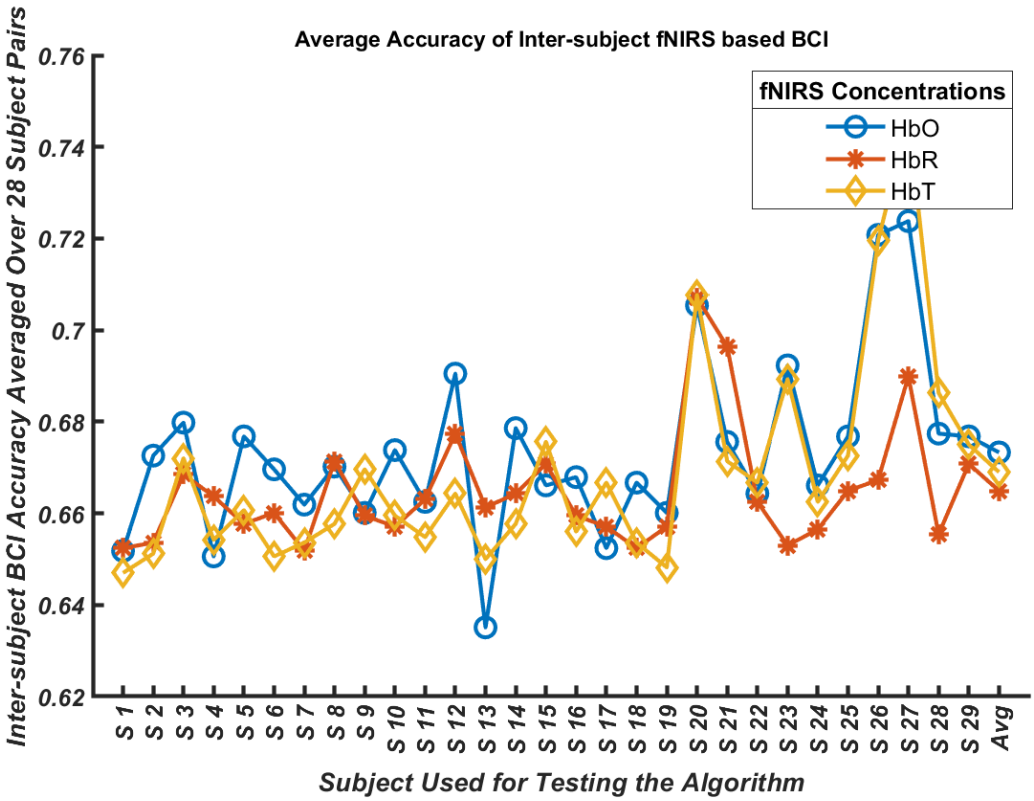

Figure 3.9: Average Accuracy of fNIRS Based Inter-subject BCI. The X-axis shows the testing subject number, and Y-axis is the average inter-subject classification accuracy. The accuracy is averaged over 28 inter-subject pairs for each testing subject. The three different lines show average accuracy for each of the three fNIRS concentrations.

ultimate target is to design a system that does not require a very long training period to provide good control performance. The objective of this experiment is to test the feasibility of an inter-subject BCI using EEG-fNIRS recordings.

We have also tested the feasibility of LSTM based deep neural network for the classification of MI activity from the EEG-fNIRS signal. Figure 3.5 to Figure 3.8 shows the average accuracy, standard deviation, maximum accuracy, minimum accuracy, respectively, for the BCI designed using EEG recordings. All the results are inter-subject results, and each subject is paired with the other twenty-nine subjects available in the dataset. For a better understanding of the results, let's consider subject S1. The average accuracy for subject S1 is the accuracy averages over twenty-

eight inter-subject pairs. In each pair, subject S1 is used as the testing subject, and another subject from the remaining list (S2, S3, …, S28, S29) is used for training the classification algorithm. Hence, the reported accuracy is averaged over twenty-eight inter-subject experiment

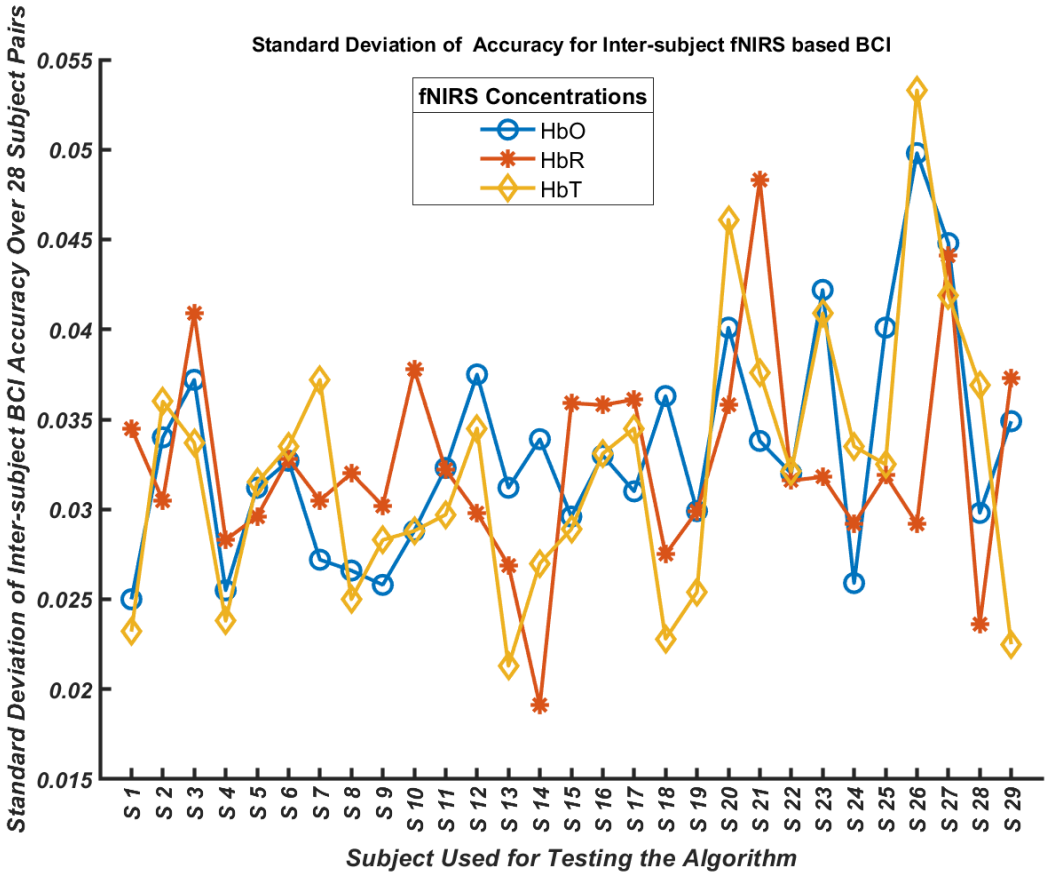

Figure 3.10: Standard Deviation of Accuracy of fNIRS Based Inter-subject BCI. The X-axis shows the testing subject number, and Y-axis is the standard deviation of inter-subject classification accuracy. The standard deviation is achieved over 28 inter-subject pairs for each testing subject. The three different lines show accuracy for each of the fNIRS concentrations.

pairs, and Figure 3.5 shows the average accuracy. Figure 3.6 shows the standard deviation of subjects. The standard deviation is also calculated from the 28 subject pairs. Figure 3.7 shows the

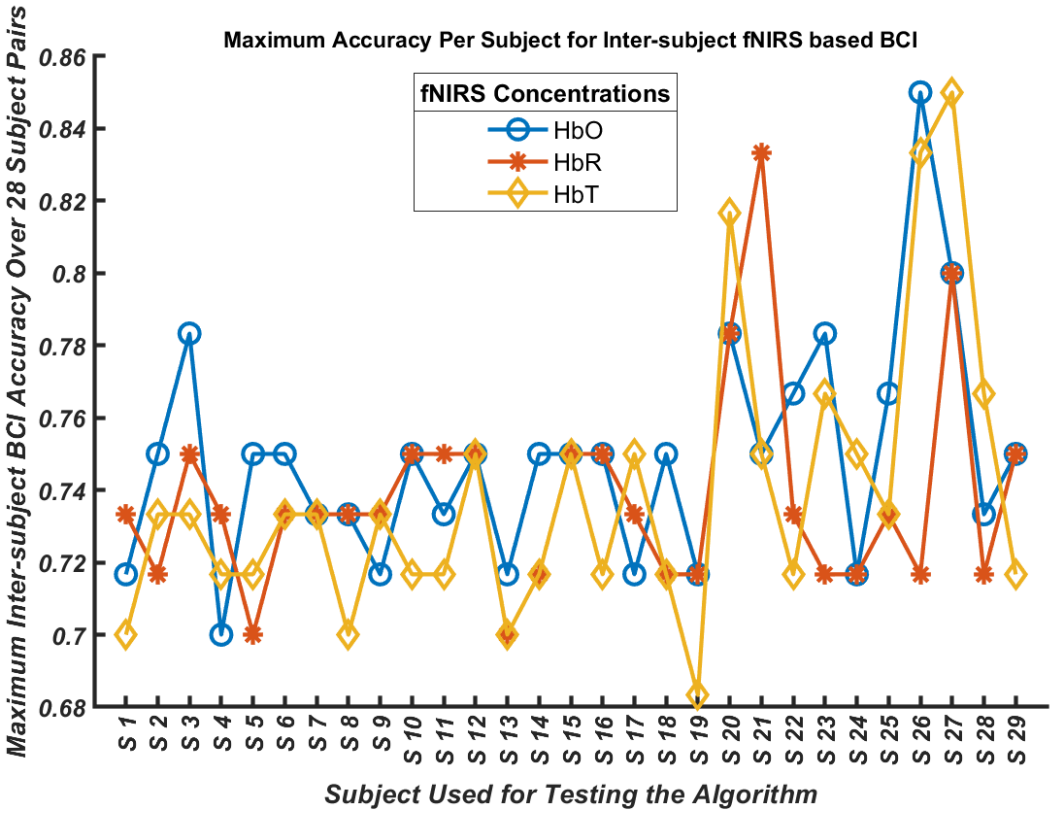

Figure 3.11: Maximum Accuracy of fNIRS Based Inter-subject BCI. The X-axis shows the testing subject number, and Y-axis is the maximum of inter-subject classification accuracy. The maximum accuracy is the maximum among 28 inter-subject pairs for each testing subject. The three different lines show accuracy for each of the three fNIRS concentrations.

maximum accuracy for each of the testing subjects. The maximum accuracy is the highest accuracy of the twenty-eight inter-subject pairs. Figure 3.8 shows the minimum accuracy for each of the testing subject. The minimum reported accuracy is the minimum among the twenty-eight inter-subject pairs. Each figure has six lines to show the performance comparison for the bandpass filtered frequencies. In Figure 3.5, we can see that subject S2 shows the maximum average accuracy using Delta wave and 0.5-49 Hz band signals. The lowest performance is recorded for S5 using 0.5-49 Hz. We can also see that for the same subject. The six different signal types show different classification accuracy. The pattern of accuracy is somewhat the same for some subjects. However, for some subjects, the variation is the classification accuracy is diverse. Delta wave shows the highest classification accuracy for S26. Theta wave also follows

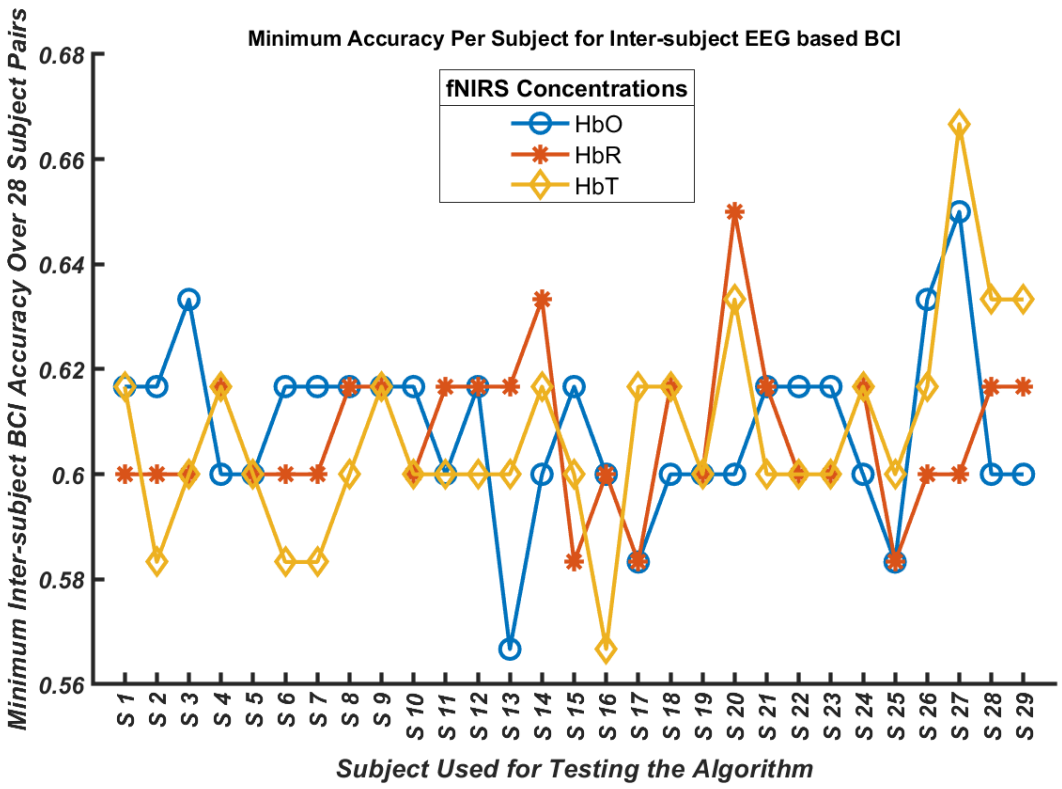

Figure 3.12: Minimum Accuracy of fNIRS Based Inter-subject BCI. The X-axis shows the testing subject number, and Y-axis is the minimum of inter-subject classification accuracy. The minimum accuracy is the minimum among 28 inter-subject pairs for each testing subject. The three different lines show accuracy for each of the three fNIRS concentrations.

the same pattern, thus showing the best performance for S26. For Mu wave, the best performance is recorded for S25. On the other hand, the Beta wave shows the best performance for S27. For the 8-32 Hz MI activity band, the best performance is obtained for S27, while S26 showed the best performance with a 0.5-49 Hz band. From the figure, we can see that the classification performance can differ widely for the same subject using different types of brain waves. It has been seen that Delta wave, Mu wave, 8-32Hz band, and 0.5 -49 Hz band showed better BCI classification performance compared to other in-terms of average accuracy variation in twenty-eight subject pairs. When the classification accuracy is averaged over twenty-nine subjects to get an understanding of the classification accuracy for the whole dataset, we can see that the best classification accuracy is 0.6620 for Delta wave, and the lowest performance is obtained for

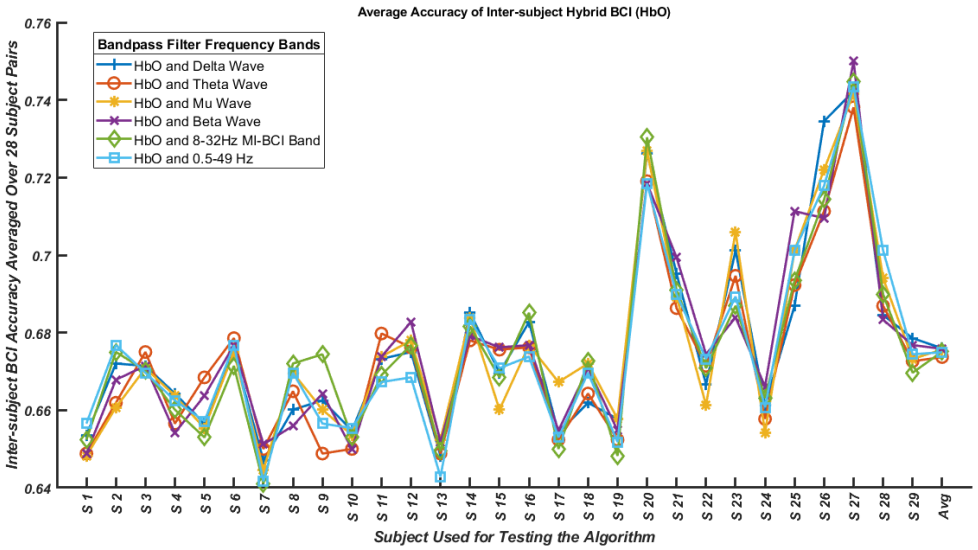

Figure 3.13: Average Accuracy of Hybrid Inter-subject BCI (HbO). The accuracy is averaged over 28 inter-subject pairs for each testing subject. The six different lines show average accuracy for each of the six EEG and HbO combinations.

Theta wave 0.6456. Mu wave also showed a very good performance. The average is 0.6514. A similar performance has been observed in terms of standard deviation (Figure 3.6). The subject pairs with lower average accuracy showed a relatively lower standard deviation. This result can be further backed by Figure 3.7 and Figure 3.8, showing maximum accuracy and minimum accuracy. The maximum accuracy performance has been found for S26 with Delta wave, Theta wave, and 0.5-49Hz band. For Mu wave and 8-32 Hz, the maximum accuracy has been found for S25. For the Beta wave, the top accuracy is recorded for S27. The top value for minimum accuracy has been found for S26 with Delta wave, Theta wave, and 0.5-49Hz band. For Mu wave, the highest value for minimum accuracy has been found for S19. For Beta wave, the top accuracy is recorded for S11, and 8-32 Hz bands showed the top value for minimum accuracy for S1, S9, S23, S24, S27. Figure 3.9, Figure 3.10, Figure 3.11, Figure 3.12 presents the average classification accuracy, standard deviation, maximum accuracy, and minimum accuracy, respectively. fNIRS based BCI has also provided a similar performance in terms of average classification accuracy.

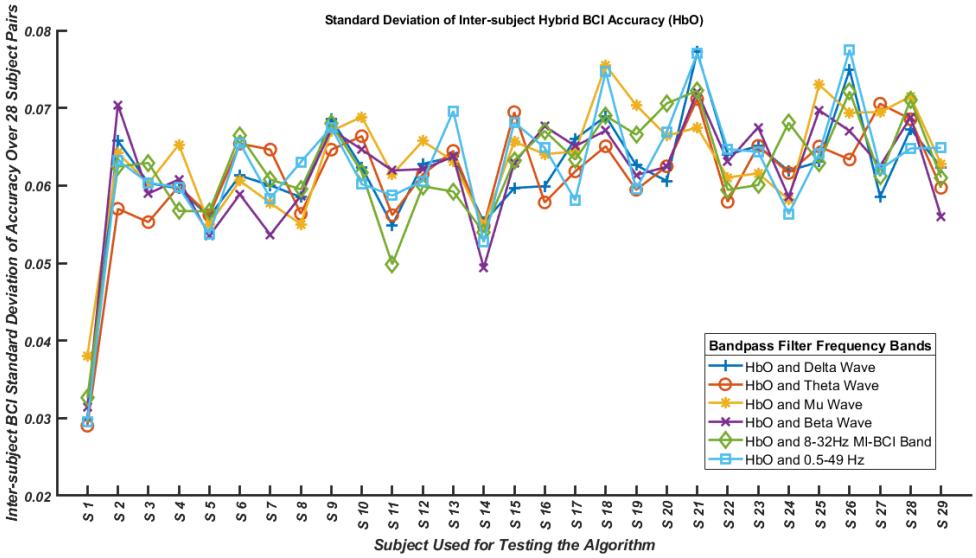

Figure 3.15: Standard Deviation of Accuracy of Hybrid Inter-subject BCI (HbO). The X-axis shows the testing subject number, and Y-axis is the standard deviation of inter-subject classification accuracy. The standard deviation is achieved over 28 inter-subject pairs for each testing subject. The six different lines show accuracy for each of the six EEG and HbO combinations.

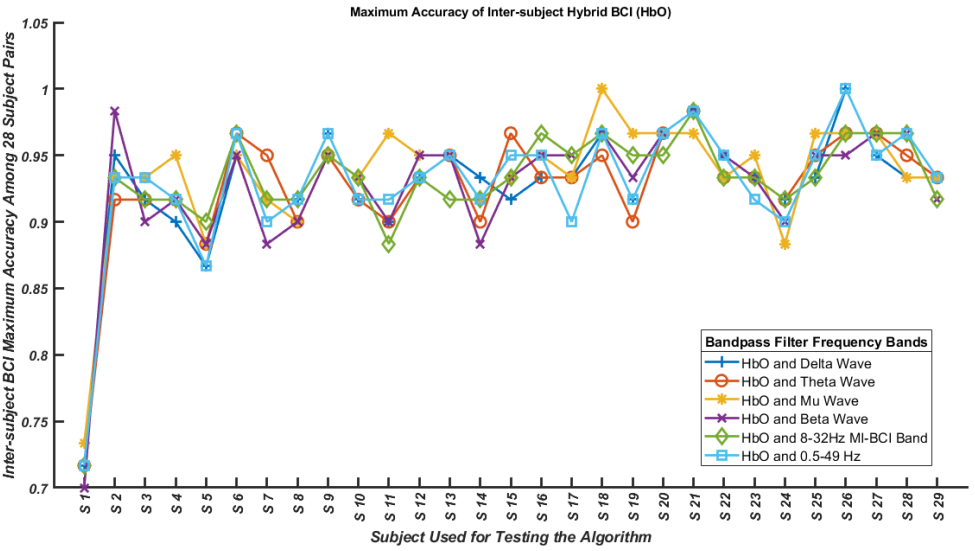

Figure 3.14: Maximum Accuracy of Hybrid Inter-subject BCI (HbO). The X-axis shows the testing subject number, and Y-axis is the maximum of inter-subject classification accuracy. The maximum accuracy is the maximum among 28 inter-subject pairs for each testing subject. The six different lines show accuracy for each of the six EEG and HbO combinations.

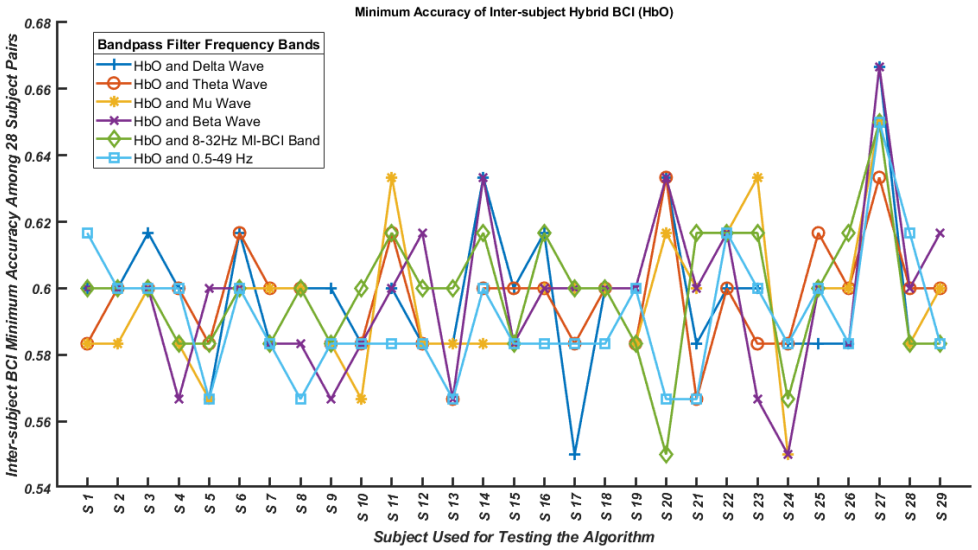

Figure 3.17: Minimum Accuracy of Hybrid Inter-subject BCI (HbO). The X-axis shows the testing subject number, and Y-axis is the minimum of inter-subject classification accuracy. The minimum accuracy is the minimum among 28 inter-subject pairs for each testing subject. The six different lines show accuracy for each of the six EEG and HbO combinations.

The highest average accuracy for HbO and HbT is obtained for S27, and for HbR the highest

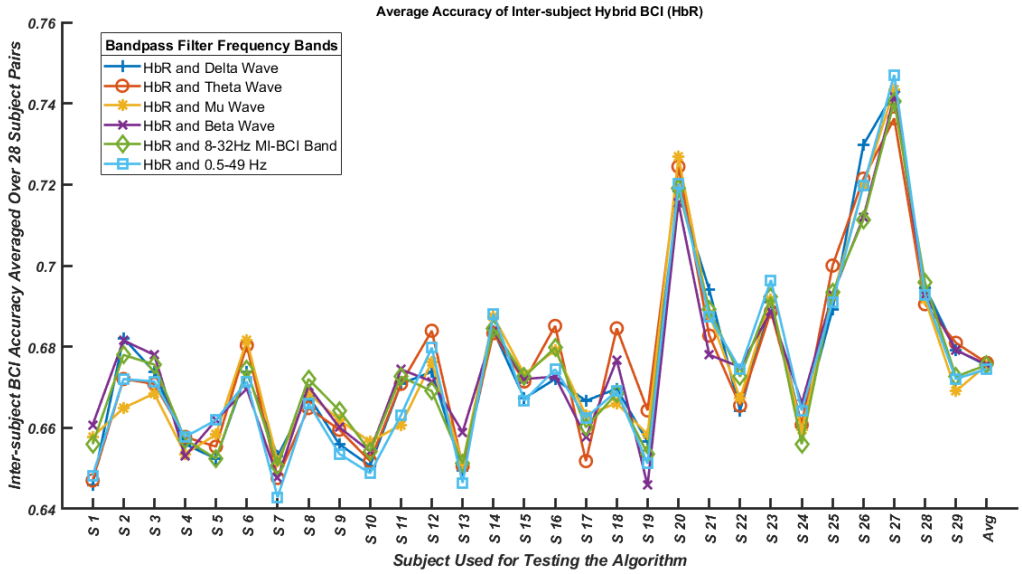

Figure 3.16: Average Accuracy of Hybrid Inter-subject BCI (HbR). The X-axis shows the testing subject number, and Y-axis is the average inter-subject classification accuracy. The accuracy is averaged over 28 inter-subject pairs for each testing subject. The six different lines show average accuracy for each of the six EEG and HbR combinations.

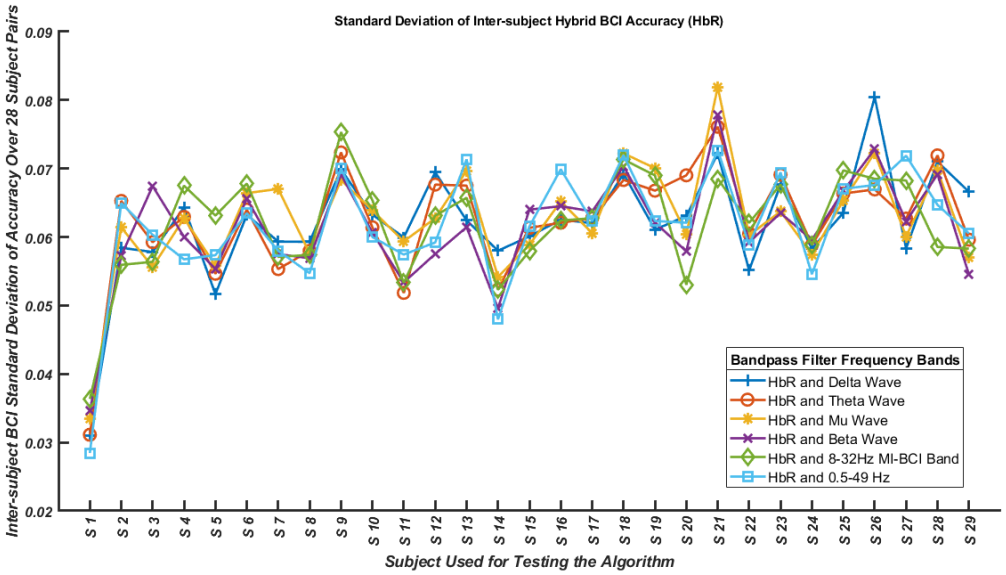

Figure 3.18: Standard Deviation of Accuracy of Hybrid Inter-subject BCI (HbR). The X-axis shows the testing subject number, and Y-axis is the average inter-subject classification accuracy. The accuracy is averaged over 28 inter-subject pairs for each testing subject. The six different lines show average accuracy for each of the six EEG and HbR combinations.

average accuracy is obtained for S20. One interesting finding for subject S20 is that the

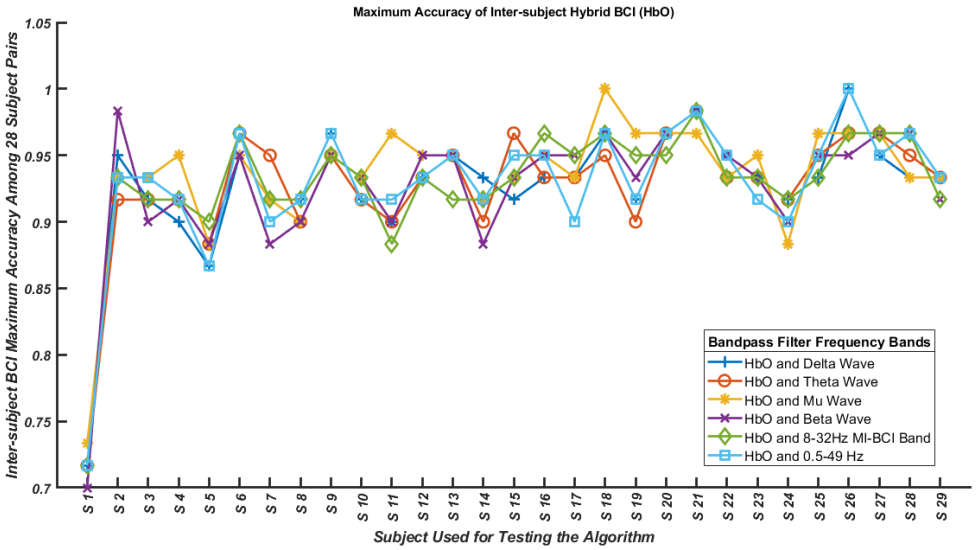

Figure 3.19: Maximum Accuracy of Hybrid Inter-subject BCI (HbR). The X-axis shows the testing subject number, and Y-axis is the maximum of inter-subject classification accuracy. The maximum accuracy is the maximum among 28 inter-subject pairs for each testing subject. The six different lines show accuracy for each of the six EEG and HbR combinations.

classification accuracies for each of the fNIRS concentration types are similar. Subject S1 showed lowest average performance for HbR and HbT, while S13 showed the lowest performance for HbO. The average accuracy for fNIRS concentrations in the dataset over twenty-nine subjects is 0.6733, 0.6649, 0.6690 for HbO, HbR, and HbT, respectively. Figure 3.10 shows the standard deviation for each testing subject over twenty-eight inter-subject pairs. The standard deviation varies widely among different types of fNIRS concentrations and among different subjects. A low value of standard deviation indicates that the classification accuracies of all the twenty-eight inter-subject pairs were comparable, and usually, this type of system is preferred for real-life implementation. A system that's performance doesn't change abruptly across subject is a stable system and preferred for inter-subject and subject independent BCIs. In our case, we cannot clearly determine based on the standard deviation that which fNIRS concentration is performing better than the other because HbO, HbR, and HbT signals show

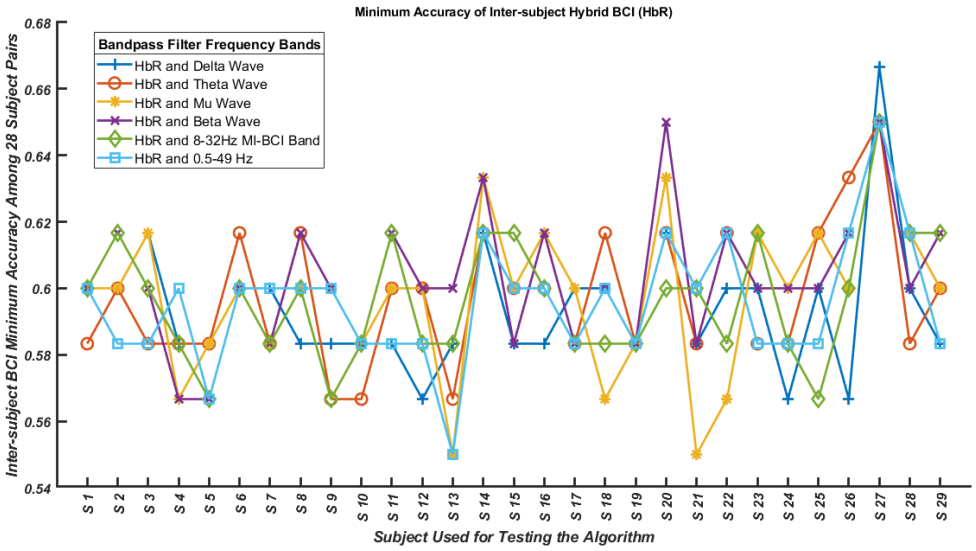

Figure 3.20: Minimum Accuracy of Hybrid Inter-subject BCI (HbR). The X-axis shows the testing subject number, and Y-axis is the minimum of inter-subject classification accuracy. The minimum accuracy is the minimum among 28 inter-subject pairs for each testing subject. The six different lines show accuracy for each of the six EEG and HbR combinations.

similar standard deviations across different testing subjects. Hence, in this regard, there are no clear superior methods to report. Figure 3.11 shows the maximum classification accuracy for each of the testing subject. The maximum accuracy in the figure is the highest accuracy among the twenty-eight inter-subject pairs tested for each subject. It is expected that the fNIRS concentration that shows the greatest number of maximum accuracies among the twenty-nine testing-subject will be considered better and be preferred for real-life implementation. From the Figure 3.11, we can see that HbO yields the best performance for seven subjects, HbR provided the best performance for three subjects, HbT yields the best performance for four subjects, and the maximum classification accuracy value is tied for the rest of the subjects. Hence, in terms of maximum classification accuracy, we can say that HbO is the clear winner. Figure 3.12 shows the minimum classification accuracy for the twenty-nine testing subjects. The reported minimum accuracy is the minimum among the twenty-eight inter-subject pairs. From the figure, we can see

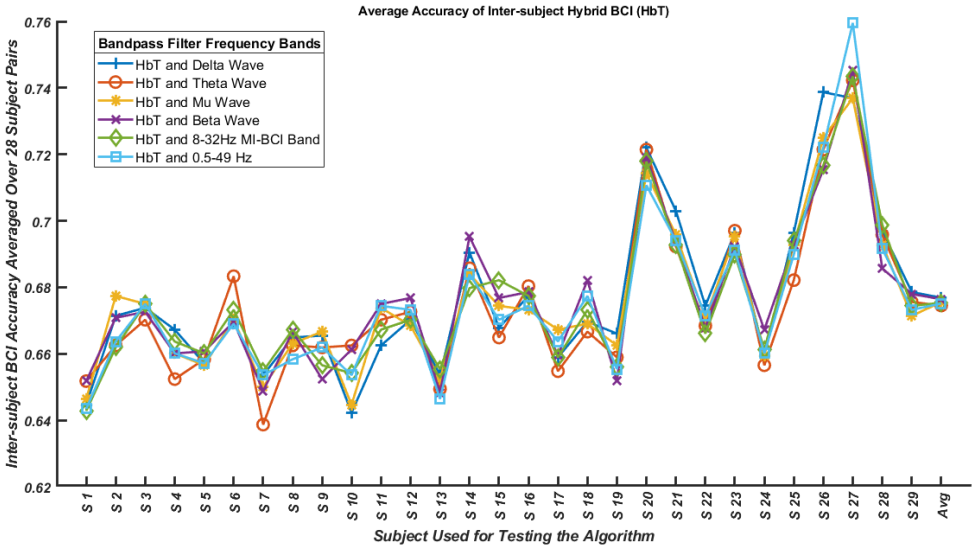

Figure 3.21: Average Accuracy of Hybrid Inter-subject BCI (HbT). The X-axis shows the testing subject number, and Y-axis is the average inter-subject classification accuracy. The accuracy is averaged over 28 inter-subject pairs for each testing subject. The six different lines show average accuracy for each of the six EEG and HbT combinations.

that HbO yields the highest values among the minimum accuracies for eight subjects, HbR provided top values for three subjects, HbT provided the best performance for four subjects, and for the rest of the subjects, we have a tie. Hence, we can clearly say that HbO is performing better in terms of both maximum accuracy and minimum accuracy. Let's look back at Figure 3.9 again and see which fNIRS concentration is performing better among the three. We can see that HbO yields the highest average accuracy for thirteen subjects, while HbR showed the best performance for three subjects. HbT yields the best average accuracy for five subjects, and for the rest of the subjects, we have a tie. Best of the results shown in Figure 3.9, Figure 3.10, Figure 3.11, Figure 3.12, we can clearly make the decision that a BCI system designed using only HbO concentrations are expected to perform better on an average that HbR standalone system and HbT standalone system. We haven't compared the accuracy performance of a combined system due to resource shortage since the experiment is highly time-consuming especially because of the

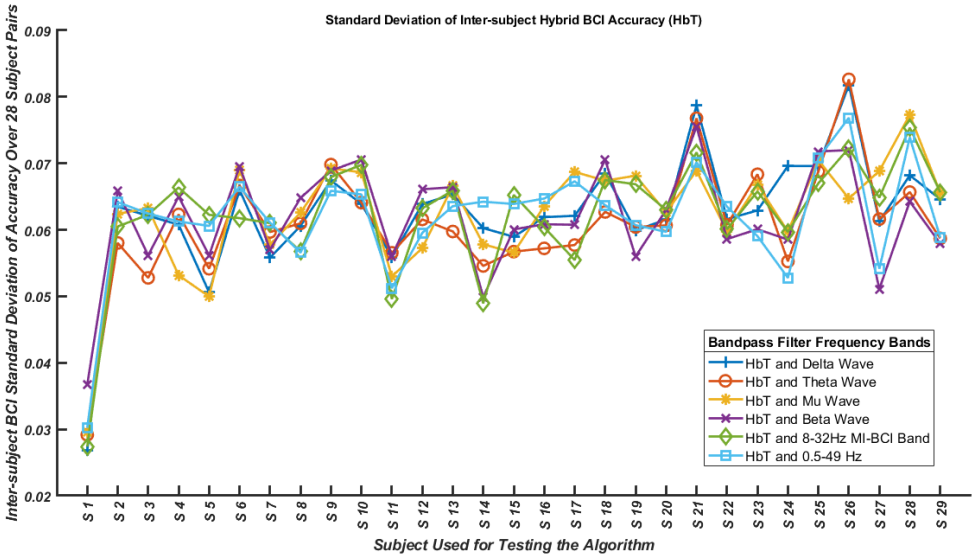

Figure 3.22: Standard Deviation of Accuracy of Hybrid Inter-subject BCI (HbT). The X-axis shows the testing subject number, and Y-axis is the standard deviation of inter-subject classification accuracy. The standard deviation is achieved over 28 inter-subject pairs for each testing subject. The six different lines show accuracy for each of the six EEG and HbT combinations.

use of LSTM based deep neural network for classification.

Figure 3.13 to Figure 3.24 shows the MI_BCI classification performance for the hybrid system. The figures are divided into three groups. The first group, Figure 3.13 to Figure 3.16, shows the classification performance for the hybrid system where the six EEG frequency bands are combined with the HbO concentration to form the hybrid combination. The second group of figures, Figure 3.17 to Figure 3.20, shows the classification performance for the hybrid system where HbR is combined with the six EEG frequency bands to get the hybrid combination. In the last group of figures, Figure 3.21 to 3.24 shows the classification accuracy comparison for hybrid BCI, where the hybrid features are achieved by combining features from HbT concentration and the six distinct frequencies of EEG. Figure 3.13 shows the average classification accuracy for the hybrid system (HbO) where each line of the graph shows the results for each combination. The legends show the name of the combinations. As we can see that the classification accuracy is higher for the last few subjects, and the accuracy is much lower for the first few subjects. These characteristics of the result are more reflective of the performance achieved using HbO based fNIRS system. Among the six different EEG frequencies, we can see that the classification accuracy is not very different anymore compared to what we observed in Figure 3.5. In Figure 3.5, we have seen a large variation in the classification accuracy for different EEG frequencies. However, in Figure 3.13, that characteristic or variation is not present, and the classification accuracies are more representative of the fNIRS concentration. Hence, we can make the claim that the classification accuracy for HbO and EEG based hybrid systems will be more representative of the classification accuracy of HbO. Also, the variation in terms of average performance for different combination is not evident enough to make a claim that this EEG frequency band is performing better than the others when combined with HbO concentrations.

Let's look at the standard deviation of the accuracies over the twenty-eight inter-subject pairs. Figure 3.14 shows the standard deviation of the HbO-EEG hybrid system. Again, the standard deviation of the performance is not representative of the EEG based system; rather, it is a combination of both the HbO-EEG system with a large similarity with the standard deviation of HbO based system. The variation of standard deviation among different EEG frequencies are also not diverse enough to make any claim on which EEG frequency performs better when combined with HbO. Let's hope for the maximum and minimum frequency graph. Figure 3.15 and Figure 3.16 show the maximum and minimum classification accuracy for the HbO-EEG hybrid BCI system, respectively. The maximum performance shows a better representation of the EEG wave performance while the minimum performance shows a better relation of HbO concentration performance. Again, the differences in the performance of EEG frequencies are not consistent enough to make a claim on which frequency is more suitable to combine with HbO. Finally, based on the results reported in the figures, we can say an HbO is a more prominent feature when combined with EEG. One of the reasons for that is we have extracted more features for fNIRS while we had a smaller number of features for fNIRS. Also, although we have normalized the features before combining them so that we can remove any unnecessary bias in the features, we might not have been able to clearly remove the effect of the different types of features. Even though the features were normalized, they had their effect on the combined feature matrix, and that effect has been clearly found on the classification performance of the hybrid system. However, this is not a firm claim since we have discussed the effect of HbR concentrations and HbT concentrations in the classification accuracy. The results of the later parts might open a new window for discussion into the trend of the results.

Figure 3.17 to Figure 3.20 shows the classification performance for the hybrid system formed by combining features of HbR or de-oxy hemoglobin concentration, and the EEG signals separated into different frequency bands. Figure 3.17 shows the average accuracy for the testing subjects averaged over their twenty-eight inter-subject pairs. A trend like HbO is found for HbR based hybrid system. The classification accuracy is following the trend of HbR performance. The average performance seems like a combination of both; however, the effect of HbR is dominant. Hence, we can say that the hybrid system is more dependent on the features generated from HbR concentrations. If we look at the individual performance of the EEG frequency band – HbR combinations, there is no clear winner. While one combination shows the highest accuracy for several subjects, the other combination provides better performance for the rest of the subjects. Figure 3.18 shows the best standard deviation of the performance for the subjects. We can see that the standard deviation has been more consistent across all subjects compared to EEG and HbR. This shows that the system has become more stable with the combination of EEG and HbR. All the EEG frequencies are showing similar standard deviation. Hence, we cannot declare one frequency band is better for the fusion than other frequency bands. Figure 3.19 and Figure 3.20 shows the maximum and minimum accuracy performance across all the testing subjects. One important finding from the figures is that the system has become more stable across different testing subjects, which makes the hybrid system more suitable for real-life implementation than the stand-alone systems. Subject S1 is performing very bad for both HbO and HbT based hybrid systems in terms of maximum accuracy. The same trend has not been found for minimum accuracy performance. Finally, we can say that when EEG signals are combined with HbR concentrations, the resultant hybrid system becomes more representative of HbR performance, and the system become more stable across different subjects.

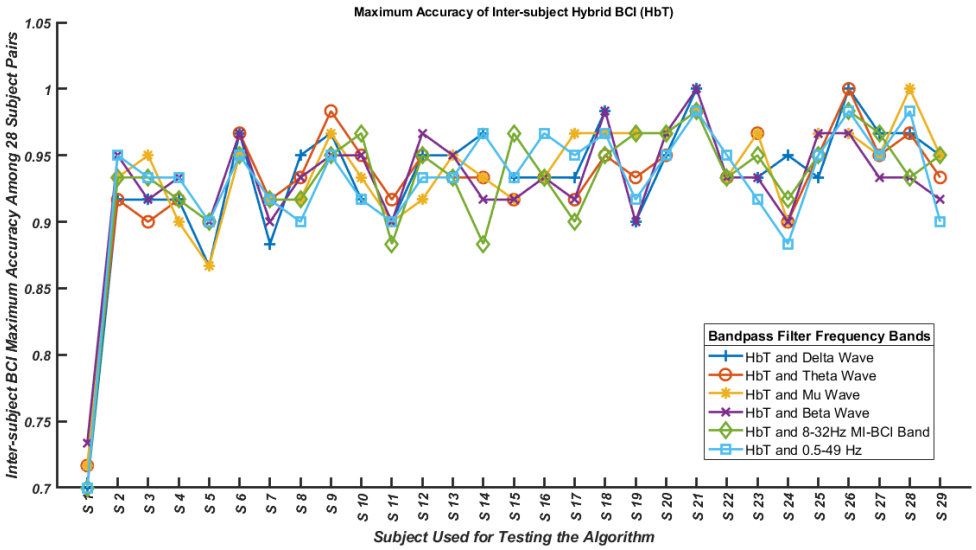

Figure 3.23: Maximum Accuracy of Hybrid Inter-subject BCI (HbT). The X-axis shows the testing subject number, and Y-axis is the maximum of inter-subject classification accuracy. The maximum accuracy is the maximum among 28 inter-subject pairs for each testing subject. The six different lines show accuracy for each of the six EEG and HbT combinations.

Figure 3.21 to Figure 3.24 presents the classification performance for the hybrid system generated by combining the HbT concentration with EEG frequency band signals. The classification performance is slightly better than the other two combination system. Figure 3.21 shows the average accuracy of the HbT based hybrid system. The top accuracy result has been increased in the HbT based system. Same as the HbO based system and HbR based system, the classification accuracy is following the trend of HbT standalone accuracy. Also, the classification performance across different frequency bands doesn't change by a large margin, and we cannot claim that one frequency band is more suited for the hybrid combination than the other. The standard deviation shown in Figure 3.22 shows a similar performance of the other two combinations. The system has become more stable across different frequency bands and different testing subjects. A similar performance like HbO and HbR has been observed for the maximum and minimum accuracy shown in Figure 3.23 and Figure 3.24, respectively. The classification

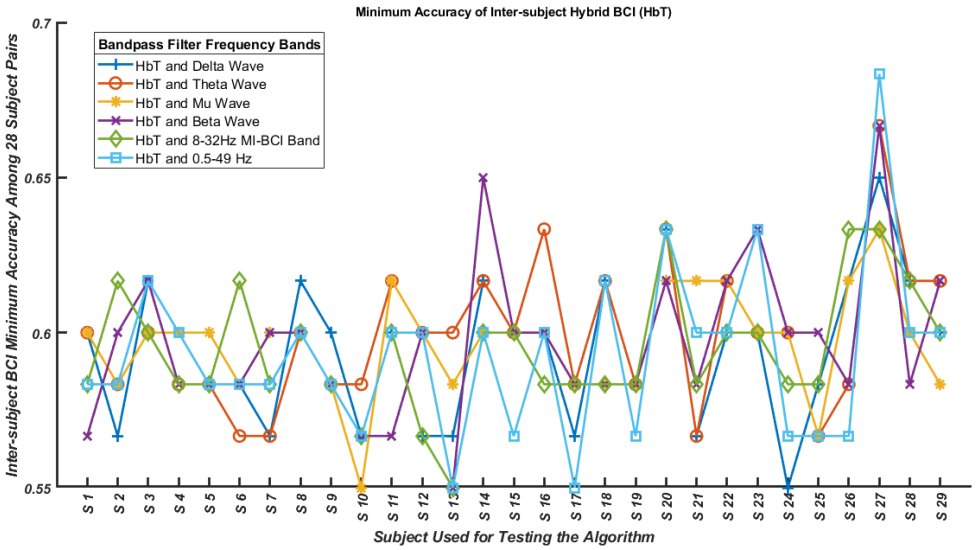

Figure 3.24: Minimum Accuracy of Hybrid Inter-subject BCI (HbT). The X-axis shows the testing subject number, and Y-axis is the minimum of inter-subject classification accuracy. The minimum accuracy is the minimum among 28 inter-subject pairs for each testing subject. The six different lines show accuracy for each of the six EEG and HbT combinations.

performance is following the performance of the standalone HbT system, and the system has become more stable.

Finally, based on the results, we can say that the hybrid system is more suitable for application is across subject experiments especially because of its ability to become a more stable system. The classification performance may or may not improve from the standalone systems, but the systems' stability will certainly increase.

In this study, it is evident that the best output is that for hybrid, while EEG shows lower performance. However, the performance variation is low for EEG and fNIRS. For EEG, the average for the set of classification accuracies is 0.6620, which is the lowest accuracy. The average accuracy range in the case of fNIRS is higher than that for EEG. Although EEG and fNIRS are somewhat similar techniques with no exact evidence for one being proposed

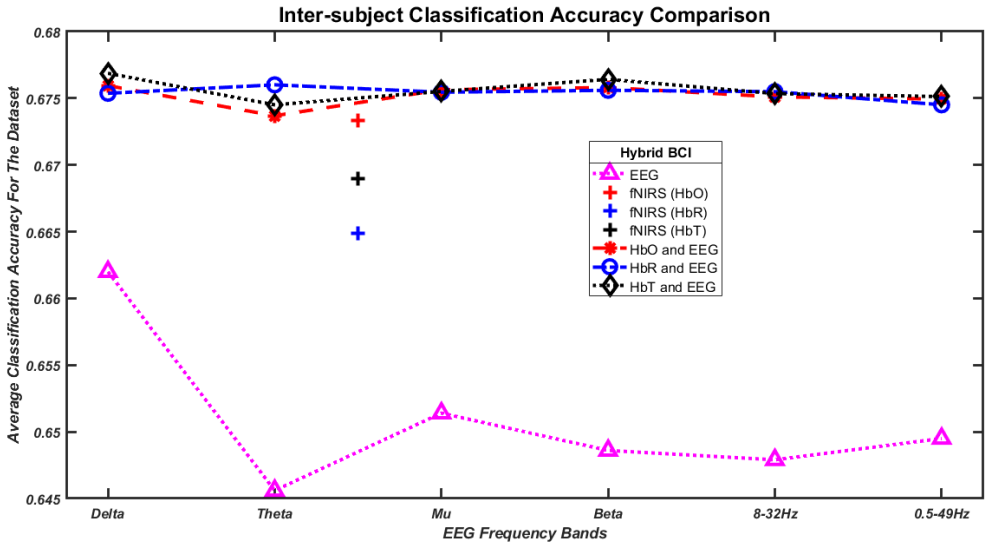

Figure 3.25: Performance Comparison of Inter-subject BCI For the Dataset. The X-axis is the different EEF frequency bands and Y-axis is the classification accuracy. The different line and markers show different types of BCI designed for the study.

experiment fused the features from EEG and fNIRS by creating a feature matrix with same with similar dimensions for each modality and then combine the features into a single matrix with combined dimension. During this fusion, it is assumed that the features are correlated for a BCI task, and the combined feature matrix would better differentiate the classes. From the results, our assumption holds perfectly, and the increased classification accuracy is proof of that. The classification accuracy comparison across different modality has been provided in Figure 3.25. The figure shows the average accuracy of each of the modalities and filtering frequency bands. As we can see, the highest average classification accuracies are obtained for the hybrid combinations. Although the average performance of the hybrid system is comparable, we can see that hybrid combination made with total hemoglobin concentration (HbT) and the different EEG bands performs the best among others. The best performance is obtained for HbT-Delta and HbT-Beta combination.

The classification accuracy improvement for the hybrid system in comparison to the EEG -based system is significant; however, this does not show the actual scenario of the improvement. The comparison with the average accuracy of fNIRS based system and the Hybrid system shows the actual improvement of the classification performance while using hybrid BCI. We have the most significant improvement for HbR based BCI comparing with HbR-EEG based system. The lowest improvement is achieved for HbO based BCI comparing with HbO-EEG. HbT-EEG based system shows the highest BCI performance but not the most significant improvement from the HbT based system. Based on the results, we can claim that our proposed hybrid system can improve the classification performance compared to the stand-alone systems.

Figure 3.26 shows a box-plot comparison of the classification performances across different BCI systems. The figure further strengthens our claim on the performance improvement using a hybrid system. Based on the results shown in Figure 3.25 and Figure 3.26, we can say that the highest classification accuracy improvement is an average of 1.2%, which is not a significant improvement in the classification performance. However, if we consider the overall performance of the hybrid-based systems compared to a single modality-based system, the hybrid system has become more stable in terms of accuracy fluctuation across subjects and frequencies. The obtained results and analysis show the suitability of the proposed algorithm for the implementation of the inter-subject hybrid BCI using simultaneous EEG and fNIRS recordings.

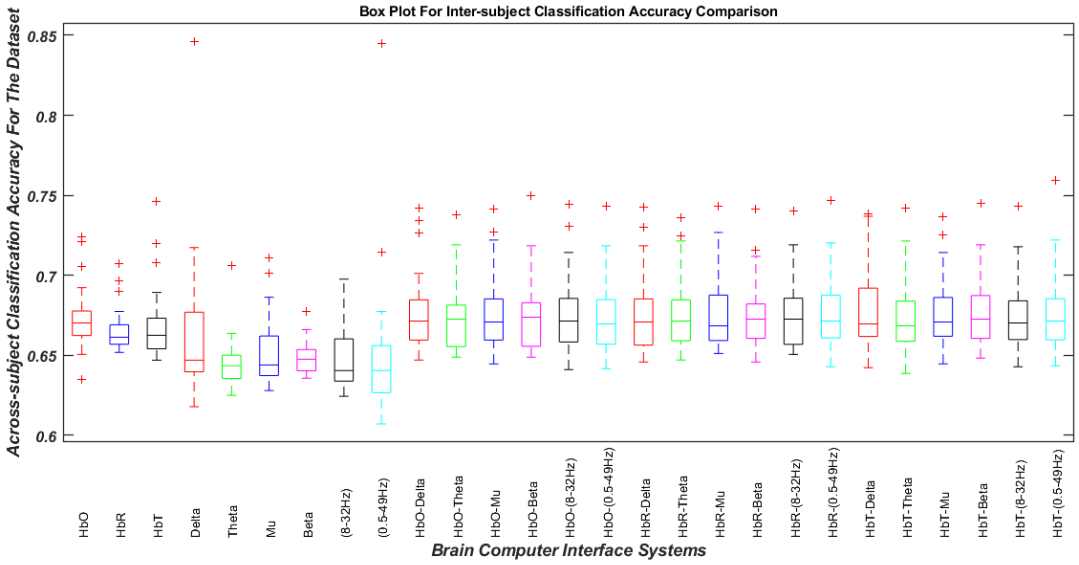

Figure 3.26: Box Plot Performance Comparison of Inter-subject BCI For the Dataset. The X-axis is the different BCI combinations and Y-axis is the classification accuracy. The bars show the range of the classification accuracy and the markers shows the outliers in each category.

Although the obtained accuracy is notable, attaining very high accuracy in inter-subject BCI is comparatively tight due to the variation of brain dynamics from person to person. Apart from the brain dynamics, there might be several impediments for the modest accuracy outcome, which may include the insufficiency in the computational approaches to merge the different features, mismatch in the temporal resolution of the two modalities, or hemodynamic responses delay. This might be enhanced by further investigation of the better correlation between the features of EEG and fNIRS.

3.4 Summary of Study 3

Hybrid brain-computer interface, hBCI commonly yields better classification accuracy by overcoming the drawbacks of a single BCI system. In our study, the EEG and fNIRS signal recordings of twenty-nine subjects were used to show that the inter-subject hybrid BCI

integrating these two modalities improves the accuracy. We have further shown that the hybrid modality based BCI system is more stable and robust for across subject variation of human brain dynamics. Hence, the proposed system can be a better candidate for the implementation of inter-subject BCI systems for better performance with reduced subject-specific training. This present study can be perceived as the first step towards the development of a technique for a universal subject independent BCI design.

CHAPTER IV

MICROWAVE BASED NON-INVASIVE GLUCOSE CONCENTRATION DETECTION BY MACHINE LEARNING

4.1 Introduction

The World Health Organization has predicted that the worldwide number of diabetes patients will increase by up to 550 million in the next ten years [134-135]. People with diabetes require frequent measuring of blood glucose levels. The traditional measurement methods using hand piercing are inconvenient and painful and cannot monitor the blood sugar level in a continuous way. Moreover, some people might have a phobia towards blood and needle piercing. There are other methods for glucose monitoring that requires saliva or iris drop. Both methods are discomforting to the user and might have a risk of infection. Hence, it is important to find a method that can avoid the above-mentioned difficulties and provide a comfortable measurement of blood glucose monitoring. Non-invasive methods are often considered as a solution to the above-mentioned difficulties and a way to monitor blood glucose continuously. Finding more comfortable and non-invasive glucose monitoring systems has led to an increased interest in non-invasive detection techniques using impedance spectroscopy, near-infrared spectroscopy, saliva, and millimeter-wave wearable sensors [134]. This work is focused on designing a non-invasive glucose monitoring system using a microwave signal.

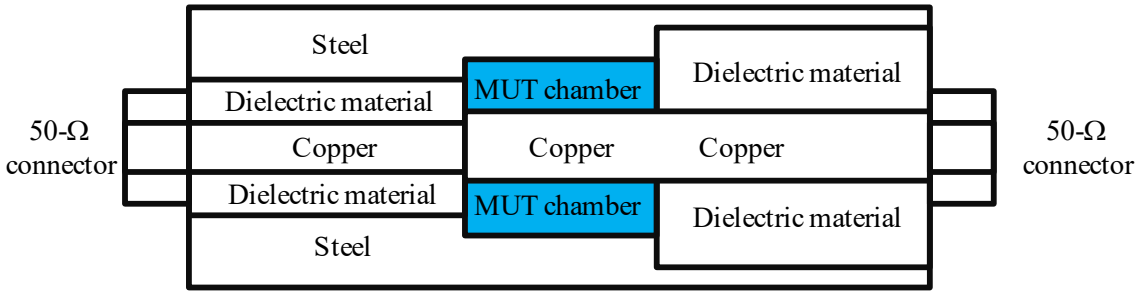

Figure 4.1: Three-segment model of N-type microwave adapter pair.

Microwave signals can harmlessly penetrate human tissue and provide important information about the medium. Microwave detection is especially widely studied among these approaches [136-139] due to its appropriate penetration depth and convenience in sensor design. Most of the reported works on the microwave approach are often focused on the deterministic measurement of dielectric parameters of glucose solution using various Debye relaxation models, whereas the sample solutions are set outside of the human body [136-137]. Some other work simply directly measured the variation of S11 or S21 coefficients or the system resonant frequencies and tried to correlate them to the glucose concentration changes [138-141]. [140-141] utilized a feature extraction-based method to determine glucose concentration; however, the works had not proposed a system that has very high accuracy or correlation values. These deterministic studies have indicated that glucose level does produce a definite change in dielectric properties. However, the variation of the glucose level within the human physiological range is less than a few hundred mg/dL (typically 60-700 mg/dL), among which the dielectric is not sensitive enough to the small variation of glucose concentration. It is still challenging for the deterministic methods to confirm a clear correlation between the dielectric properties and the glucose levels.

In this work, we report an alternative approach to use machine learning classification based on the large set of features extracted from the measured scattering parameters (S11) on the glucose solution with various concentrations. The hypothesis is that given enough glucose measurement data, machine learning-based approaches can model the relationship between the measurement data and measured glucose concentration, and the model can be used to detect glucose concentration from solution with unknown concentrations. In other words, in this work, we are trying to use machine learning algorithms to learn the characteristics of S11 parameters measured for different glucose concentrations and use that information to classify glucose concentrations from unknown solutions.

4.2 Experimental Methods

4.2.1 Microwave Data Description

An N-type microwave adapter pair was utilized to measure the S11 parameters of the glucose solutions with variable glucose concentration. The S11 parameters were measure using a frequency sweep from 10 MHz to 18GHz. The solution was an aqueous glucose solution with binary concentration (fixed concentration). They have prepared solutions for ten separate glucose concentrations. The concentrations are 0 mg/dL or pure water, 50 mg/dL, 100 mg/dL, 150 mg/dL, 200 mg/dL, 250 mg/dL, 300 mg/dL, 400 mg/dL, 500 mg/dL, 1000 mg/dL. We know that the normal glucose concentration range for the human body is usually in the range of 60 mg/dL to 700 mg/dL. The concentration can vary sharply depending on the time, mood, health condition, eating habits, etc. Hence, we have selected a variety of glucose concentrations with changes amount them being a variable number. The adaptor pair was modelized into a three-segment coaxial transmission line (Figure 4.1, Figure 4.2) to accurately determine the S-

parameters. S-parameters vary with the complex dielectric of the glucose aqueous solution filled inside the adapter chamber. Six Debye dielectric parameters (infinite frequency permittivity $\varepsilon_{r\infty}$, $\Delta\varepsilon_{r1}$, $\Delta\varepsilon_{r2}$, the relaxation time $\tau 1$ and $\tau 2$, and low-frequency conductivity σ) were then retrieved from the measured wideband complex S-parameters:

$$\varepsilon_r(\omega) = \varepsilon_{r\infty} + \frac{\Delta\varepsilon_{r1}}{1 + j\omega\tau_1} + \frac{\Delta\varepsilon_{r2}}{1 + j\omega\tau_2} + \frac{\sigma}{j\omega\varepsilon_0} \qquad (4.1)$$

The glucose concentrations vary from 0 (pure water), 50, 100, 150, 200, 250, 300, 400, 500 to 1000 mg/dL. In the original experiment with the solution, each concentration was measured six times. These low numbers of samples are possible drawbacks for implementing machine learning algorithms. Because machine learning algorithms are often data-driven algorithms and require lots of training samples to provide acceptable performance. To solve this problem, we have proposed to create additional data samples from the original recordings by adding gaussian noise to the original recordings.

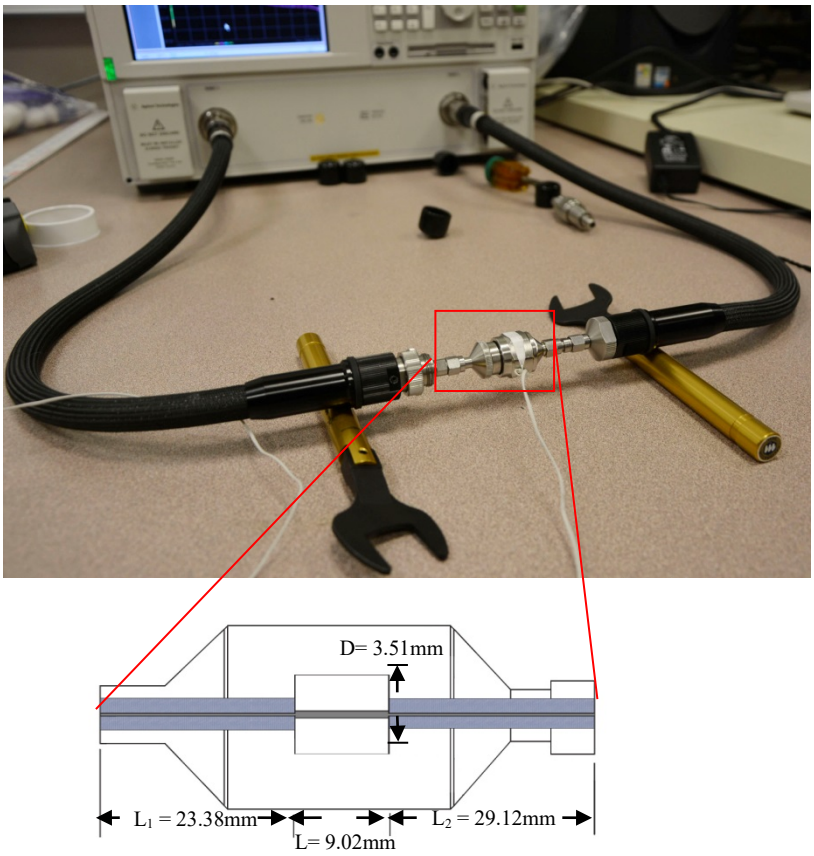

Figure 4.2: The Measurement System and Geometry of the Connector with Dimensions.

There are several ways to generate additional data samples from the original recordings. One way is that we can simply replicate the number of trials and create a larger dataset. However, this type of dataset will not provide good performance and suffer from overfitting since all the data samples will be known to the algorithms, even the trials which are used for testing. Other ways are using an artificial neural network to generate an additional dataset from the original dataset. This process is sophisticated, and the performance of the process depends on the availability of a good number of data in the beginning. Since we have only six trials per concentration, this method was not feasible for our problem, and one of the requirements of the project was to design a simple algorithm. Another possible way was to add synthetic noise to the replicated dataset and get a fairly different dataset. That would serve the purpose; however, no such

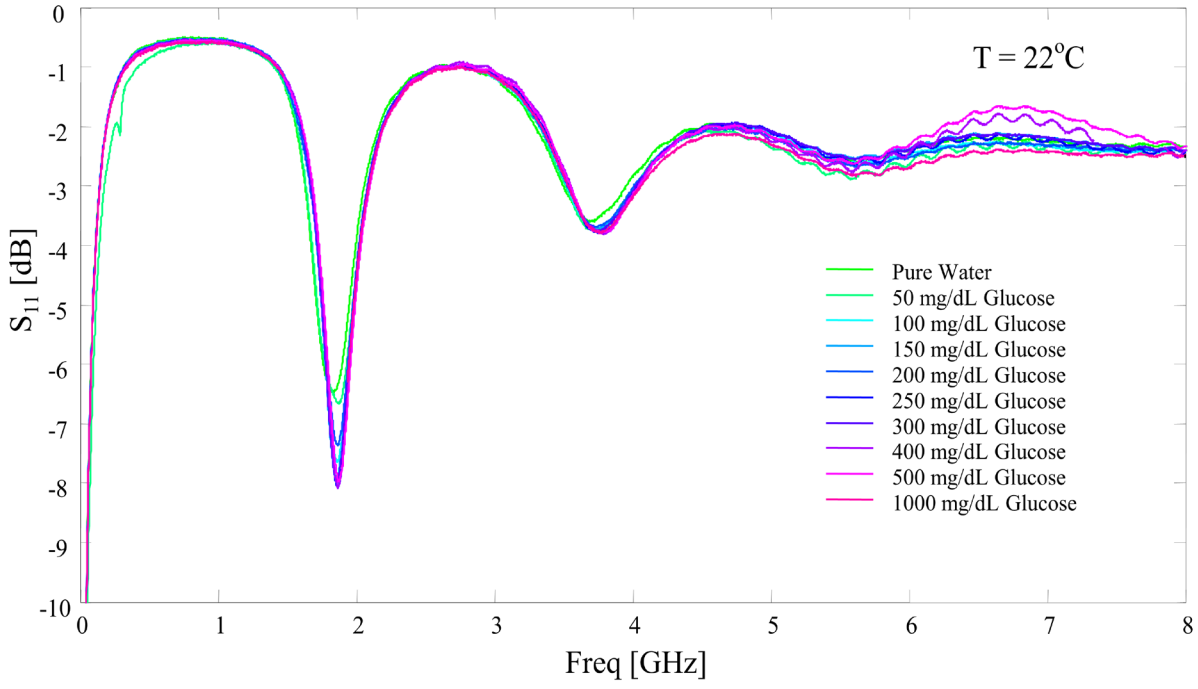

Figure 4.3: Measured S11 for the glucose aqueous solutions with various concentrations.

synthetic noise was available for this type of application. Another way is to generate additional samples by using dielectric parameters and Gaussian noise. In this method, Gaussian noises at various levels were added to the extracted Debye dielectric parameters to create two large datasets. The generated dataset has two distinct advantages. One, the generated samples are not the same for each of the trials. Two, the generated dataset is heavily distorted with noise, which helps us to realizes the noise generated by human muscle activity and tissues. Finally, the generated dataset was feed to the machine learning algorithms for the glucose concentration classification.

Two datasets of 240 trials per concentration were created with a total of 2400 trials for ten concentrations for training and another 2400 for validation. Figure 4.3 shows a set of measured S11 frequency sweeping data for the aqueous glucose solutions with various concentrations. The S11 curves shown in Figure 4.3 are the dB-scale magnitude plots of the measured broadband complex S11 signals. The raw complex signals are quite different in phase shift. The dips are determined by the actual geometry of the N-type adaptor chamber, as shown in Figure 4.2. We can see the slight magnitude shift around the dips with varying glucose concentrations. We can see from the S11 magnitude plots in Figure 4.3 that the changes in the S11 magnitude are fairly small. This small change is often hard to characterize with a deterministic equation or model-based methods. As we can see, there are only sharp changes in the deeps and the slopes. Tracking these sharp changes for deferent glucose concentrations is a tough job for deterministic methods. Hence, it was important to look for alternatives algorithm to study the S11 graphs to accurately detect the glucose concentration. We have already mentioned that the aqueous solutions had binary glucose concentrations, which means the concentration for a solution is fixed. However, this is not the scenario for the actual blood glucose. Hence, the importance of

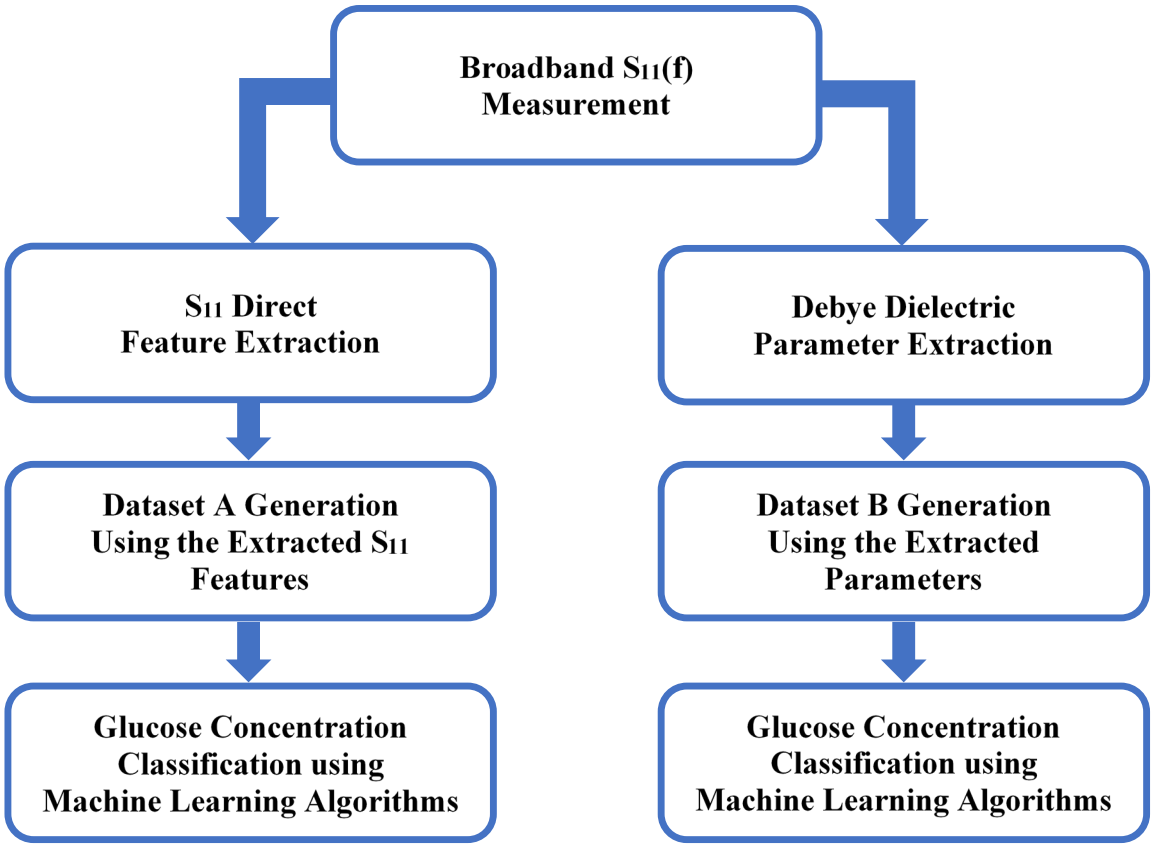

Figure 4.4: Flowchart of the Classification System.

using artificial intelligence is a necessity to detect the concentrations accurately. As this study is mainly focused on the test to see if the statistical methods could work on glucose concentration detection, in this work, the data was truncated at 10 MHz to 8GHz, although the measurement was done for up to 18 GHz. This could be done since this frequency range already included most features.

4.2.2 Classification Arrangement

Two different datasets were created: dataset A was created from the directly measured broadband S11 parameters (6401). Twelve features were extracted from the dataset A. The features are as follows,

- Four slopes of the S11 coefficient graph.
- Peak to RMS difference of the graph.
- The variance of the S11 magnitude.
- Amplitude range.
- Standard deviation.
- Arithmetic average or mean.

Dataset B was created from the extracted Debye dielectric parameters from S11 parameters. From the original six trials per concentration, 240 trials were created for each concentration by adding different levels of Gaussian noise for both datasets. Several machine learning-based classification algorithms were then applied to both datasets each at a time to obtain the classification accuracy. The noise level in training and testing data is changed. The noise was added with MATLAB random number generator algorithm, which made sure that for the same noise level, the generated dataset is reasonably different. 10-fold cross-validation was adopted to validate the performance of the training algorithms and prevent the classifier from overfitting. Algorithms with the most significant classification accuracies are listed in the next section. Figure 4.4 shows a simplified flowchart of the classification system.

Among all the tested machine learning algorithms, four methods showed the best accuracies: Decision Tree Classifier (DTC), Bagged Tree Ensemble Classifier, Cubic Kernel-based Support Vector Machine (Cubic-SVM), and Linear Discriminant Analysis (LDA). The decision tree classifier performs well when a large number of training samples can be provided. A decision tree classifier continuously splits the training dataset until a decision is made on the output class [142]. In our dataset, we have generated a large number of samples to make it a perfect case for DTC. LDA yields linear discriminant functions by modeling training features within each class

as normally distributed with a common covariance matrix [143]. SVM constructs an optimal hyperplane known as decision surface so that the margin of separation between two classes in the data is maximized. It uses support vectors containing a small subset of training data to determine the optimal position of the hyperplane boundary [144]. The classifier mentioned above can provide excellent classification performance by learning class-specific features independently. In some cases, combining all the learners from different algorithms could yield even better classification performance. Ensemble classifier combines previously trained weak learner models and training data and predicts the ensemble responses for new data by aggregating responses from weak learners [145]. The ensemble classifier needs a weakly learned model to combine the model and generate a better one. For our case, the input learners to Ensemble classifiers are various combinations of DTC, SVM, and several discriminant analysis methods. All the input learners provided a consistent performance, and the Ensemble classifier provided the best performance by combining input from the other learners. The following four sub-sections are dedicated to the description of all the four classification methods that showed the best performance.

4.2.3 Support Vector Machine (SVM)

Support vector machines (SVMs) with the cubic kernel is used to classify the glucose concentration from the extracted features. Support vector machines (SVMs) is a supervised machine learning algorithm popular as a classification technique for increasing the margin between the given data and distinguishing hyperplane via decreasing the upper value of the generalization error. Shortly after the invention of SVMs by Vapnik [146] it became the most used machine learning algorithm for binary classification. SVM tries to create an optimal hyperplane separating two classes in a way so that the margin of separation between classes is

maximized. Let's consider the following training set to understand how the SVM creates the separable pattern,

$$\{(f_i, d_i)\}_{i=1}^{N} \qquad (4.2)$$

Here d_i is the target corresponding to an input vector f_i of n dimension. $d_i = 1$ represent the input pattern for a positive group while $d_i = -1$ represents the input pattern for the negative group. Based on the input patterns and the target class, we can select an optimal separating hyperplane from a pool of possible hyperplanes. The decision surface can be described as $w.f + b = 0$. In the equation, *w* is the weight vector that can be regulated, and *b* is the bias. We can write the equation for the separating hyperplane as $w.f + b \geq +1$ for a positive group of data and $w.f + b \geq -1$ for a negative group of data. These two equations can be combined [147] as

$$d_i(w.f + b) - 1 \geq 0 \qquad (4.3)$$

The distance from the starting point to the optimal hyperplane is $\frac{(\|b\|)}{(\|w\|)}$ and $(\|w\|)$ is the Euclidean norm of the w. We can write the optimized [147] equation for the given training samples to be solved to w and b as follows

$$Min\, J(w, b, e) = \frac{1}{2} w^T w + \frac{1}{2} c \sum_{i=1}^{l} e_i^2 \qquad (4.4)$$

Subject to the constraints:

$$d_i(w^T \Phi(f_i) + b) \geq 1 - e_i,\ e_i \geq 0\ for\ i = 1, \ldots\ldots, l \qquad (4.5)$$

In the equation 4.4, the cost function is given by the variable *J*. *C* referred to as the regularization parameter, and e_i is the classification error. This type of SVM used a linear decision boundary for the classification and referred to as linear SVM. However, for our problem, we have used a nonlinear decision boundary as the classification boundary for glucose detection. This nonlinearity in the decision boundary can be achieved by increasing the complexity of the

classifier using the kernel trick [148]. For our experiment, we have used polynomial (cubic) kernel function with a third-degree polynomial to achieve a cubic kernel function [149].

The kernel is defined $K(f, f_i) = \Phi(f)^T \Phi(f_i) = (f^T f + 1)^n$

Here n is 3 for cubic kernel function [149].

4.2.4 Linear Discriminant Analysis (LDA)

Linear discriminant analysis (LDA) is a dimensionality reduction technique that reduces the number of dimensions (features) in a dataset while retaining as much information as possible. Let's consider a dataset contains two features. In the usual feature reduction methods, we can simply ignore one of the feature dimensions to projects the features in a signal dimension. However, this method will be considered as a wrong method since it will ignore the information provided by the other feature dimension. On the other hand, in LDA, information from both features are utilized to generate a new axis, and the data is projected on the newly formed axis. This new representation minimizes the variance and maximizes the distance between the means of two classes. For our experiment, a multiclass LDA classifier is used to classify the ten classes of glucose concentration. LDA is widely known for its simplicity and used for classification in various fields. It shows a good compromise between computational cost and classification performance. Let $x_k \in R^2 (k = 1,2,3, \dots 240)$ denotes the samples, μ_i be the sample mean of class i, and μ be the total mean of all the samples [150]. That is

$$\mu_i = \frac{1}{n_i} \sum_{x \epsilon c_i} x, \mu = \frac{1}{n} \sum_{xi} xi \,, \qquad (4.6)$$

Where n_i is the number of samples of class i, and n is the total number of samples.

Then, the multiclass LDA problem is to find the optimal projection matrix V that maximized the following Fisher's criterion,

$$J(V) = \frac{\det(V^T S_B V)}{\det(V^T S_W V)} \qquad (4.7)$$

Where S_B and S_w are the between-class scatter matrix and the with-in class scatter matrix, respectively, defined by,

$$S_W = \sum_{i=1}^{m} \sum_{x_k \epsilon\, class\ i} (x_k - \mu_i)(x_k - \mu_i)^T \qquad (4.8)$$

$$S_B = \sum_{i=1}^{m} n_i\, (\mu_i - \mu)(\mu_i - \mu)^T \qquad (4.9)$$

Where m is the number of classes and for our work, we have ten classes. It is noted that a matrix V satisfying (equation 4.7) can be reformulated as a generalized eigenvalue problem as follows.

$$S_W^{-1} S_B V = \lambda V \qquad (4.10)$$

The optimal V is then the matrix corresponding to the most significant two eigenvalues of $S_W^{-1} S_B$. Finally, we have used Matlab classifier learners to train and test the classifier. 10-fold cross-validation is used for validation.

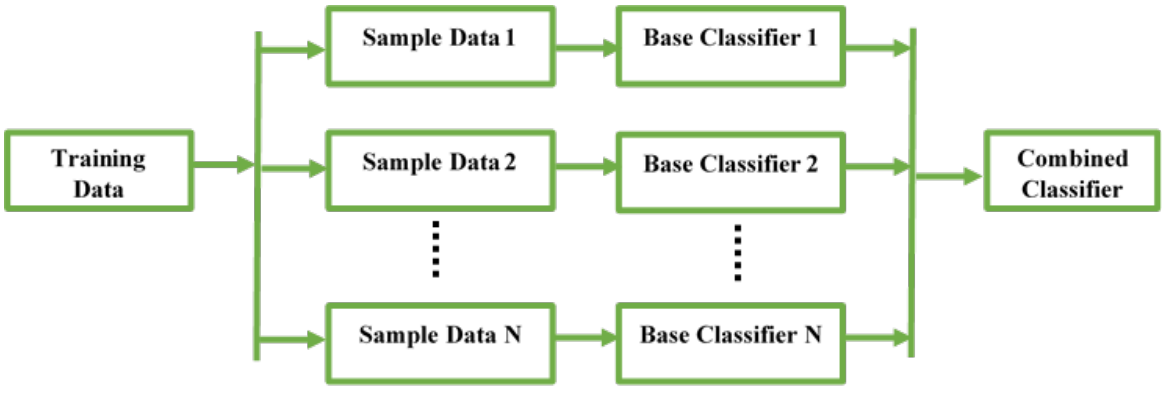

Figure 4.5: A simple flowchart for ensemble learning classifier.

4.2.5 Decision Tree Classifier

This algorithm constructs a decision tree with branches and nodes based on the feature vector set. A decision tree starts with a root node *r* derived from the feature that minimizes the distance in two sibling nodes [151]. The measure of the impurity at node r, denoted by $im(r)$, is shown in the following equation:

$$im(r) = -\sum_{i=1}^{m} p\left(\frac{w_i}{r}\right) \log p\left(\frac{w_i}{r}\right) \qquad (4.11)$$

Where $p\left(\frac{w_i}{r}\right)$ is the proportion of the patterns x_i allocated to class w_i at the node r. Eac none-terminal node is then divided into two further nodes, r_1 and r_2, such that p_1, p_2 are the proportions of the entities passed to new nodes r_1 , r_2 respectively. The most appropriate division is the which maximizes the difference given in the equation,

$$\Delta im(d, r) = im(r) - p_1 im(r_1) - p_2 im(r_2) \qquad (4.12)$$

The decision tree grows unto a phase when the difference cannot be further minimized with additional division d is implemented. When this phase is reached, the node r is not subdivided further, and automatically becomes a terminal node. The class w_i, associated with the terminal node r is that which maximizes the conditional probability $p\left(\frac{w_i}{r}\right)$. Eventually, in the testing phase, test samples are classified using the calculated optimal decision tree model [152].

4.2.6 Ensemble Learning Classifier

Ensemble learning is basically based on a combined decision over multiple learners. The working principle is the same as consulting with multiple doctors before deciding on surgery or making decisions on a product purchase based on reading the reviews. The aim of ensemble learning is like improve the confidence level before making the right decision. The block

diagram (Figure 4.5) can be referred for a better understanding [153]. In ensemble learning, multiple classifier learners are generated from training data and the decision from the classifiers combined to generate a final decision on the class. Ensemble architecture has root (training), several intermediate nodes referred to as intermediate classifiers, and leaf-node, also referred to as classification decision. An ensemble architecture is efficient for cases where there is diversity among base classifiers, which mean the individual learners commit an error on different instances. Diversity allows an ensemble classifier to exhibit higher accuracy than the average accuracy of its individual models. For our ensemble classifier, several types of SVMs, LDAs, Decision Tree classifiers are considered as base classifiers for the ensemble learning algorithm. Bagging boosting is used for ensemble learning. A highly popular independent ensemble

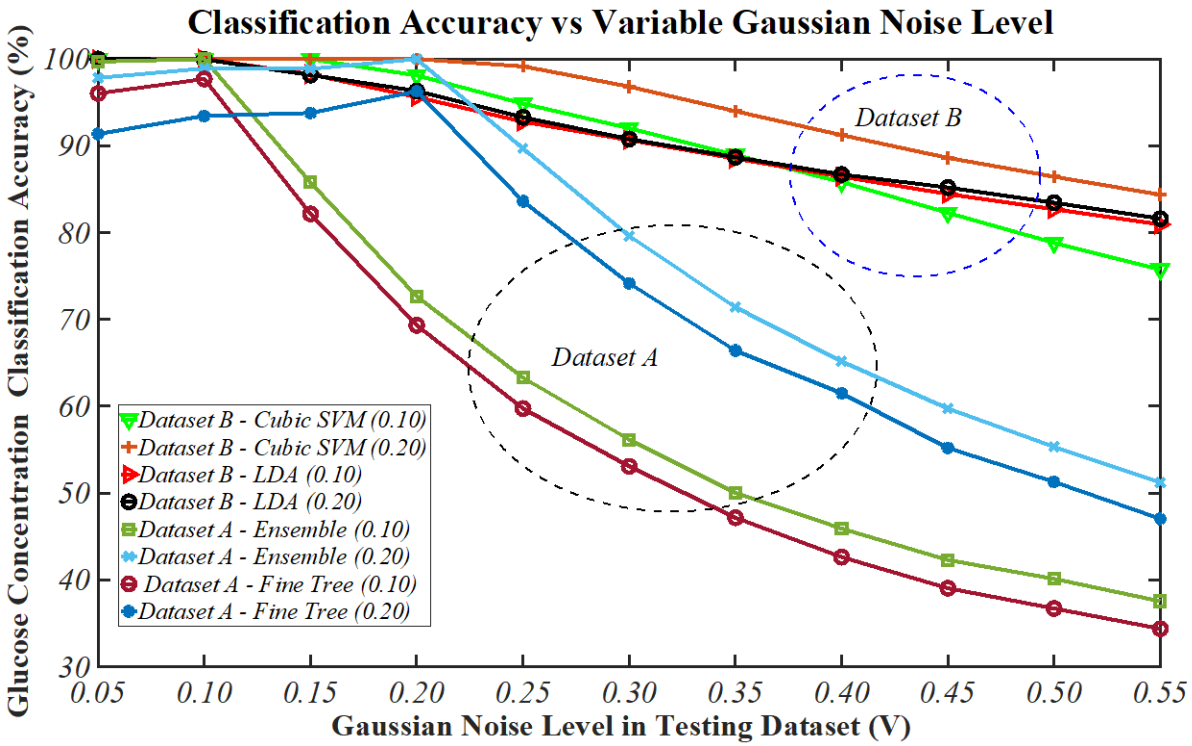

Figure 4.6: Comparison of classification accuracy with respect to change in Gaussian Noise Level (V).

classifier method is “bagging.” As per the theory of bagging, subsets are created by sampling with replacement method on the training set. “With replacement” means that some of the original instances may appear more than once in a bag subset. The size of the bag subset is less than the size of the actual training-set. So, a subset of training set may be different from each other. Multiple prediction models are built from different bags, and those models are used to classify unknown instances (test-set). The prediction outputs from all the bags are combined, and the final output is determined. The composite classifier (combined model of bagged classifiers) outperforms a single model for the same training-set.

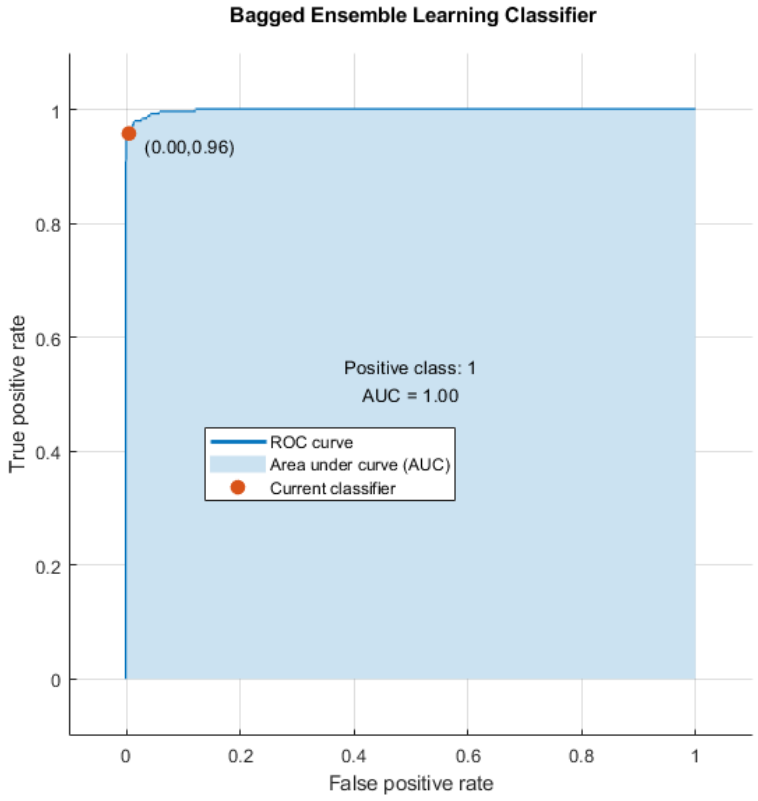

Figure 4.7: Area under the curve (AUC) for Bagging Ensemble Learning Classifier.

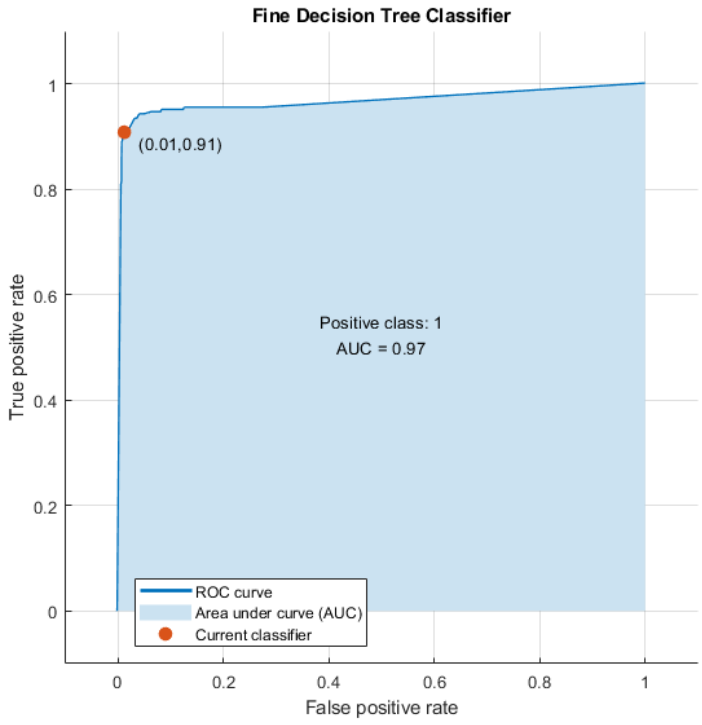

Figure 4.8: Area under the curve (AUC) for Fine Decision Tree Classifier.

4.3 Results and Discussions

The tested machine learning-based methods are data-driven and perform better if trained with a large dataset. The most used machine learning techniques have been used to classify the dataset and determine the glucose concentration levels and showed good classification accuracy. Among them, two methods, Fine Decision Tree (Highest recorded accuracy of 97.7% for noise level 0.10 in the training dataset and 0.20 in the testing dataset) and Bagged Tree Ensemble classifier (Highest recorded accuracy of 100% for noise level 0.10, 0.20 and noise level 0.10. and 0.20 in training and testing dataset respectively) resulted in the best performance for dataset A. Among all the methods employed on the dataset B, the support vector machine (SVM) with cubic kernel function and linear discriminant analysis (LDA) showed a perfect 100% classification accuracy for training dataset noise levels at 0.10 and 0.20 while the testing noise

level at 0.10, 0.15, and 0.20. Only the best results are presented here to remove complexity due to the large volume of data. The area under the curve (AUC) for bagged ensemble classifier (Figure 4.7), and fine decision tree classifier (Figure 4.8) is shown the figure. As the AUC curve suggests, the classification accuracy is 97% for fine decision trees and 100% for ensemble learning classifier. Figure 4.9 shows the confusion matric for cubic-SVM. As the figure shows, all the classes are perfectly classified as the true positive class, and the classification accuracy is 100%.

Considering the in vivo scenario that the scattering signals from the variation of the targeted glucose would be deeply buried inside the noise signals from the surrounding tissues, we have added Gaussian noises to the measured data to make the dataset more realistic. Various levels of Gaussian noises were tested to investigate their effect on classification accuracy. The noise level was incremented every six samples, with the varying noise level given $N(S) = 1.5 + V \times S$. Here, V is from 0.05 to 0.55, with an incremental increase of 0.05, and S varies from 1 to 40 and changes every six samples. The resulted dataset has different incremental noise levels for every six samples to test the robustness of the classification algorithm to the noise. The results indicate a strong correlation between classification accuracy and noise levels. Figure 4.6 shows the correlation between noise level and classification accuracy for different classifiers. As predicted, the classification accuracy decreases with the increase of the noise level. In Figure 4.6, the x-axis is the different V values for the noise added to the testing dataset, and each curve represents one training dataset, with V indicated in the parenthesis. The legends in Figure 4.6 are representing the noise level in training data. The table has information about the noise level in both training and testing data (Training level, Testing Level). It was found that as V exceeds 0.40, the S11 data starts to get heavily deformed by the noise, and the classification accuracy quickly drops

with the increased noise level for dataset A. On the other hand, the classification results using the features from dataset B shows evident higher robustness to the increasing noise and is more appropriate to be used for the classification in a realistic scenario. Even at high noise levels, some classifiers can still give satisfactory classification results (Table 4.1). The classification results in Table 4.1 indicate a perfect 100% classification accuracy when the noise parameter $V \leq 0.1$ for dataset A and $V \leq 0.2$ for dataset B.

Measured broadband data indicates that the changes to both S11 and dielectric properties are small, even with 50 mg/dL glucose concentration variation. It makes the conventional deterministic methods challenging to detect and determine the concentration change accurately. The proposed method can differentiate glucose concentration changes in 50 mg/dL ranges and also in 100 mg/dL ranges with very high classification accuracy. The study suggests a proposing way to develop the non-invasive glucose detection method using big data machine learning.

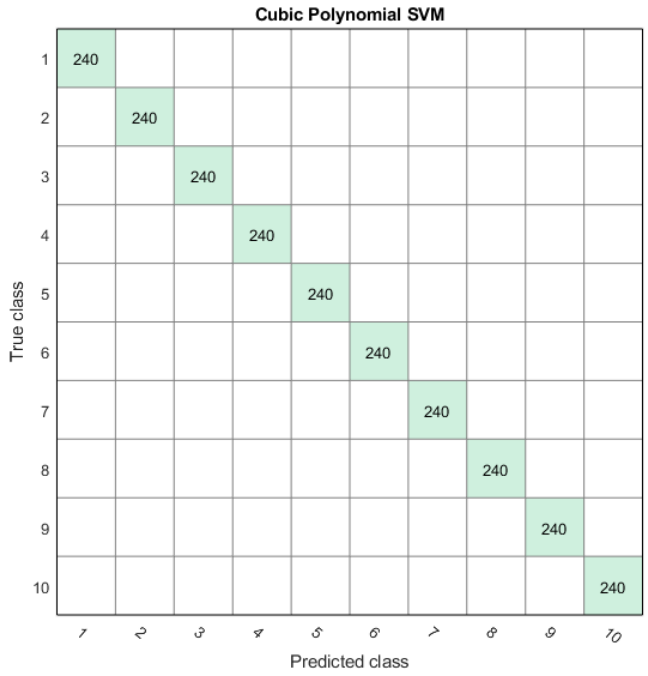

Figure 4.9: Confusion matrix for Bagging Ensemble Learning Classifier.

Table 4.1: Accuracy comparison of glucose concentration detection of various classifiers

Dataset	***Classification Algorithm***	***[a]Accuracy***	***Noise Levels (V) Training, Test***
A	Decision Tree (Fine Tree)	97.7	0.10, 0.20
A	Ensemble	100	0.10, 0.10 0.20, 0.20
B	LDA	100	0.10, 0.10 0.20, 0.10
B	Cubic SVM	100	0.10, 0.15 0.20, 0.20

a The best classification accuracies at the highest noise levels are listed. The fourth column shows the noise level V in the training and testing dataset.

This particular model of testing glucose concentration from aqueous solution is specially adapted to check if the statistical methods could work better than the deterministic methods on glucose concentration detection. The future sensor system to be applied to the human would be a different system. For the same purpose, the tested solutions in this paper are binary glucose aqueous solutions with various concentrations. Our next work planned to move on to the blood solutions with controllable glucose concentrations. In our next work, we are planning on designing hardware for real-life human blood samples with varying glucose concentrations. The target is to design a system that enables continuous glucose monitoring.

4.4 Summary of Study 4

Various machine learning classifiers are tested on the glucose concentration determination by using the large sets of measured microwave scattering signals from the glucose solution with various concentrations. The classification results indicate that satisfactory classification accuracy

can still be achieved even with high noise levels in the feature parameters. The work has successfully shown that microwave scattering signals combined with machine learning are a promising and robust approach for non-invasive glucose concentration determination. The presented method will be extended to in vivo data in the future.

CHAPTER V

CONCLUSIONS

Combinations of state-of-the-art signal processing algorithms and standard machine learning approaches were studied in this thesis in the context of the brain-computer interface (BCI) and non-invasive blood glucose detection. Four independent studies were carried out in the thesis work. The first three studies were designed for BCI, and the last study is about a microwave signal based non-invasive glucose detection. In all the first three BCI studies, brain signal was used to decode mental command. Three different types of BCI structure was studied. Inter-subject BCI using the EEG signal was studied in the first study. I have designed the second experiment to study if the classification accuracy can be improved for multimodal hybrid BCI using simultaneous EEG-fNIRS signals. An inter-subject multimodal hybrid BCI was designed in the third study using simultaneous EEG-fNIRS recordings. The target of the studies was to improve the BCI classification accuracy by employing different preprocessing algorithms, extracting meaningful signal attributes or features, and then using machine learning algorithms to classify the features to decode brain commands. In the last study, a non-invasive glucose detection technique was proposed using broadband microwave scattering parameters and machine learning algorithms.

The target of the study was to analyze machine learning algorithms and microwave scattering parameters aa a potential candidate for blood glucose measurement.

In the BCI studies, state-of-the-art signal processing algorithms (e.g., Butterworth bandpass filter to reduce or eliminate low-frequency or high-frequency artifacts, baseline normalization to reduce noisy signals, common spatial pattern with (RCSP) and without regularization (CSP) as spatial filtering algorithms to increase the separability between classes and improve classification accuracy) were used to preprocess the acquired brain signals. Commonly used features (e.g., sub-band wavelet energy, sub-band wavelet entropy, band power, sample entropy, signal maximum, signal minimum, signal average, signal standard deviation, signal variance, signal peak to RMS difference, slope index, number of positive and negative peaks, and amplitude range) were extracted from both EEG and fNIRS signals. Standard machine learning classifiers (e.g., feed-forward neural network, support vector machine with error-correcting output codes) and deep learning classifiers using LSTM Neural Network were used to classify the extracted features and decode the mental command. Finally, the decoded commands were compared with original commands to calculate the classification accuracy for the system.

In the last project on glucose concentration detection, broadband microwave scattering parameters (S-parameters) were measured for different glucose solution placed in an n-type microwave adapter chapter. Measurement was done for different glucose solutions with concentration from 0 mg/dL to 1000 mg/dL. S-parameters were measured for a sweeping frequency of 10 MHz to 18 GHz. Debye dielectric relaxation parameters were extracted from the complex S-parameters. Dielectrics were used to create a large dataset from the original six measurements per concentrations. The effect of tissue noise was analyzed using Gaussian noise. Features were extracted from the datasets and used for the classification of the glucose solutions.

Standard machine learning algorithms (e.g., support vector machine, discriminant analysis, decision tree classifier, ensemble learning classifier) were used for the classification, and their results were compared to comment on the best classification algorithms for glucose detection.

In study 1, it has been shown that participants in inter-subject BCIs show associativity in SMR dynamics and that associativity can be utilized to predict the control performance of inter-subject BCI. Kullback-Leibler Divergence (KLD) based predictors have been proposed as the measurement of across-subject associativity. The proposed predictor has been tested for a subject independent BCI paradigm where no information from the testing subject is used for the training of the system. Linear regression between the proposed predictor and inter-subject classification accuracy shows a strong negative correlation ($r = -0.62$) between the proposed predictor and classification accuracy for forty-five inter-subject pairs. The results show the suitability of the proposed predictors in inter-subject BCIs.

In study 2, a successful classification of multi-class motor execution tasks in multimodal hybrid EEG-fNIRS based BCIs have been shown. Hybrid BCIs have been shown in the literature to improve the classification performance for binary BCI; however, multiclass BCI is essential to enable the usage of a hybrid BCI system for multitasking. The results showed that classification accuracy could be improved significantly when mutually correlated information from neurophysiological and hemodynamic brain activity. The study can be perceived as an essential step towards hybrid BCIs with more degrees of freedom.

An inter-subject hybrid BCI using simultaneously recorded EEG-fNIRS signals has been reported in study 3. The objective of the study is to see if the hybrid combination of modalities can overcome the barrier of inter-subject brain dynamics variation. In our study, the EEG and fNIRS signal recordings from twenty-nine subjects were used to show that the inter-subject

hybrid BCI integrating these two modalities improves the accuracy. We have shown that the hybrid modality based BCI system is more stable and robust for across subject variation of human brain dynamics. Hence, the proposed system can be a better candidate for the implementation of inter-subject BCI systems for better performance with reduced subject-specific training.

Study 4 shows that machine learning algorithms can be utilized to design a non-invasive glucose detection system from microwave scattering parameters. Traditional algorithms measure microwave scattering parameters for glucose solutions and use the Debye relaxation model to extract dielectric properties. The studies show a correlation between the measured parameters and the glucose solution; however, the dielectric is not sensitive enough to track small changes in the glucose concentration. Hence, the studies fail to make any firm conclusion about the suitability of the detection techniques. On the other hand, the method proposed in study 4 achieved medical-grade classification accuracies for microwave scattering parameter datasets containing a high level of noise, which can be perceived as tissue noise of blood glucose measurements. In this study, it has been shown a Debye dielectric parameter combined with machine learning is a robust and promising technique of glucose concentration detection. This study is planned to be extended for real blood solution and finally for a realistic non-invasive blood glucose monitoring device.

In conclusion, several studies were designed to test the application of signal processing algorithms and machine learning classifiers in the context of BCI and glucose measurement. The results showed the suitability of the proposed algorithms to achieve better performance in BCIs as well as in glucose detection.

REFERENCES

1. L. Nicolas-Alonso and J. Gomez-Gil, "Brain Computer Interfaces, a Review", Sensors, vol. 12, no. 2, pp. 1211-1279, 2012.

2. J. Wolpaw, N. Birbaumer, D. McFarland, G. Pfurtscheller and T. Vaughan, "Brain–computer interfaces for communication and control", Clinical Neurophysiology, vol. 113, no. 6, pp. 767-791, 2002.

3. Meng, J. et al. Noninvasive Electroencephalogram Based Control of a Robotic Arm for Reach and Grasp Tasks. Sci. Reports 6, 38565 (2016).

4. Frolov, A. A. et al. Post-stroke Rehabilitation Training with a Motor-Imagery-Based Brain-Computer Interface (BCI)-Controlled Hand Exoskeleton: A Randomized Controlled MulticenterTrial. Front. Neurosci. 11, 400 (2017).

5. Cecotti, H. Spelling with non-invasive brain-computer interfaces - current and future trends. J Physiol Paris 105, 106–114 (2011).

6. F. Ortiz Carreon, J. Gonzalez Serna, A. Montes Rendon, N. Gonzalez Franco, A. Pena Jimenez and J. Hernandez Gomez, "Induction of emotional states in people with disabilities through film clips using brain computer interfaces", IEEE Latin America Transactions, vol. 14, no. 2, pp. 563-568, 2016.

7. L. Farwell, D. Richardson, G. Richardson and J. Furedy, "Brain fingerprinting classification concealed information test detects US Navy military medical information with P300", Frontiers in Neuroscience, vol. 8, 2014.

8. Shende, P. M. & Jabade, V. S. Literature review of brain computer interface (bci) using electroencephalogram signal. In International Conference on Pervasive Computing, 1–5 (2015).

9. G. Pfurtscheller and C. Neuper, "Motor imagery and direct brain-computer communication", Proceedings of the IEEE, vol. 89, no. 7, pp. 1123-1134, 2001.

10. J. Millán, "Combining brain-computer interfaces and assistive technologies: state-of-the-art and challenges", Frontiers in Neuroscience, vol. 1, 2010.

11. K. Ang and C. Guan, "Brain-Computer Interface in Stroke Rehabilitation", Journal of Computing Science and Engineering, vol. 7, no. 2, pp. 139-146, 2013.

12. A. Ramos-Murguialday, D. Broetz, M. Rea, L. Läer, Ö. Yilmaz, F. Brasil, G. Liberati, M. Curado, E. Garcia-Cossio, A. Vyziotis, W. Cho, M. Agostini, E. Soares, S. Soekadar, A. Caria, L. Cohen and N. Birbaumer, "Brain-machine interface in chronic stroke rehabilitation: A controlled study", Annals of Neurology, vol. 74, no. 1, pp. 100-108, 2013.

13. A. Lecuyer, F. Lotte, R. Reilly, R. Leeb, M. Hirose and M. Slater, "Brain-Computer Interfaces, Virtual Reality, and Videogames", Computer, vol. 41, no. 10, pp. 66-72, 2008.

14. J. van Erp, F. Lotte and M. Tangermann, "Brain-Computer Interfaces: Beyond Medical Applications", Computer, vol. 45, no. 4, pp. 26-34, 2012.D. Coyle, J. Principe, F. Lotte and A. Nijholt, "Guest Editorial: Brain/neuronal - Computer game interfaces and interaction", IEEE Transactions on Computational Intelligence and AI in Games, vol. 5, no. 2, pp. 77-81, 2013.

15. B. Allison and C. Neuper, "Could Anyone Use a BCI?", Brain-Computer Interfaces, pp. 35-54, 2010.

16. C. Guger, G. Edlinger, W. Harkam, I. Niedermayer and G. Pfurtscheller, "How many people are able to operate an eeg-based brain-computer interface (bci)?", IEEE Transactions on Neural Systems and Rehabilitation Engineering, vol. 11, no. 2, pp. 145-147, 2003.

17. E. Hammer, T. Kaufmann, S. Kleih, B. Blankertz and A. KÃ¼bler, "Visuo-motor coordination ability predicts performance with brain-computer interfaces controlled by modulation of sensorimotor rhythms (SMR)", Frontiers in Human Neuroscience, vol. 8, 2014.

18. Ray, R. Sitaram, M. Rana, E. Pasqualotto, K. Buyukturkoglu, C. Guan, K. Ang, C. Tejos, F. Zamorano, F. Aboitiz, N. Birbaumer and S. Ruiz, "A subject-independent pattern-based Brain-Computer Interface", Frontiers in Behavioral Neuroscience, vol. 9, 2015.

19. Reuderink, J. Farquhar, M. Poel and A. Nijholt, "A subject-independent brain-computer interface based on smoothed, second-order baselining", 2011 Annual International Conference of the IEEE Engineering in Medicine and Biology Society, 2011.

20. S. Hatamikia, A. Nasrabadi and N. Shourie, "Plausibility assessment of a subject independent mental task-based BCI using electroencephalogram signals", 2014 21th Iranian Conference on Biomedical Engineering (ICBME), 2014.

21. Shijian Lu, Cuntai Guan and Haihong Zhang, "Unsupervised Brain Computer Interface Based on Intersubject Information and Online Adaptation", IEEE Transactions on Neural Systems and Rehabilitation Engineering, vol. 17, no. 2, pp. 135-145, 2009.

22. S. Saha, K. Ahmed, R. Mostafa, L. Hadjileontiadis and A. Khandoker, "Evidence of Variabilities in EEG Dynamics During Motor Imagery-Based Multiclass Brain–Computer Interface", IEEE Transactions on Neural Systems and Rehabilitation Engineering, vol. 26, no. 2, pp. 371-382, 2018.

23. B. Blankertz, C. Sannelli, S. Halder, E. M. Hammer, A. Kübler, K.-R. Müller, G. Curio, and T. Dickhaus, Neurophysiological predictor of SMR-based BCI performance, NeuroImage, vol. 51, no. 4, pp. 1303–1309, 2010

24. M. Grosse-Wentrup, B. Schölkopf and J. Hill, "Causal influence of gamma oscillations on the sensorimotor rhythm", NeuroImage, vol. 56, no. 2, pp. 837-842, 2011.

25. M. Grosse-Wentrup and B. Schölkopf, "High gamma-power predicts performance in sensorimotor-rhythm brain–computer interfaces", Journal of Neural Engineering, vol. 9, no. 4, p. 046001, 2012.

26. H. Suk, S. Fazli, J. Mehnert, K. Müller and S. Lee, "Predicting BCI Subject Performance Using Probabilistic Spatio-Temporal Filters", PLoS ONE, vol. 9, no. 2, p. e87056, 2014.

27. Y. Zhang, P. Xu, D. Guo and D. Yao, "Prediction of SSVEP-based BCI performance by the resting-state EEG network", Journal of Neural Engineering, vol. 10, no. 6, p. 066017, 2013.

28. J. Mak, D. McFarland, T. Vaughan, L. McCane, P. Tsui, D. Zeitlin, E. Sellers and J. Wolpaw, "EEG correlates of P300-based brain–computer interface (BCI) performance in people with amyotrophic lateral sclerosis", Journal of Neural Engineering, vol. 9, no. 2, p. 026014, 2012.

29. S. Fazli, J. Mehnert, J. Steinbrink and B. Blankertz, "Using NIRS as a predictor for EEG-based BCI performance", 2012 Annual International Conference of the IEEE Engineering in Medicine and Biology Society, 2012.

30. M. Ahn, H. Cho, S. Ahn and S. Jun, "High Theta and Low Alpha Powers May Be Indicative of BCI-Illiteracy in Motor Imagery", PLoS ONE, vol. 8, no. 11, p. e80886, 2013.

31. M. Ahn, S. Ahn, J. Hong, H. Cho, K. Kim, B. Kim, J. Chang and S. Jun, "Gamma band activity associated with BCI performance: simultaneous MEG/EEG study", Frontiers in Human Neuroscience, vol. 7, 2013.

32. X. Shu, S. Chen, L. Yao, X. Sheng, D. Zhang, N. Jiang, J. Jia and X. Zhu, "Fast Recognition of BCI-Inefficient Users Using Physiological Features from EEG Signals: A Screening Study of Stroke Patients", Frontiers in Neuroscience, vol. 12, 2018.

33. Bamdadian, C. Guan, K. Ang and J. Xu, "The predictive role of pre-cue EEG rhythms on MI-based BCI classification performance", Journal of Neuroscience Methods, vol. 235, pp. 138-144, 2014.

34. E. Combrisson and K. Jerbi, "Exceeding chance level by chance: The caveat of theoretical chance levels in brain signal classification and statistical assessment of decoding accuracy", Journal of Neuroscience Methods, vol. 250, pp. 126-136, 2015.

35. Daum, B. Rockstroh, N. Birbaumer, T. Elbert, A. Canavan and W. Lutzenberger, "Behavioural treatment of slow cortical potentials in intractable epilepsy: neuropsychological predictors of outcome.", Journal of Neurology, Neurosurgery & Psychiatry, vol. 56, no. 1, pp. 94-97, 1993.

36. N. Neumann, "Predictors of successful self-control during brain-computer communication", Journal of Neurology, Neurosurgery & Psychiatry, vol. 74, no. 8, pp. 1117-1121, 2003.

37. F. Nijboer, A. Furdea, I. Gunst, J. Mellinger, D. McFarland, N. Birbaumer and A. Kübler, "An auditory brain–computer interface (BCI)", Journal of Neuroscience Methods, vol. 167, no. 1, pp. 43-50, 2008.

38. Burde W, Blankertz B. “Is the locus of control of reinforcement a predictor of brain-computer interface performance?”, Proceedings of the 3rd International Brain-Computer Interface Workshop and Training Course. 2006; 2006:108–09.

39. E. Hammer, S. Halder, B. Blankertz, C. Sannelli, T. Dickhaus, S. Kleih, K. Müller and A. Kübler, "Psychological predictors of SMR-BCI performance", Biological Psychology, vol. 89, no. 1, pp. 80-86, 2012.

40. O. Alkoby, A. Abu-Rmileh, O. Shriki and D. Todder, "Can We Predict Who Will Respond to Neurofeedback? A Review of the Inefficacy Problem and Existing Predictors for Successful EEG Neurofeedback Learning", Neuroscience, vol. 378, pp. 155-164, 2018.

41. M. Ahn, H. Cho, S. Ahn and S. Jun, "User's Self-Prediction of Performance in Motor Imagery Brain–Computer Interface", Frontiers in Human Neuroscience, vol. 12, 2018.

42. C. Jeunet, B. N'Kaoua, S. Subramanian, M. Hachet and F. Lotte, "Predicting Mental Imagery-Based BCI Performance from Personality, Cognitive Profile and Neurophysiological Patterns", PLOS ONE, vol. 10, no. 12, p. e0143962, 2015.

43. M. Ahn and S. Jun, "Performance variation in motor imagery brain–computer interface: A brief review", Journal of Neuroscience Methods, vol. 243, pp. 103-110, 2015.

44. L. Botrel and A. Kubler, "Reliable predictors of SMR BCI performance — Do they exist?", 2018 6th International Conference on Brain-Computer Interface (BCI), 2018.

45. S. Saha and M. Baumert, "Intra- and Inter-subject Variability in EEG-Based Sensorimotor Brain Computer Interface: A Review", Frontiers in Computational Neuroscience, vol. 13, 2020.

46. B. H. Dobkin, "Brain-computer interface technology as a tool to augment plasticity and outcomes for neurological rehabilitation", The Journal of Physiology, vol. 579, no. 3, pp. 637–642, 2007.

47. Y. Wang and T.-P. Jung, "A Collaborative Brain-Computer Interface for Improving Human Performance", PLoS ONE, vol. 6, no. 5, 2011.

48. S. Saha, K. I. Ahmed, R. Mostafa, A. H. Khandoker, and L. Hadjileontiadis, "Enhanced inter-subject brain computer interface with associative sensorimotor oscillations", Healthcare Technology Letters, vol. 4, no. 1, pp. 39–43, Jan. 2017.

49. S. Saha, M. S. Hossain, K. Ahmed, R. Mostafa, L. Hadjileontiadis, A. Khandoker, and M. Baumert, “Wavelet Entropy-Based Inter-subject Associative Cortical Source Localization for Sensorimotor BCI”, Frontiers in Neuroinformatics, vol. 13, 2019.

50. D. J. Krusienski, M. Grosse-Wentrup, F. Galán, D. Coyle, K. J. Miller, E. Forney, and C. W. Anderson, “Critical issues in state-of-the-art brain–computer interface signal processing”, Journal of Neural Engineering, vol. 8, no. 2, p. 025002, 2011.

51. V. Jayaram, K.-H. Fiebig, J. Peters, and M. Grosse-Wentrup, “Transfer Learning for BCIs”, Brain–Computer Interfaces Handbook, pp. 425–442, Sep. 2018.

52. Nijboer, “The influence of psychological state and motivation on brain-computer interface performance in patients with amyotrophic lateral sclerosis - a longitudinal study”, Frontiers in Neuroscience, 2010.

53. M. Ahn and S. C. Jun, “Performance variation in motor imagery brain–computer interface: A brief review”, Journal of Neuroscience Methods, vol. 243, pp. 103–110, 2015.

54. T. Dickhaus, C. Sannelli, K.-R. Müller, G. Curio, and B. Blankertz, “Predicting BCI performance to study BCI illiteracy”, BMC Neuroscience, vol. 10, no. Suppl 1, 2009.

55. M. Wronkiewicz, E. Larson, and A. K. C. Lee, “Leveraging anatomical information to improve transfer learning in brain–computer interfaces”, Journal of Neural Engineering, vol. 12, no. 4, p. 046027, 2015.

56. B. J. Edelman, J. Meng, D. Suma, C. Zurn, E. Nagarajan, B. S. Baxter, C. C. Cline, and B. He, “Noninvasive neuroimaging enhances continuous neural tracking for robotic device control”, Science Robotics, vol. 4, no. 31, 2019.

57. H. Kang, Y. Nam, and S. Choi, “Composite Common Spatial Pattern for Subject-to-Subject Transfer”, IEEE Signal Processing Letters, vol. 16, no. 8, pp. 683–686, 2009.

58. H. Ramoser, J. Muller-Gerking, and G. Pfurtscheller, “Optimal spatial filtering of single trial EEG during imagined hand movement”, IEEE Transactions on Rehabilitation Engineering, vol. 8, no. 4, pp. 441–446, 2000.

59. M. Arvaneh, C. Guan, K. K. Ang, and C. Quek, “EEG Data Space Adaptation to Reduce Intersession Nonstationarity in Brain-Computer Interface”, Neural Computation, vol. 25, no. 8, pp. 2146–2171, 2013.

60. Brunner, C., et al., “BCI Competition 2008–Graz data set A. Institute for Knowledge Discovery (Laboratory of BrainComputer Interfaces)”, Graz University of Technology, p. 136-142, 2008.

61. S. Saha, K. I. Ahmed, and R. Mostafa, “Unifying sensorimotor dynamics in multiclass brain computer interface”, 2016 5th International Conference on Informatics, Electronics and Vision (ICIEV), 2016.

62. S. Kullback and R. A. Leibler, “On Information and Sufficiency,The Annals of Mathematical Statistics”, vol. 22, no. 1, pp. 79–86, 1951.

63. C. Granero-Belinchón, S. G. Roux, and N. B. Garnier, “Kullback-Leibler divergence measure of intermittency: Application to turbulence”, Physical Review E, vol. 97, no. 1, 2018.

64. É. Roldán and J. M. R. Parrondo, “Entropy production and Kullback-Leibler divergence between stationary trajectories of discrete systems”, Physical Review E, vol. 85, no. 3, 2012.

65. S. V. Weijs, R. V. Nooijen, and N. V. D. Giesen, “Kullback–Leibler Divergence as a Forecast Skill Score with Classic Reliability–Resolution–Uncertainty Decomposition,” Monthly Weather Review, vol. 138, no. 9, pp. 3387–3399, 2010.

66. Y. Ma, X. Ding, Q. She, Z. Luo, T. Potter, and Y. Zhang, “Classification of Motor Imagery EEG Signals with Support Vector Machines and Particle Swarm Optimization”, Computational and Mathematical Methods in Medicine, vol. 2016, pp. 1–8, 2016.

67. F. Lotte and C. Guan, “Regularizing Common Spatial Patterns to Improve BCI Designs: Unified Theory and New Algorithms”, IEEE Transactions on Biomedical Engineering, vol. 58, no. 2, pp. 355–362, 2011.

68. X. Mao, M. Li, W. Li, L. Niu, B. Xian, M. Zeng, and G. Chen, “Progress in EEG-Based Brain Robot Interaction Systems, Computational Intelligence and Neuroscience”, vol. 2017, pp. 1–25, 2017.

69. F. Nijboer, A. Furdea, I. Gunst, J. Mellinger, D. McFarland, N. Birbaumer and A. Kübler, An auditory brain–computer interface (BCI), Journal of Neuroscience Methods, vol. 167, no. 1, pp. 43-50, 2008.

70. M. Witte, S. Kober, M. Ninaus, C. Neuper, and G. Wood, “Control beliefs can predict the ability to up-regulate sensorimotor rhythm during neurofeedback training”, Frontiers in Human Neuroscience, vol. 7, 2013.

71. S. Saha and M. Baumert, “Intra- and Inter-subject Variability in EEG-Based Sensorimotor Brain Computer Interface: A Review,” Frontiers in Computational Neuroscience, vol. 13, 2020.

72. Hong, Keum-Shik, and Muhammad Jawad Khan. "Hybrid Brain–Computer Interface Techniques for Improved Classification Accuracy and Increased Number of Commands: A Review". Frontiers in Neurorobotics, vol 11, 2017. Frontiers Media SA, doi:10.3389/fnbot.2017.00035. Accessed 15 Apr 2019.

73. Sadeghi, Sahar, and Ali Maleki. "Methodological Note: Recent Advances in Hybrid Brain-Computer Interface Systems: A Technological and Quantitative Review". Basic and Clinical Neuroscience Journal, vol 9, no. 5, 2018, pp. 373-388. Negah Scientific Publisher, doi:10.32598/bcn.9.5.373. Accessed 15 Apr 2019.

74. Ahn, Sangtae, and Sung C. Jun. "Multi-Modal Integration Of EEG-Fnirs For Brain-Computer Interfaces – Current Limitations and Future Directions". Frontiers in Human Neuroscience, vol 11, 2017. Frontiers Media SA, doi:10.3389/fnhum.2017.00503. Accessed 15 Apr 2019.

75. Fazli, Siamac et al. "Enhanced Performance by A Hybrid NIRS–EEG Brain Computer Interface". Neuroimage, vol 59, no. 1, 2012, pp. 519-529. Elsevier BV, doi: 10.1016/j.neuroimage.2011.07.084. Accessed 15 Apr 2019.

76. Koo, Bonkon et al. "A Hybrid NIRS-EEG System for Self-Paced Brain Computer Interface with Online Motor Imagery". Journal of Neuroscience Methods, vol 244, 2015, pp. 26-32. Elsevier BV, doi: 10.1016/j.jneumeth.2014.04.016. Accessed 15 Apr 2019.

77. Yin, Xuxian et al. "A Hybrid BCI Based on EEG And Fnirs Signals Improves the Performance of Decoding Motor Imagery of Both Force and Speed of Hand Clenching". Journal of Neural Engineering, vol 12, no. 3, 2015, p. 036004. IOP Publishing, doi:10.1088/1741-2560/12/3/036004. Accessed 15 Apr 2019.

78. Khan, M. Jawad et al. "Early Detection of Hemodynamic Responses Using EEG: A Hybrid EEG-Fnirs Study". Frontiers in Human Neuroscience, vol 12, 2018. Frontiers Media SA, doi:10.3389/fnhum.2018.00479. Accessed 15 Apr 2019.

79. Li, Rihui et al. "Enhancing Performance of a Hybrid EEG-Fnirs System Using Channel Selection and Early Temporal Features". Frontiers in Human Neuroscience, vol 11, 2017. Frontiers Media SA, doi:10.3389/fnhum.2017.00462. Accessed 15 Apr 2019.

80. Ge, Sheng et al. "A Brain-Computer Interface Based On A Few-Channel EEG-Fnirs Bimodal System". IEEE Access, vol 5, 2017, pp. 208-218. Institute of Electrical and Electronics Engineers (IEEE), doi:10.1109/access.2016.2637409. Accessed 15 Apr 2019.

81. Al-Shargie, Fares et al. "Stress Assessment Based on Decision Fusion of EEG And Fnirs Signals". IEEE Access, vol 5, 2017, pp. 19889-19896. Institute of Electrical and Electronics Engineers (IEEE), doi:10.1109/access.2017.2754325. Accessed 15 Apr 2019.

82. Chiarelli, Antonio Maria et al. "Deep Learning for Hybrid EEG-Fnirs Brain–Computer Interface: Application to Motor Imagery Classification". Journal of Neural Engineering, vol 15, no. 3, 2018, p. 036028. IOP Publishing, doi:10.1088/1741-2552/aaaf82. Accessed 15 Apr 2019.

83. Trakoolwilaiwan, Thanawin et al. "Convolutional Neural Network for High-Accuracy Functional Near-Infrared Spectroscopy in A Brain–Computer Interface: Three-Class Classification of Rest, Right-, And Left-Hand Motor Execution". Neurophotonics, vol 5, no. 01, 2017, p. 1. SPIE-Intl Soc Optical Eng, doi: 10.1117/1.nph.5.1.011008. Accessed 15 Apr 2019.

84. Buccino, Alessio Paolo et al. "Hybrid EEG-Fnirs Asynchronous Brain-Computer Interface for Multiple Motor Tasks". PLOS ONE, vol 11, no. 1, 2016, p. e0146610. Public Library of Science (Plos), doi: 10.1371/journal.pone.0146610. Accessed 15 Apr 2019.

85. Müller-Gerking, Johannes et al. "Designing optimal Spatial Filters for Single-Trial EEG Classification In A Movement Task". Clinical Neurophysiology, vol 110, no. 5, 1999, pp. 787-798. Elsevier BV, doi:10.1016/s1388-2457(98)00038-8.

86. Blankertz, Benjamin et al. "Optimizing Spatial Filters for Robust EEG Single-Trial Analysis". IEEE Signal Processing Magazine, vol 25, no. 1, 2008, pp. 41-56. Institute of Electrical and Electronics Engineers (IEEE), doi:10.1109/msp.2008.4408441.

87. Übeyli, E. (2007). ECG beats classification using multiclass support vector machines with error correcting output codes. Digital Signal Processing, 17(3), pp.675-684.

88. Y. Tomita, F. B. Vialatte, G. Dreyfus, Y. Mitsukura, H. Bakardjian, and A. Cichocki, "Bimodal BCI using simultaneously NIRS and EEG," IEEE Trans. Biomed. Eng., vol. 61, no. 4, pp. 1274–1284, 2014.

89. S. Niknamian, "The Introduction of Designing a Hybrid Brain Computer Interface System," SSRN Electron. J., 2018.

90. J. Mellinger et al., "An MEG-based brain–computer interface (BCI)," Neuroimage, vol. 36, no. 3, pp. 581–593, Jul. 2007.

91. J. Yu, K. K. Ang, C. Guan, and C. Wang, "A multimodal fNIRS and EEG-based BCI study on motor imagery and passive movement," Int. IEEE/EMBS Conf. Neural Eng. NER, pp. 5–8, 2013.

92. H. Wang, W. Chang, and C. Zhang, "Functional brain network and multichannel analysis for the P300-based brain computer interface system of lying detection," Expert Syst. Appl., vol. 53, pp. 117–128, Jul. 2016.

93. B. Van De Laar, H. Gürkök, D. Plass-Oude Bos, M. Poel, and A. Nijholt, "Experiencing BCI control in a popular computer game," IEEE Trans. Comput. Intell. AI Games, vol. 5, no. 2, pp. 176–184, 2013.

94. G. Kristo et al., "Work package: WP2 Due: M9 Type: X PU 1 PP 2 RE 3 CO 4 Main author: Mariska van Steensel (UMCU)," 2013.

95. X. Yin et al., "A hybrid BCI based on EEG and fNIRS signals improves the performance of decoding motor imagery of both force and speed of hand clenching," J. Neural Eng., vol. 12, no. 3, 2015.

96. "Functional Near-Infrared Spectroscopy (fNIRS) Cognitive Brain Monitor." [Online]. Available: https://technology.nasa.gov/patent/LEW-TOPS-84. [Accessed: 03-Oct-2019].

97. F. Herold, P. Wiegel, F. Scholkmann, and N. Müller, "Applications of Functional Near-Infrared Spectroscopy (fNIRS) Neuroimaging in Exercise–Cognition Science: A Systematic, Methodology-Focused Review," J. Clin. Med., vol. 7, no. 12, p. 466, Nov. 2018.

98. S. Sadeghi and A. Maleki, “Recent advances in hybrid brain-computer interface systems: A technological and quantitative review,” Basic Clin. Neurosci., vol. 9, no. 5, pp. 373–388, Sep. 2018.

99. G. Pfurtscheller, “The hybrid BCI,” Front. Neurosci., 2010.

100. Y. Punsawad, Y. Wongsawat, and M. Parnichkun, “Hybrid EEG-EOG brain-computer interface system for practical machine control,” in 2010 Annual International Conference of the IEEE Engineering in Medicine and Biology Society, EMBC’10, 2010, pp. 1360–1363.

101. K. Pollmann, M. Vukelic, and M. Peissner, “Towards affect detection during human-technology interaction: An empirical study using a combined EEG and fNIRS approach,” in 2015 International Conference on Affective Computing and Intelligent Interaction, ACII 2015, 2015, pp. 726–732.

102. M. Arvaneh, K. K. Ang, and C. Quek, “Optimizing the Channel Selection and Classification Accuracy in EEG-Based BCI,” IEEE Trans. Biomed. Eng., vol. 58, no. 6, p. 1865, 2011.

103. J. Giedd, J. R.- Neuron, and undefined 2010, “Structural MRI of pediatric brain development: what have we learned and where are we going?” Elsevier.

104. C. Neuper, G. R. Müller-Putz, R. Scherer, and G. Pfurtscheller, “Motor imagery and EEG-based control of spelling devices and neuroprostheses,” 2006, pp. 393–409.

105. S. Coyle, T. Ward, C. Markham, and G. McDarby, “On the suitability of near-infrared (NIR) systems for next-generation brain-computer interfaces,” in Physiological Measurement, 2004, vol. 25, no. 4, pp. 815–822.

106. N. Naseer and K. S. Hong, “Classification of functional near-infrared spectroscopy signals corresponding to the right- and left-wrist motor imagery for development of a brain-computer interface,” Neurosci. Lett., vol. 553, pp. 84–89, Oct. 2013.

107. S. Fazli et al., “Enhanced performance by a hybrid NIRS-EEG brain computer interface,” Neuroimage, vol. 59, no. 1, pp. 519–529, Jan. 2012.

108. J. Shin, A. Von Lühmann, D. W. Kim, J. Mehnert, H. J. Hwang, and K. R. Müller, “Data descriptor: Simultaneous acquisition of EEG and NIRS during cognitive tasks for an open access dataset,” Sci. Data, vol. 5, Feb. 2018.

109. Hong, K., and Khan, M., 2017. Hybrid Brain–Computer Interface Techniques for Improved Classification Accuracy and Increased Number of Commands: A Review. Frontiers in Neurorobotics, 11.

110. Corsi, M., Chavez, M., Schwartz, D., Hugueville, L., Khambhati, A., Bassett, D. and De Vico Fallani, F., 2019. Integrating EEG and MEG Signals to Improve Motor Imagery Classification in Brain–Computer Interface. International Journal of Neural Systems, 29(01), p.1850014.

111. Khalaf, A., Sejdic, E. and Akcakaya, M., 2019. A novel motor imagery hybrid brain computer interface using EEG and functional transcranial Doppler ultrasound. Journal of Neuroscience Methods, 313, pp.44-53.

112. J. Shin et al., “Open Access Dataset for EEG+NIRS Single-Trial Classification,” IEEE Trans. Neural Syst. Rehabil. Eng., vol. 25, no. 10, pp. 1735–1745, Oct. 2017.

113. Hochreiter, S., and J. Schmidhuber. "Long short-term memory." Neural computation. Vol. 9, Number 8, 1997, pp.1735–1780

114. M. Kudo, J. Toyama, and M. Shimbo. "Multidimensional Curve Classification Using Passing-Through Regions." Pattern Recognition Letters. Vol. 20, No. 11–13, pages 1103–1111.

115. Fazli, S., Popescu, F., Danóczy, M., Blankertz, B., Müller, K. and Grozea, C., 2009. Subject-independent mental state classification in single trials. Neural Networks, 22(9), pp.1305-1312.

116. Abibullaev, B., An, J., Jin, S., Lee, S. and Moon, J., 2013. Minimizing inter-subject variability in fNIRS-based brain–computer interfaces via multiple-kernel support vector learning. Medical Engineering & Physics, 35(12), pp.1811-1818.

117. Li, F., Tao, Q., Peng, W., Zhang, T., Si, Y., Zhang, Y., Yi, C., Biswal, B., Yao, D. and Xu, P., 2020. Inter-subject P300 variability relates to the efficiency of brain networks reconfigured from resting- to task-state: Evidence from a simultaneous event-related EEG-fMRI study. NeuroImage, 205, p.116285.

118. Halme, H., Parkkonen, L., “Across-subject offline decoding of motor imagery from MEG and EEG”. Sci Rep 8, 10087 (2018).

119. P. Gaur, R. B. Pachori, H. Wang and G. Prasad, "A multivariate empirical mode decomposition based filtering for subject independent BCI," 2016 27th Irish Signals and Systems Conference (ISSC), Londonderry, 2016, pp. 1-7, doi: 10.1109/ISSC.2016.7528480.

120. Fahimi, F., Zhang, Z., Goh, W., Lee, T., Ang, K. and Guan, C., 2019. Inter-subject transfer learning with an end-to-end deep convolutional neural network for EEG-based BCI. Journal of Neural Engineering, 16(2), p.026007.

121. Herff C., Heger D., Putze F., Guan C., Schultz T. (2012) Cross-Subject Classification of Speaking Modes Using fNIRS. In: Huang T., Zeng Z., Li C., Leung C.S. (eds) Neural Information Processing. ICONIP 2012. Lecture Notes in Computer Science, vol 7664. Springer, Berlin, Heidelberg

122. Liu, Y., Ayaz, H. and Shewokis, P., 2017. Multisubject “Learning” for Mental Workload Classification Using Concurrent EEG, fNIRS, and Physiological Measures. Frontiers in Human Neuroscience, 11.

123. O. Kwon, M. Lee, C. Guan and S. Lee, "Subject-Independent Brain-Computer Interfaces Based on Deep Convolutional Neural Networks," in IEEE Transactions on Neural Networks and Learning Systems, doi: 10.1109/TNNLS.2019.2946869.

124. P. Wang, A. Jiang, X. Liu, J. Shang and L. Zhang, "LSTM-Based EEG Classification in Motor Imagery Tasks," in IEEE Transactions on Neural Systems and Rehabilitation Engineering, vol. 26, no. 11, pp. 2086-2095, Nov. 2018, doi: 10.1109/TNSRE.2018.2876129.

125. D. Zhang, L. Yao, K. Chen and J. Monaghan, "A Convolutional Recurrent Attention Model for Subject-Independent EEG Signal Analysis," in IEEE Signal Processing Letters, vol. 26, no. 5, pp. 715-719, May 2019, doi: 10.1109/LSP.2019.2906824.

126. G. Zhang, V. Davoodnia, A. Sepas-Moghaddam, Y. Zhang and A. Etemad, "Classification of Hand Movements From EEG Using a Deep Attention-Based LSTM Network," in IEEE Sensors Journal, vol. 20, no. 6, pp. 3113-3122, 15 March15, 2020, doi: 10.1109/JSEN.2019.2956998.

127. S. Yoo, S. Woo and Z. Amad, "Classification of three categories from prefrontal cortex using LSTM networks: fNIRS study," 2018 18th International Conference on Control, Automation and Systems (ICCAS), Daegwallyeong, 2018, pp. 1141-1146.

128. Huve G., Takahashi K., Hashimoto M. (2018) fNIRS-Based Brain–Computer Interface Using Deep Neural Networks for Classifying the Mental State of Drivers. In: Kůrková V., Manolopoulos Y., Hammer B., Iliadis L., Maglogiannis I. (eds) Artificial Neural Networks and Machine Learning – ICANN 2018. ICANN 2018. Lecture Notes in Computer Science, vol 11141. Springer, Cham

129. Lu J., Yan H., Chang C., Wang N. (2020) Comparison of Machine Learning and Deep Learning Approaches for Decoding Brain Computer Interface: An fNIRS Study. In: Shi Z., Vadera S., Chang E. (eds) Intelligent Information Processing X. IIP 2020. IFIP Advances in Information and Communication Technology, vol 581. Springer, Cham

130. Ghonchi, H., Fateh, M., Abolghasemi, V., Ferdowsi, S. and Rezvani, M., 2020. Deep recurrent–convolutional neural network for classification of simultaneous EEG–fNIRS signals. IET Signal Processing, 14(3), pp.142-153.

131. Asgher U, Khalil K, Khan MJ, Ahmad R, Butt SI, Ayaz Y, Naseer N and Nazir S (2020) Enhanced Accuracy for Multiclass Mental Workload Detection Using Long Short-Term Memory for Brain–Computer Interface. Front. Neurosci. 14:584. doi: 10.3389/fnins.2020.00584

132. Chiarelli, A., Croce, P., Merla, A. and Zappasodi, F., 2018. Deep learning for hybrid EEG-fNIRS brain–computer interface: application to motor imagery classification. Journal of Neural Engineering, 15(3), p.036028.

133. W. V. Gonzales, A. T. Mobashsher and A. Abbosh, “The Progress of Glucose Monitoring-A Review of Invasive to Minimally and Non-Invasive Techniques, Devices and Sensors”, Sensors, 19(4), p.800, 2019

134. W. R. Rowley, C. Bezold, Y. Arikan, E. Byrne, and S. Krohe, “Diabetes 2030: Insights from Yesterday, Today, and Future Trends”, Popul Health Manag., 20(1): 6–12, 2017

135. T. Yilmaz, R. Foster and Y. Hao, “Radio-Frequency and Microwave Techniques for Non-Invasive Measurement of Blood Glucose Levels”, Diagnostics, 9(1), p.6, 2019

136. M. Hofmann, G. Fischer, R. Weigel, and D. Kissinger, "Microwave-Based Non-invasive Concentration Measurements for Biomedical Applications," IEEE Trans. Microw. Theory Tech., vol. 61, pp. 2195-2204, 2013

137. H. Choi, et al., “Design and in vitro interference test of microwave noninvasice blood glucose monitoring sensor,” IEEE Trans. Microw. Theoiry Techn., vol. 63, no. 10, pp. 3016-3025, October 2015

138. A. Omer, G. Shaker and S. Safavi-Naeini, “Non-invasive Glucose Monitoring at mm-Wave Frequencies”, J. Compu. Vision Imaging Sys., 4(1), p.3, 2018.

139. B. Bababjanyan, H. Melikyan, S. Kim, J. Kim, K. Lee and B. Friedman, "Real-Time Non-invasive Measurement of Glucose Concentration Using a Microwave Biosensor", Journal of Sensors, vol. 2010, pp. 1-7, 2010.

140. X. Xiao and Q. Li, "A Non-invasive Measurement of Blood Glucose Concentration by UWB Microwave Spectrum", IEEE Antennas and Wireless Propagation Letters, vol. 16, pp. 1040-1043, 2017.

141. Breiman, L., J. Friedman, R. Olshen, and C. Stone. Classification and Regression Trees. Boca Raton, FL: CRC Press, 1984

142. Guo, Y., T. Hastie, and R. Tibshirani. Regularized linear discriminant analysis and its application in microarrays. Biostatistics, Vol. 8, No. 1, pp. 86–100, 2007

143. Hastie, T., R. Tibshirani, and J. Friedman. The Elements of Statistical Learning, second edition. New York: Springer, 2008

144. Breiman, L. “Bagging Predictors.” Machine Learning. Vol. 26, pp. 123–140, 1996.

145. V. Vapnik, “The nature of statistical learning theory. Springer-Verlag, 1995.

146. G. M Foody, and A. Mathur, “A relative evaluation of multiclass image classification by support vector machines,” IEEE Transactions on Geoscience and Remote Sensing, vol.6, pp.1335–1343, 2004.

147. S. Haykin, “Neural networks: A comprehensive foundation”, 2nd ed., Pearson Education, 1999.

148. S. K. Saha et al, "A Filtering Approach to Clean EEG Signal Based on EMD-DF to Improve Classification Accuracy during Hands Movement," International Journal of Computer Science Issues (IJCSI), vol. 16, (1), pp. 14-20, 2019.

149. K. Hong, N. Naseer and Y. Kim, "Classification of prefrontal and motor cortex signals for three-class fNIRS–BCI", Neuroscience Letters, vol. 587, pp. 87-92, 2015. Available: 10.1016/j.neulet.2014.12.029.

150. L. Breiman et al., Classification and Regression Trees, Chapman & Hall, Boca Raton, 1993.

151. O. Aydemir et al., Comparing Common Machine Learning Classifiers in Low-Dimensional Feature Vectors for Brain Computer Interface Applications, International Journal of Innovative Computing, Information and Control, Volume 9, Number 3, March 2013.

152. R. Chatterjee, A. Datta and D. Sanyal, "Ensemble Learning Approach to Motor Imagery EEG Signal Classification", Machine Learning in Bio-Signal Analysis and Diagnostic Imaging, pp. 183-208, 2019. Available: 10.1016/b978-0-12-816086-2.00008-4

BIOGRAPHICAL SKETCH

Md Shakhawat Hossain was born on June 05, 1995. He has completed a Bachelor of Science in Electrical and Electronic Engineering (EEE) from United International University (UIU), Dhaka, Bangladesh in 2017. After completing his degree, he worked as Teaching Assistant (TA) and worked as a Graduate Research Assistant (GRA) at UIU EEE department. He also served UIU as a Part-time Lecturer of EEE from February 2018 to October 2018. After completing around 2 years of research activity at UIU, Shakhawat left UIU in November 2018.

He has completed a Master of Science in Engineering degree in Electrical Engineering from The University of Texas Rio Grande Valley (UTRGV), Texas, USA in 2020. He worked as a Research Assistant in NanoBio Lab at UTRGV from January 2019 to December 2019 which research is presented in this thesis. For teaching experiences, he also worked as a Graduate Teaching Assistant in ECE department at UTRGV January 2020 to August 2020.

His Publications:

1. S Saha, MS Hossain, K Ahmed, R Mostafa, L Hadjileontiadis, A Khandoker, and M Baumert, “Wavelet Entropy-Based Inter-subject Associative Cortical Source Localization for Sensorimotor BCI.” Front. Neuroinform. 13:47, 2019, DOI: 10.3389/fninf.2019.00047.
2. M.S. Hossain, Samir M. Iqbal, Yong Zhou, “Microwave Based Glucose Concentration Classification by Machine Learning,” 2020 IEEE Texas Symposium on Wireless & Microwave Circuits & Systems, 2020.
3. M.S. Hossain, S. Saha, K. Ahmed, and R. Mostafa, "cMEM-based Motor Imagery Induced Cortical Source Localization for Computationally Efficient Brain Computer Interface," 2017 IEEE Region 10 Humanitarian Technology Conference (R10-HTC), 2017
4. M.S. Hossain, S. Saha, M. Habib, A. Noman, T. Sharfuddin, and K. Ahmed, "Application of Wavelet-based Maximum Entropy on the Mean in Channel Optimization for BCI," 2016 International Conference on Medical Engineering, Health Informatics and Technology (MediTec), 2016.